NERC
NORTH AMERICAN ELECTRIC RELIABILITY CORPORATION

# Technical Reference Document

## Dynamic Load Modeling

December 2016

RELIABILITY | ACCOUNTABILITY


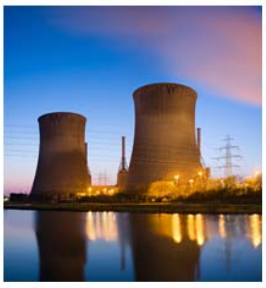

3353 Peachtree Road NE
Suite 600, North Tower
Atlanta, GA 30326
404-446-2560 | www.nerc.com

# Table of Contents

# Acknowledgments

The NERC Load Modeling Task Force (LMTF) gratefully acknowledges the invaluable assistance of the following industry experts in the preparation of this technical reference paper:

- Richard Bravo (Southern California Edison)
- Donald Davies (Western Electricity Coordinating Council)
- Pavel Etingov (Pacific Northwest National Laboratory)
- Joe Eto (Lawrence Berkeley National Laboratory)
- Anish Gaikwad (Electric Power Research Institute)
- Scott Ghiocel (Mitsubishi Electric Power Products, Inc.)
- Hamody Hindi (Bonneville Power Administration)
- Dmitry Kosterev (Bonneville Power Administration)
- John Kueck (Consultant)
- Bernie Lesieutre (University of Wisconsin-Madison)
- Rob O'Keefe (American Electric Power)
- Pouyan Pourbeik (Power and Energy, Analysis, Consulting and Education, PLLC)
- Steven Robles (Southern California Edison)
- Jay Senthil (Siemens PTI)
- John Undrill (Consultant)
- Song Wang (PacifiCorp)

# Preface

The North American Electric Reliability Corporation (NERC) is a not-for-profit international regulatory authority whose mission is to assure the reliability of the bulk power system (BPS) in North America. NERC develops and enforces Reliability Standards; annually assesses seasonal and long-term reliability; monitors the BPS through system awareness; and educates, trains, and certifies industry personnel. NERC's area of responsibility spans the continental United States, Canada, and the northern portion of Baja California, Mexico. NERC is the electric reliability organization (ERO) for North America, subject to oversight by the Federal Energy Regulatory Commission (FERC) and governmental authorities in Canada. NERC's jurisdiction includes users, owners, and operators of the BPS, which serves more than 334 million people.

The North American BPS is divided into eight Regional Entity (RE) boundaries as shown in the map and corresponding table below.

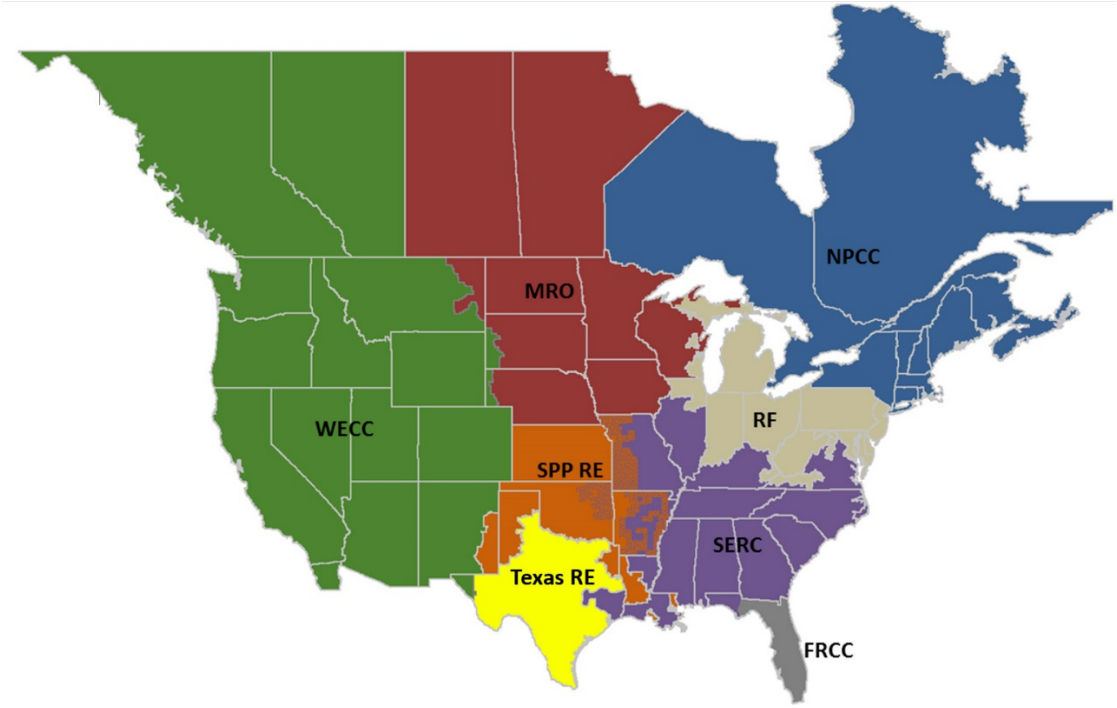


*The North American BPS is divided into eight Regional Entity (RE) boundaries. The highlighted areas denote overlap as some load-serving entities participate in one Region while associated transmission owners/operators participate in another.*

| | |
|---|---|
| **FRCC** | Florida Reliability Coordinating Council |
| **MRO** | Midwest Reliability Organization |
| **NPCC** | Northeast Power Coordinating Council |
| **RF** | ReliabilityFirst |
| **SERC** | SERC Reliability Corporation |
| **SPP RE** | Southwest Power Pool Regional Entity |
| **Texas RE** | Texas Reliability Entity |
| **WECC** | Western Electricity Coordinating Council |

# Executive Summary

The North American Electric Reliability Corporation (NERC) held a Technical Workshop on Dynamic Load Modeling and Fault Induced Delayed Voltage Recovery (FIDVR) in September 2015, which highlighted the current state-of-the-art in dynamic load modeling and the motor testing and simulation studies performed that provide the technical basis for the current dynamic load models. The workshop highlighted the composite load model and the physical nature of end-use loads that drive the various components of the model including induction motor load. This Technical Reference Document provides a detailed overview of the material covered in the workshop and acts as a technical reference for Transmission Planners (TPs) and Planning Coordinators (PCs) in the understanding of dynamic load models and modeling practices. The report highlights the following topics:

- **Changing End-Use Loads:** End-use loads are rapidly changing as energy efficiency and power electronics drive performance requirements and benefits from an energy efficiency standpoint. Understanding the fundamental behavior of these loads is critical for accurate modeling and awareness of load performance.
- **Recent History of Dynamic Load Modeling:** The development of dynamic load models, particularly the Composite Load Model (CLM), has occurred over the past 10-20 years. Recent improvements in the WECC have driven the use of the cmpldw model and more work is needed to expand its use and performance across all software platforms and utilities.
- **Physical Nature of End-Use Loads:** To accurately represent and study end-use load performance, an understanding of the nature of the end-use loads is required with respect to different motor types, power electronic loads, lighting loads, etc.
- **Testing Programs of Motors and Electronically Coupled Loads:** Much work has gone into testing end-use loads, primarily different types of motors and electronically coupled loads. High-level testing results are provided here with references to the actual testing programs.
- **Electromagnetic Simulations:** In addition to testing, much has been learned from 3-phase, electromagnetic transient simulations that model different types of motors in greater detail. The findings and how they influence the development of the composite load model are provided here as a reference.
- **Composite Load Model Data:** The CLM provides a flexible and detailed model of multiple induction motor types, electronic loads, static load, and protection settings. To reasonably model these types of loads, realistic parameters should be used. A reference to "default" or expected parameters and the reasoning behind these parameters is described here for reference by TPs and PCs.
- **Field Measurements:** Field measurements have played a critical role in understanding transient voltage response and end-use load behaviors for residential and commercial loads. The use of distribution-level monitoring is provided here with reference to multiple utility practices across North America.
- **System Studies and Sensitivity Analysis:** Examples of system studies using the CLM and an overview of sensitivity analysis is provided to give TPs and PCs an understanding of how sensitivities in the model parameters can drive simulation results.
- **Future Improvements to the Composite Load Model:** There is ongoing research in the area of improving the current composite load model to more accurately represent the reality of aggregates of end-use loads. Recent findings and concepts are described to share where the CLM is headed in the near future, including progressive stalling and tripping, phasor-based models, and plug-and-play modularized load modeling.
- **Creation of the NERC Load Modeling Task Force (LMTF):** Based on the outcomes of the workshop and industry need for sharing lessons learned and expertise in the area of dynamic load modeling, NERC has formed the Load Modeling Task Force (LMTF) to serve as a focal point for utility planners, subject matter experts, and software vendors to address emerging load modeling issues and further improve existing models in a cohesive and efficient manner.

# Introduction and Background

## Changing Nature of Electrical Loads

The composition and utilization of end-use loads is continually evolving based on technological advances and economics. The performance characteristics of these loads is also changing. Historically, residential end-use loads consisted primarily of resistive heating (space heating), cooking, and lighting (incandescent) along with small single-phase induction motor loads driving small appliances and some residential air-conditioners. Today, these loads are rapidly disappearing for more advanced and higher efficiency end-use loads. Many of these loads include power electronic converters that convert alternating current (AC) to direct current (DC). Examples of these loads are shown in Figure 1 and include many household devices such as cell phones, tablets, clocks, televisions, entertainment systems, and other consumer electronic products. In addition, distributed energy resources such as rooftop photovoltaic (PV) are increasing in penetration at the residential and commercial loads. Residential air-conditioning is considered a staple in many parts of North America today. Furthermore, electric vehicles are continually decreasing in consumer price, making them a growing component of the end-use loads. Advancements in small battery storage systems are continuing to bring that technology to the residential and small commercial consumers.

Larger 3-phase and smaller 1-phase motor loads have historically been direct drives, meaning the motor was directly connected to the electrical network. These types of motor loads are expected to be a major component of the aggregate load moving forward due to economic reasons. Advanced motor drives and higher efficiency motor drives have moved towards an electronic interface between the grid, which enables more energy efficient control of the motor loading over time. These types of loads include Electronically Commutated Motors (ECMs) and Variable Frequency Drives (VFDs). To the electrical grid, these motors do not exhibit the same response as a conventional direct drive motor and must be considered moving forward.

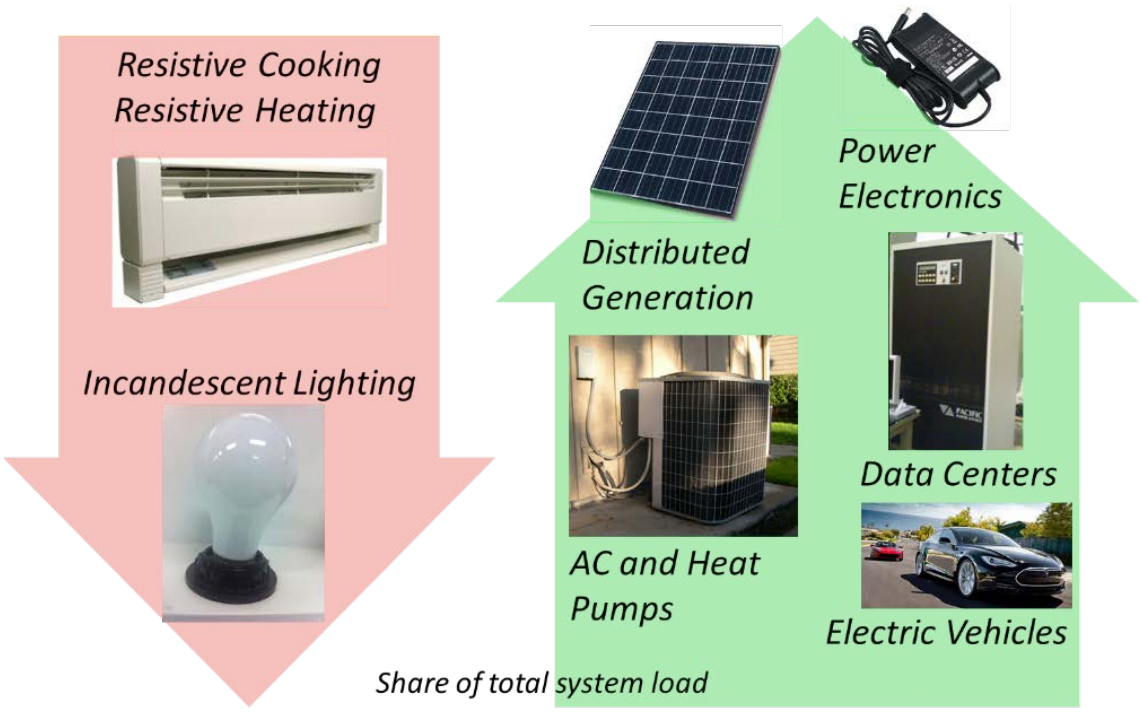


**Figure 1: Changing Share of End-Use Loads**

Table 1 shows a high level overview of how the end-use loads on the grid have evolved over the past few decades, and illustrates the rapid changes in load technology and composition.

**Table 1: Progression of Load Types**

| Then | Now |
|---|---|
| Resistive Heating | Heat Pumps (VFD) |
| Conventional Air-Conditioner Cooling | High-Efficiency Air-Conditioner Cooling (VFD) |
| Incandescent (Resistive) Lighting | Compact Fluorescent & LED Lighting |
| Resistive Cooking | Gas Cooking (Load Reduction) |
| Residential Appliances – Washers, dryers, refrigerators | Same (higher-efficiency) |
| No residential/commercial vehicle load | (Plug-In) Electric Vehicles |
| No energy storage load | Battery storage systems |
| Commercial Fans – Direct Drive | Commercial Fans – ECM |
| Commercial Pumps – Direct Drive | Commercial Pumps - VFD |

Many of these end-use loads will be considered in this technical report, to provide information on their performance characteristics and how to model the aggregate behavior of these types of loads in bulk power system studies.

# History of Dynamic Load Modeling

The history of dynamic load modeling and testing the behavior of loads goes back multiple decades. This section highlights some of the early developments that led to the creation of the composite load model in the Western Interconnection used for studying wide-area oscillatory behavior that led to one of the 1996 outages in the Western Interconnection.

## Early Load Modeling Efforts

- 1980s – Constant current real, constant impedance reactive models connected to transmission level bus
  - Primarily due to limitations in computing technologies at that time
- 1990s – EPRI Loadsyn Program
  - Several utilities using a static polynomial characteristic for load representation
- 1990s – IEEE Task Force recommends dynamic load modeling improvements
  - Recommendations warranted but do not gain much traction in the industry
- 1996 – Model validation study of August 10, 1996 outage demonstrates the need the for motor load modeling to represent oscillations and transient voltage instability
- 2001 – WECC develops “Interim” Load Model

- Consisted of 20% load represented as three-phase induction motors with remaining load represented as static load with constant current active and constant impedance reactive components
- This was identified as the only practical option in 2001
- Intended to be a temporary solution to address oscillations observed at the California-Oregon Intertie (COI)
- Model limitations and need for a composite load representation were recognized
- Model was used for planning and operating the Western Interconnection power system until 2014

## Siemens PTI and Southern California Edison

- Late 1980s – Southern California Edison observed delayed voltage recovery events, attributed to stalling of residential air conditioners
  - Tested residential air conditioner units in the laboratory, developed empirical model
- 1997 – Southern California Edison performs model validation study on Lugo event
  - Illustrated the need to represent the distribution equivalent network
  - Illustrated the need to have special models for air conditioner load – single-phase model rather than three-phase model

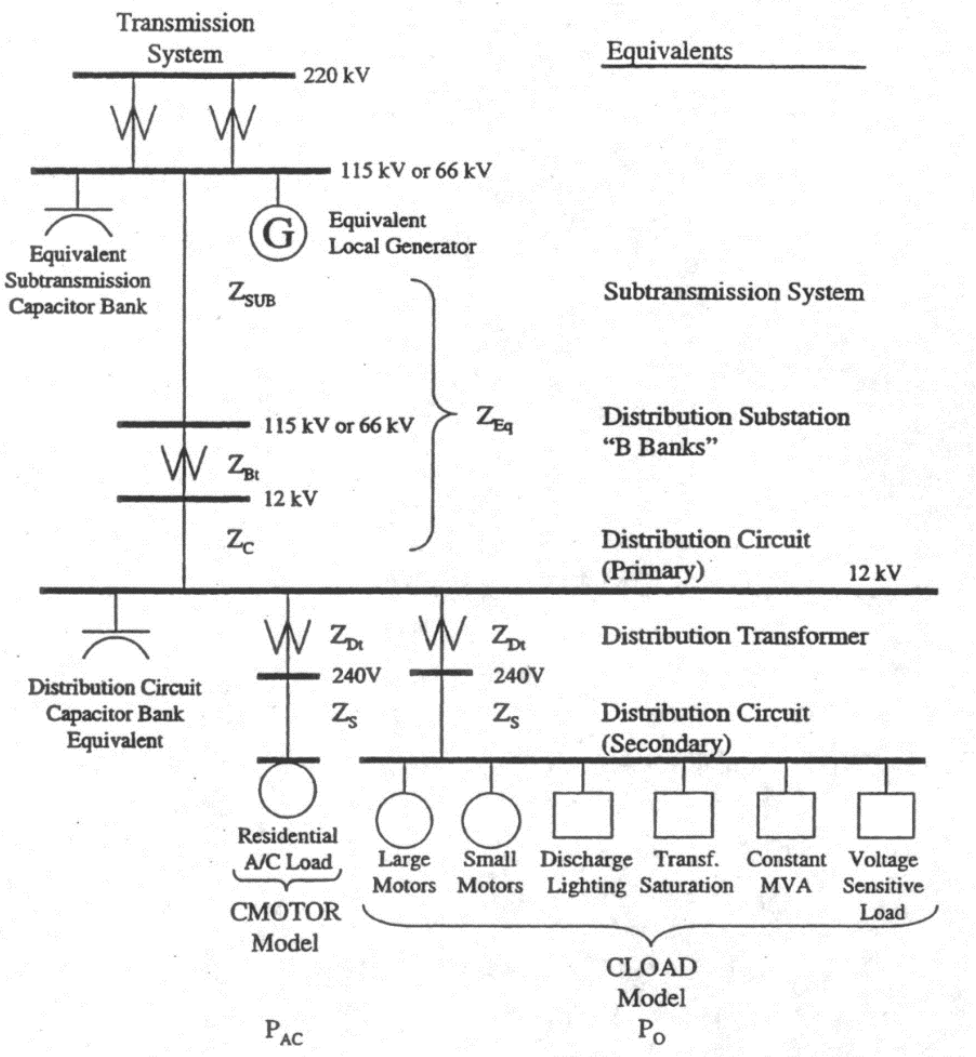


**Figure 2: Model Used by Southern California Edison in PTI PSS®E Simulator**

## Eastern Interconnection Dynamic Load Modeling

- 1994 – Florida Power & Light published an IEEE paper using a similar load model structure
- 1998 – Delayed voltage recovery event in Atlanta area in Southern Company territory
  - Events observed, analyzed, modeled, and benchmarked to recreate event
- Both models, in principle, use similar approach to the SCE model and eventual WECC model
- These models were used for special studies in local areas, but beginning to get traction
- 2013 – Northeast Power Coordinating Council (NPCC) created the NPCC Load Modeling Working Group
- 2015 – Southwest Power Pool (SPP) created the SPP Dynamic Load Task Force[1]

[1] The SPP DLTF is a successor to the SPP Transient Stability Task Force (TSTF) active from 2011-2013. The TSTF developed the original SPP Disturbance Performance Requirements that are in use in SPP today.

## WECC Load Modeling Task Force

- 2005 – WECC developed 'explicit' model
  - Included distribution equivalent circuit, induction motor load and static load
  - Numerical stability achieved in interconnection-wide study for the first time
- 2007 – First version of the composite load model in GE PSLF developed
  - Three phase motor models only, no single phase models represented
- 2006-2009 – Single-phase air conditioners tested by Electric Power Research Institute (EPRI), Bonneville Power Administration (BPA), and Southern California Edison (SCE)
  - Led to development of performance model for single-phase air conditioners
- 2009 – Single-phase air conditioner performance model added to composite load model
- 2011 – WECC adopts a phased approach for composite load modeling, starts system impact studies
- 2013 – WECC approved use of Phase 1 composite load models for planning and operational studies

# Electrical End Use Loads

This sections contextualizes the various end-use loads that exist on the system. This provides background information necessary to fully understand the composite load model and the parameters used in the model. This section is based on a compilation of research and testing performed by utilities to better understand the performance of these loads.

## Contactors

To fully understand the various end-use loads and their response, it is important to also understand the basic elements of these loads, including added controls and contactors. Electrical contactors are electrically controlled switches used for operating or switching a circuit, often controlling electric motors, lighting or heating load, and other electrical loads. These contactors are controlled by a secondary low-power circuit as shown in Figure 3.

A contactor consists of three major components:

1. Contacts carrying the current of the supply circuit;
2. Electromagnet ("coil") providing force to close the contacts;
3. Enclosure housing the contact and coil.

For a normally open "Form A" contact, current passing through the coil produces a magnetic field, attracting the moving core of the contactor. The coil draws current initially, until its inductance increases when the metal core enters the coil. The moving contact is pulled by the moving core, and the force created by the coil holds the contacts together. When the contactor is de-energized, gravity or a spring mechanism return the coil to its initial position and opens the contact. This is known as the contactor "dropping out".

As the figure shows, the supply voltage for the coil is pulled off the main circuit to establish the contact connection and maintain the force necessary to close the contacts. However, when supply voltage drops out or reduces significantly, there is insufficient electromagnetic force to maintain the contact connection and it may drop out. This is a critical consideration for modeling motor loads, as contactors have proved to drop out at voltage levels around 45-55% nominal voltage in about 1-3 cycles. When voltage recovers, the contactor will reclose relatively quickly. Testing has shown that contactors reclose between 2 to 9 cycles depending on recovery voltage; a reasonable assumption is that reclosing occurs within 6 cycles (100 ms). Tests have also shown reclosing voltage to be around 65% or so relatively consistently.

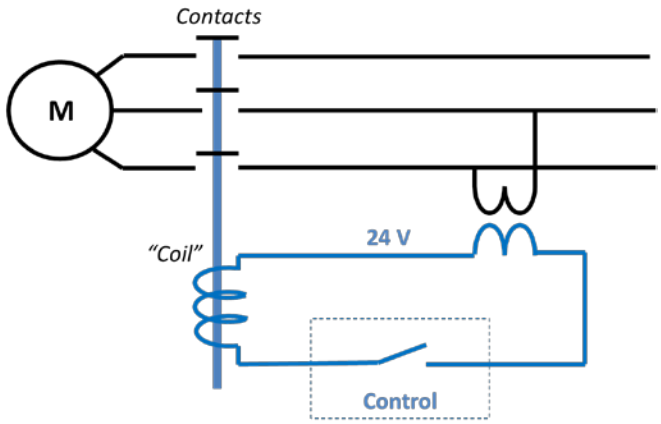


**Figure 3: Contactor and Control Circuit**

## End-Use Load Energy Management Systems

In addition to the supply voltage opening the contactors, a control system can also separate the low-power circuit path and therefore extinguish the magnetic field. This is the case of manual control or control by ancillary systems such as building Energy Management Systems (EMS)[2].

A motor load can be disconnected by EMS in two different ways. First, the EMS can open the contactors as designed to protect the motor from under voltage disturbances. Second, the EMS itself can shut off due to a low voltage disturbance. In the first case the EMS remains in control the entire time, and the EMS will typically reclose the contactors within 1 to 8 cycles after the voltage recovers. The second case is more complex and is discussed below.

EMS are highly complex and the controls can be drastically different between EMS vendors and installations based on the end-use loads being served. However, testing of EMS has shown that they can ride through voltage sags down to about 65% of nominal voltage and take a longer time to drop out (2-3 seconds) after the event occurs. The EMS will go through a reset sequence upon voltage returning that can take anywhere from a few seconds to a few minutes. Even with battery-backed EMS, these systems will likely still drop out; the clock is typically for maintaining internal clock and operating system power while external power is unavailable.

Reset sequences are based on the load being served by the EMS. Pre-programmed sequences in the controller will run from the beginning upon restart. Some loads may return quickly while others may restart after some time. This is to avoid any issues associated with restarting a block of load or motors at the same time. Testing has shown that voltage sags below 60% of nominal will result in EMS controller resetting[3]. However, this same research showed no reaction of the EMS to 5-cycle sags even for very low voltages. Figure 4 shows a standard EMS equipment restart time sequence (for illustrative purposes).

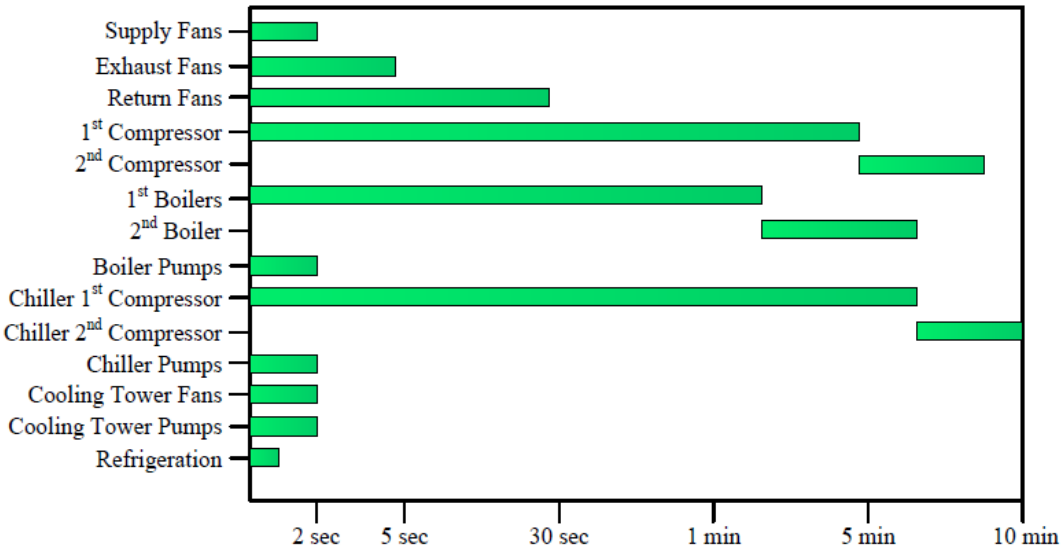


**Figure 4: Standard EMS Equipment Restart Time (Source: PNNL)**

[2] In this case, Energy Management System (EMS) refers to the building or load-related controls generally consisting of a central computer and field devices that control relays and contactors on the end-use loads.

[3] D. James, J. Kueck, "Commercial Building Motor Protection Response Report," Pacific Northwest National Laboratory: Report PNNL-24468, June 2015.

# Drive Load of Motors

The driven load behind the motor has a measurable impact on the motor performance, particularly with respect to the following:

- Reacceleration (or failure to reaccelerate and stall) following transmission faults
- Damping of power oscillations
- Frequency response

The mechanical input torque, $T_m$, of the load drives the motor performance and this torque characteristics is often described (in the models) by

$$T_m = T_{m0} * \omega^{E_{trq}}$$

where $T_{m0}$ is the initial mechanical input torque, ω is motor speed, and $E_{trq}$ is the torque damping coefficient. Constant torque loads that are not dependent on motor speed such as compressors have a damping coefficient of 0 while speed dependent loads such as fans and pumps have a damping coefficient of 2 (torque proportional to the square of speed). This explains why the driven load has an impact on stalling and reacceleration. As motor speed (and torque) decrease from full load torque for a depressed voltage, a speed dependent mechanical torque will be more grid-friendly to motor reacceleration while a constant load torque will not. Similarly, speed dependent response of electrical end-use motors support asymptotic stability of the grid by responding to small perturbations in voltage and frequency.

# Inertia of Motors and Loads

The inertia constant H of a motor is its normalized polar moment of inertia about a rotational axis. The moment of inertia of an object is essentially indicative of the resistance provided by the object to changes in its rotational motion. The procedure of estimating the polar moment of inertia is given in the Appendix. .

For power system studies, the value of the inertia constant H used in the motor swing equation must also reflect the inertia of the load connected to the motor. The reflected inertia of the load would be the effective inertia seen by the motor at the motor shaft. The driven load can be connected to the motor in numerous ways. For a rotating load, the connection to the motor can be either directly connected or through a gear or belt drive.

**Load directly connected to the motor**

Assume a fan load directly connected to the motor shaft, the total inertia constant would include the sum of the kinetic energy of the motor and the fan. Additionally, as the speed of rotation of the load would be the same as the motor shaft, primarily, loads requiring low torque and operable at high speed are connected directly to the motor. The kinetic energy can be calculated as

$$KE = \frac{1}{2} I \omega^2$$

where, $I$ is the polar moment of inertia and ω is the angular speed of rotation in rad/s. Thus, the inertia constant can be calculated as,

$$H_{m+l} = \frac{KE_m + KE_l}{S_{base}} = \frac{\frac{1}{2}(I_m + I_l)\omega^2}{S_{base}}$$

where, $I_m$ and $I_l$ are the polar moment of inertia of the motor and the directly connected load (fan in this example), respectively and $S_{base}$ is the MVA power base.

**Load connected through a gear box**

Consider a load connected to a motor through a gear as shown in Figure 5.

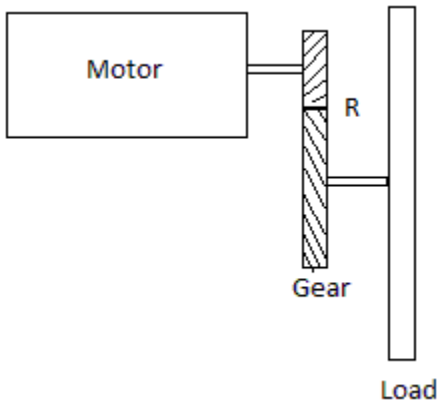


**Figure 5: Load connected through gear box**

The motor speed $\omega_m$ and torque $T_m$ are related to the load speed $\omega_l$ and torque $T_l$ though the gear ratio R as $\omega_m=R\omega_l$ and $T_l=RT_m$. Newton's second law, for rotational motion, thus gives

$$T_l = I_l \frac{d\omega_l}{dt}$$

Substituting for $\omega_l$ and $T_l$ in terms of $\omega_m$ and $T_m$ gives

$$T_m = \frac{I_l}{R^2}\frac{d\omega_m}{dt}$$

Thus, the reflected moment of inertia of the load onto the motor shaft (or the effective moment of inertia of the load as seen by the motor) is $I_l/R^2$. The inertia constant can now be calculated as,

$$H_{m+l} = \frac{KE_m + KE_l}{S_{base}} = \frac{\frac{1}{2}\left(I_m + \frac{I_l}{R^2}\right)\omega_m^2}{S_{base}}$$

By means of the gear box, a large load requiring high torque and operating at low speed can be driven by a small motor delivering low torque and running at high speed. For example, for a gear ratio of R=5, the torque required by the load is 5 times the torque deliverable by the motor and the speed of rotation of the load is $1/5^{th}$ the speed of the motor. The effective moment of inertia of the load as seen by the motor shaft is thereby $1/25^{th}$ the actual moment of inertia of the load. Further with operation at rated motor speed, $I_l$ of a directly connected load would be nearly equivalent to $I_l/R^2$ of a load connected through a gear box. Thus, the total inertia constant of the motor and load would be almost the same value for a given motor whether the load is connected through a gear box or directly connected to the motor.

**Motor driving a conveyor belt with load**

Consider a motor driving a conveyor belt with load through a pulley as shown in Figure 6.

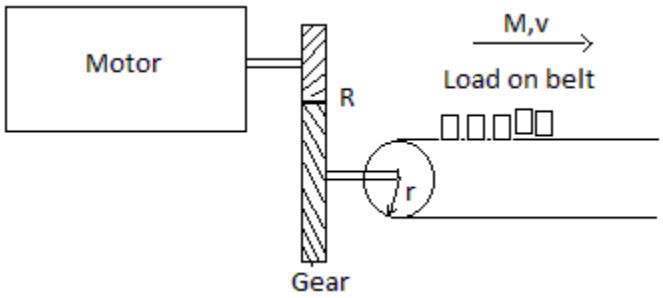


**Figure 6: Conveyor belt with load**

The inertia of the pulley is generally much smaller than the inertia of the belt with load and can thus be neglected. Let the linear velocity of the belt with load be *v*. Thus, for a total belt plus load mass M with a pulley radius *r*, the load torque $T_l$ is given as

$$T_l = rM\frac{dv}{dt} = rM\frac{d\omega r}{dt} = r^2M\frac{d\omega}{dt}$$

Thus, the load moment of inertia is given as $I_l=Mr^2$. Again, with the drive pulley connected to the motor through a gear box of ratio R, the effective moment of inertia of the conveyor belt plus load as seen by motor would be $Mr^2/R^2$. The inertia constant would then be calculated as

$$H_{m+l} = \frac{KE_m + KE_l}{S_{base}} = \frac{\frac{1}{2}\left(I_m + \frac{Mr^2}{R^2}\right)\omega_m^2}{S_{base}}$$

It should be pointed out that for inclined conveyor belts, there will be two velocity components and appropriately the moment of inertia would be impacted.

# Three-Phase Induction Motors

There are multiple types of three-phase induction motors that drive a myriad of end-use loads. This section simply provides some context around examples of three-phase induction motor loads commonly accounted for in dynamic load modeling studies.

Roof Top Unit (RTU) Direct Expansion compressor motors in the range of 5-15 HP are commonly used for building HVAC (Figure 7). These motors have a relatively small inertia constant due to their small size and inertia of the end-use load being driven by the motors. These motors typically have a local control board and motor contactors drop out between 55-65% voltage. These three-phase motors will typically stall around 50% voltage; therefore, it is expected that the contactors will drop out before motor stalling. However, unbalanced faults can still cause motor stalling if the contactors are supplied a voltage from the unfaulted phase(s). Testing has shown that if contactors drop out on these motors, they do not reclose for multiple minutes[4]. Some of these types of motors may have undervoltage protection that may operate around 2 seconds for voltage depressions of 80%.

[4] S. Robles, "Commercial 3-Phase Rooftop Air Conditioner Test Report," Southern California Edison, June 2015.

**Figure 7: Small Three-Phase (Rooftop A/C) Induction Motor Example**

Larger three-phase motors such as large chiller motors that are in the range of 200-500 HP typically have a more advanced local control board with multiple forms of protection such as undervoltage, overcurrent, and phase unbalance. Typical numbers for undervoltage protection from PNNL analysis include 90% voltage for 2 seconds and 65-80% voltage for 0.1 seconds. These motors are not expected to restart quickly and are assumed to remain offline for the timeframes associated with dynamic load modeling studies. Figure 8 shows an example of a 200-250 HP compressor for a large central cooling system.


**Figure 8: Large Three-Phase (Chiller) Induction Motor Example**

Server farms and data centers are another example of three-phase induction motors, particularly the cooling associated with data center buildings. It is generally assumed that approximately 65-70% of the load is power electronic or constant power load while most the remainder of the load is small three-phase rooftop air-conditioner compressor motors.

**Figure 9: Data Centers Loads – Power Electronic and Cooling**

To contextualize, Figure 10 shows the three-phase motors for a hotel in downtown Salt Lake City with approximately 125 hotel rooms. The building includes the following motors.

- 2 Compressor Motors:
  - 3-ph, 460 V, 139 RLA, ~94kW / 70 hp
  - 3-ph, 460 V, 118 RLA, ~ 80 kW / 60 hp
- 9 Fan Motors:
  - 3-ph, 460 V, 1.25 hp each


**Figure 10: Three-Phase Motors Outside Hotel in Salt Lake**

## Stalling Considerations for Three-Phase Motors

To describe the issue of three-phase motor stalling, let us consider laboratory tests conducted by Southern California Edison (SCE). Based on tests of multiple large 3-phase rooftop air conditioners, the following conclusions are drawn:

- **3-Phase Faults:** Contactors drop out before stalling can occur for balanced undervoltage conditions
- **2-Phase Faults:** Most tested units stall for undervoltage conditions
  - Stalling generally occurs between 10-30% voltage within 10-60 cycles
  - Stall time quicker for lower voltages
  - Compressor restarts within 5 cycles after voltage recovers
- **1-Phase Faults:** No stalling observed for 1-phase unbalanced undervoltages

Consider Figure 11, which shows the torque-speed characteristic for a small (15 HP) and large (250 HP) NEMA[5] B motor. Note that the characteristic torque curve is fundamentally one of the reasons why stalling is avoided or mitigated. During fault conditions, low voltages drives the speed of the motor down, pulling the machine torque down from full load torque. At very low speeds, the motor actually exhibits an increase in torque which does not occur for single-phase motors (discussed in subsequent section). In many cases, this torque remains higher than the torque required by the end-use load and stalling does not occur.

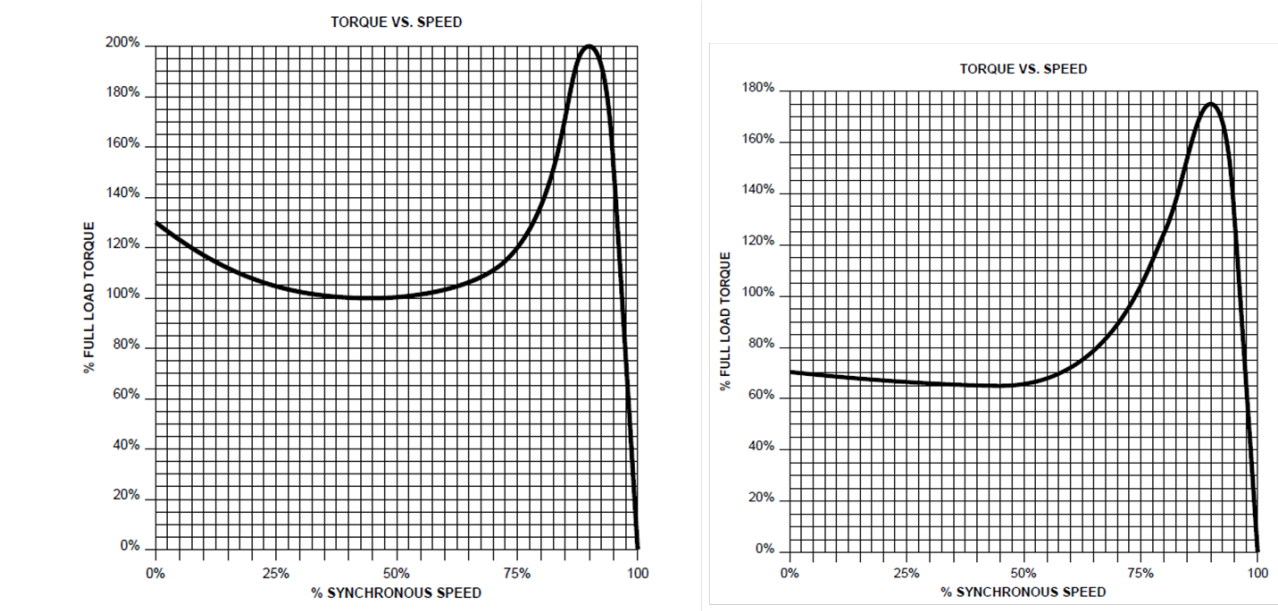


**Figure 11: NEMA B Motor Torque-Speed Curves – 15 HP (left) and 250 HP (right) [Source: Siemens]**

[5] National Electric Manufacturers Association (NEMA), *The Association of Electrical Equipment and Medical Imaging Manufacturers*, Online. www.nema.org/.

## Electrical Data for Small and Large Three-Phase Motors

Table 2 shows electrical data for large and small three-phase motors. This data was compiled from review of actual motors tested in the laboratories and in service in commercial buildings. It also includes expert opinion from testing and design of industrial and commercial processes.

**Table 2: Electrical Data for Induction Motors**

| Parameter | Name | Small Motor | Large Motor |
|---|---|---|---|
| Rs | Stator Resistance [pu] | 0.03 to 0.04 | < 0.01 |
| Ls | Synchronous Reactance [pu] | 1.8 to 3.0 | 2.5 to 5.5 |
| L' | Transient Reactance [pu] | 0.15 to 0.18 | 0.18 to 0.2 |
| L'' | Sub-Transient Reactance [pu] | 0.12 to 0.15 | 0.15 to 0.18 |
| $T_0'$ | Transient Time Constant [sec] | 0.12 to 0.20 | 0.8 to 1.8 |
| $T_0''$ | Sub-Transient Time Constant [sec] | 0.0024 to 0.003 | 0.003 to 0.005 |

The transient and sub-transient time constants are a measure of how long it would take for the energy to be dissipated in the respective circuits. The small sub-transient time constant, indicative of very quick energy dissipation, can cause numerical instability issues in large interconnected power system simulations using typical commercial simulation tools.

Most positive sequence power system simulation tools represent the dynamic behavior of a majority of elements by representative differential equations supplemented by corresponding algebraic equations. The differential equations provide information on the rate of change of certain characteristic variables of the element. In order to obtain the behavioral trend of the elements over a period of time, simulator programs perform a numerical integration of these differential equations thereby obtaining the specific amount of change of each characteristic variable over a certain time step. The time constant of a circuit defines the time element of the rate of change of the characteristic variables of that particular circuit. Thus, if the time step of integration is greater than the time constant of the circuit, the perceived change in the characteristic variable of the circuit, for that time step could be extremely large numerically. Subsequent iterations could then result in an increased rate of change of the variable, leading to numerical instability. Further, due to the nonlinear nature of the power system, the appearance of numerical instability in one characteristic variable could affect the numerical instability of multiple variables.

Few techniques are available to resolve this issue:

1. The time step of integration of the entire system of equations is taken as a value which is lower than the lowest time constant in the system. The drawback of this is however, due to the presence of few elements with small time constants, the computation time of the solution of the entire system increases.
2. The time step of integration is halved or quartered or reduced appropriately only for those elements which have low time constants. While this too increases the computation time, the increase is not as large as that when the entire system ran at the lower integration time step.
3. Using variable time-step numerical integration techniques. The drawback is that if the parameters of the variable time-steps are not suitably chosen with some knowledge of the phenomena under study, certain

dynamic responses can be entirely missed. Also, such numerical methods are not available in all commercial software tools.

4. Using engineering judgement and depending on the type of study being performed, representation of the circuits with low time constants can be neglected. For an induction motor example, the sub-transient circuit represents the second cage of a "two-cage" induction motor. Thus, representing this motor as a single cage motor would result in effectively neglecting the sub-transient circuit and hence the low time constants.

# Residential Air Conditioners – Single-Phase Induction Motors

Single-phase air conditioning load can be a substantial component of the overall load composition, particularly during heavy load conditions such as hot summer days. In highly residential areas or feeders, these loads dominate the overall composition in terms of size and characteristic response due to the nature of their operation. Figure 12 shows an example of a residential air conditioning unit commonly found in suburban neighborhoods. Some regions of the country have a higher penetration of window-mounted air-conditioning units while other areas are predominantly central air conditioning or heat pump units ("residential A/C").

**Figure 12: Residential Air Conditioner**

## Scroll-Type vs. Reciprocating Compressor

There are two main types of single-phase compressor motors used in air-conditioning installations: scroll-type and reciprocating compressors. A reciprocating compressor is a positive-displacement compressor that uses pistons driven by a crankshaft that is turned by a motor to deliver gases at high pressure. A scroll compressor is an orbiting positive-displacement compressor that compresses gases at high pressure with two inter-fitting, spiral-shaped scroll members.

Mechanical load is a function of position. For reciprocating compressors, the characteristic is approximated by a saw tooth waveform (blue line) with average constant torque (green line) as shown in Figure 13. The increasing portion of the waveform lasts one quarter of a mechanical revolution and the decreasing portion lasts three quarters of a revolution based on the reciprocating nature of the machine.

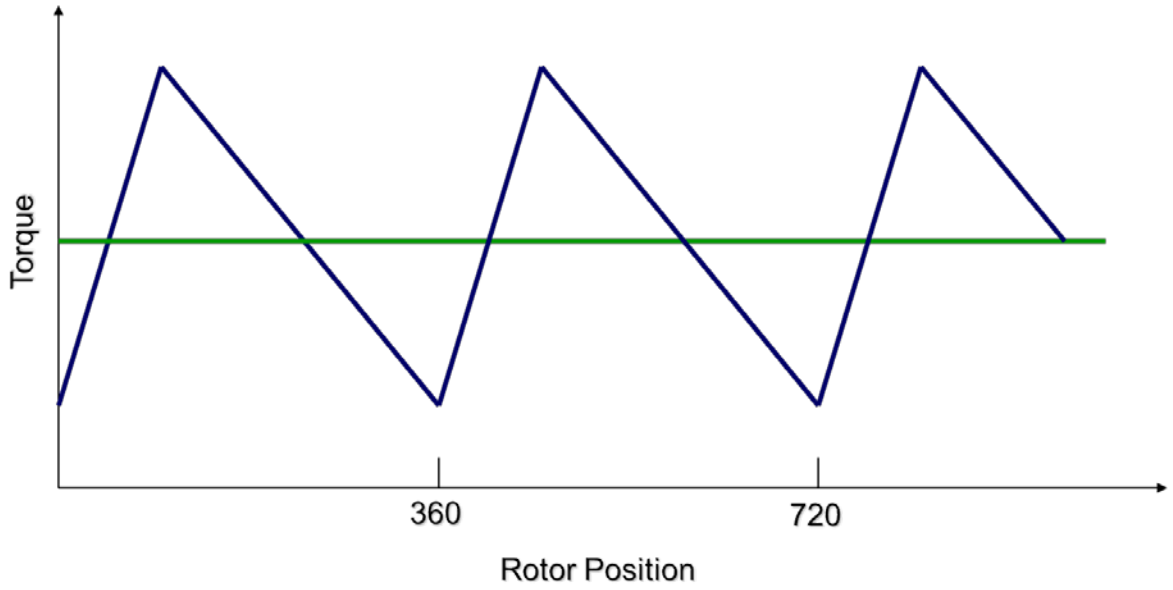


**Figure 13: Residential Air Conditioner Torque**

Figure 14 shows an example of a 3.5-ton compressor motor from a residential air-conditioner, weighing about 4.6 kg with dimensions of 310 x 75 mm. The small size of the motor and the load driven by the motor are what drive the very small inertia constant these motors have.

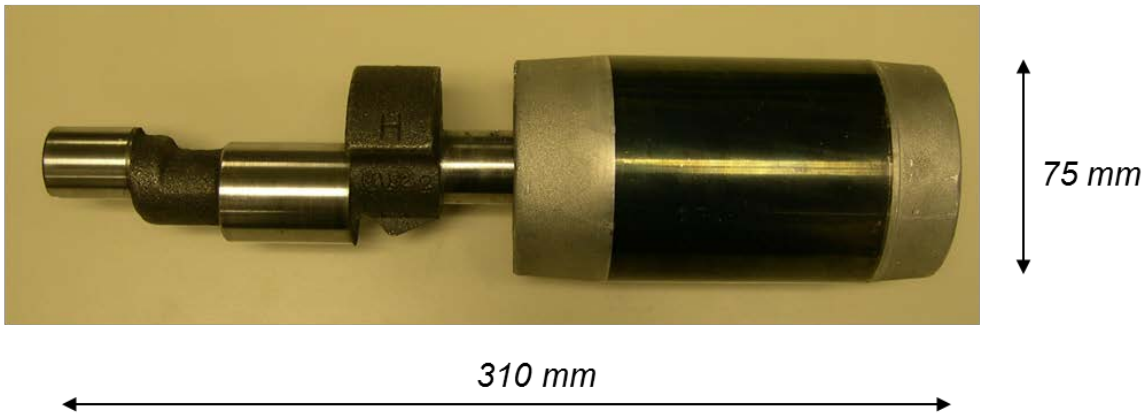


**Figure 14: Example of a Residential Air Conditioner Compressor Motor**

The electrical configuration of a single phase induction motor is as shown in Figure 15. For a motor to start to rotate, a rotating magnetic field must be developed. The rotating magnetic field is produced in three phase motors due to the spatial distribution of the three phase windings and the time distribution of the three phase voltage waveforms. In a single phase motor however, with only one main winding and a single phase supply, only a pulsating magnetic field is produced. This pulsating magnetic field would enable the motor to rotate, but it is not able to cause the motor to self-start and hence the motor requires an external start/push.

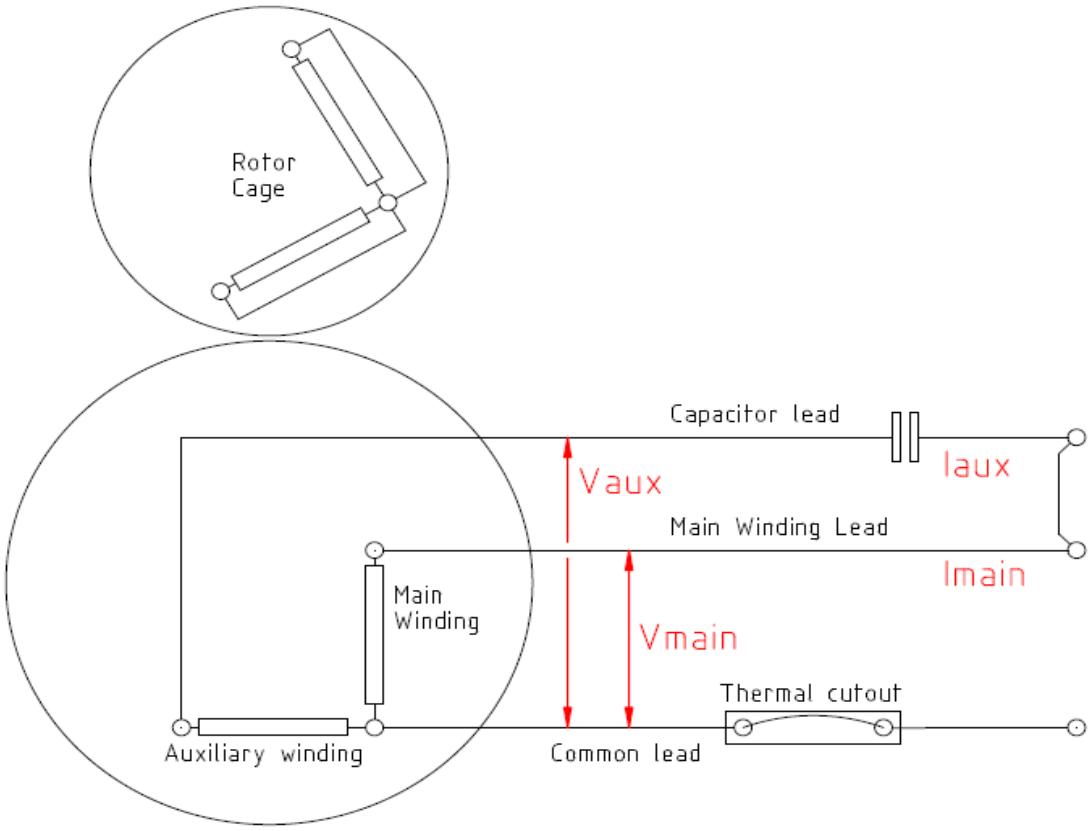


**Figure 15: Electrical Configuration of a Single-Phase Induction Motor**

To bring about self-start, a second winding known as the auxiliary winding is added in the stator in parallel to the main winding. Additionally, a capacitor is added in series to this winding to cause an additional phase shift in the voltage applied to that phase. The capacitor and auxiliary winding would ensure that the current through the auxiliary winding leads the current through the main winding by about $60^{o}$ - $80^{o}$ thereby bringing about a pseudo two phase supply source in the stator. The magnetic field that will now be set up in the air gap will no longer be pulsating and will be a rotating magnetic field causing the motor to self-start. The amount of starting torque developed is directly proportional to the size of the capacitor. However, the maximum torque developed is inversely proportional to the size of the capacitor and thus a trade-off has to be made. The presence of the capacitor also results in a quieter operation of the motor as the auxiliary winding circuit acts as an RLC filter and absorbs most of the backward flux that could be present from the main winding flux. The rotor of the motor is usually a single cage motor with the rotor bars short circuited by the end rings. The magnetic flux produced by each winding of the stator induces currents in the rotor cage.

### Stalling of Single-Phase Motors

Single phase motor stalling is a relatively complex topic dependent on many different variables. This section highlights the fundamentals of single phase motor stalling based on early laboratory testing and recent simulation work.

The Bonneville Power Administration (BPA)[6], Southern California Edison (SCE)[7], and Electric Power Research Institute (EPRI)[8] have tested single phase air conditioner compressor motors extensively over the years. Early tests measuring the compressor active and reactive power demand for changes in voltage illustrated the distinction between two states of operations – run state and stall state. Figure 16 illustrates how as supply voltage is decreased, the motor slowly begins to consume a higher amount of active and reactive power. At some voltage level ("stall voltage"), the supply voltage is no longer adequate to maintain stable motor operation and the motor "stalls[9]" (stops). There is insufficient motor torque to overcome the load torque and therefore the motor stalls. Head pressure is built up in the compressor, so the motor is unable to reaccelerate until that pressure is reduced. At this point, the motor exhibits the behavior as shown in Figure 16 on the STALL curve, drawing extremely high amounts of current particularly when the voltage recovers to normal operating level. This is because once the motor stops (stalls), its electrical behavior is essentially that of a resistive plus inductive load (i.e., a shunt reactor to ground). Ambient temperature also plays a clear role in stall characteristic. The tests performed in Figure 16 were completed under varying ambient temperatures. It is clear that as the ambient temperature increases, the stall voltage will also increase.

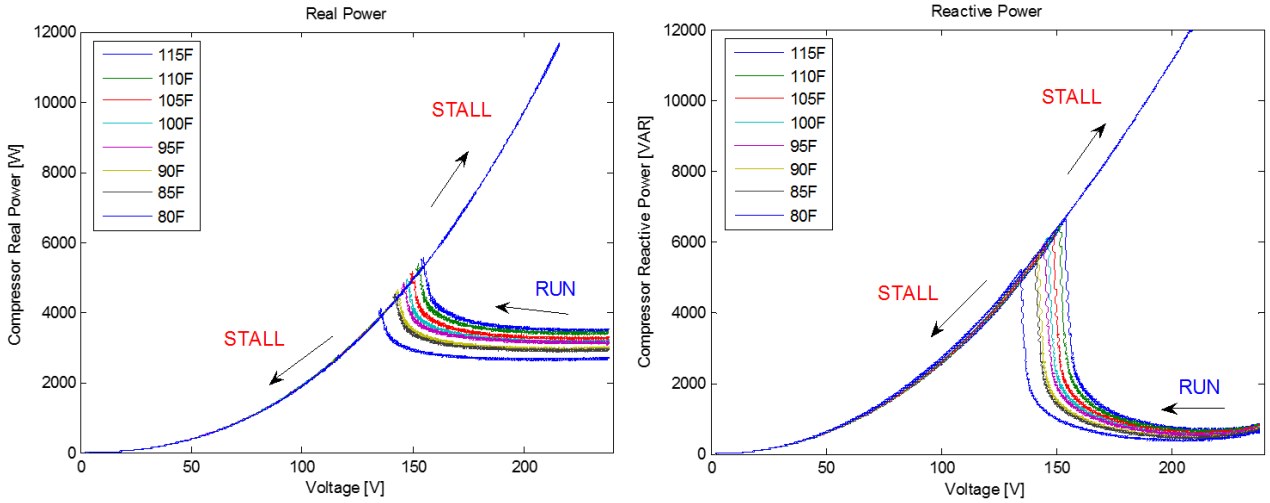


**Figure 16: Power Consumption vs. Voltage – Temperature Sensitivity**

To explain visually why single phase motors are prone to stalling as compared with three-phase motors, Figure 17 shows the torque-speed curve for both types of motors. Three-phase motors exhibit a torque characteristic where at low speed the torque increases and may stay above the load torque level[10]. However, single phase induction motors have a much different torque curve with very low torque at low speeds. Therefore, low voltage levels lead to motor deceleration and the potential for stalling where the load torque cannot be overcome by the electrical torque provided to the motor. This is particularly true for air-conditioner motors where the compressor load exhibits a constant torque characteristic with respect to speed.

The red dot shown on the single phase motor torque curve indicates the minimum speed at which a motor might recover after a disturbance if the terminal voltage returns to nominal. Below that speed the motor does not have enough torque to overcome the mechanical load.

[6] R. Bravo, J. Wen, D. Kosterev, B. Price, R. Yinger, "WECC Air Conditioner Motor Model Test Report," Western Electricity Coordinating Council.

[7] R.J. Bravo, R.R. Yinger, D. Martinez, L. Gaillac, "SCE Air Conditioner Testing Report", Southern California Edison, 2007.

[8] A. Gaikwad, A. Maitra, B. Philips, J. Harding, P. Pourbeik, and Daniel Brooks, "Air Conditioner Testing Report: Results of the Residential Air Conditioner Testing Efforts for APS", EPRI Project Report issued to APS, 2007.

[9] This is a locked rotor condition.

[10] The torque speed curve at lower voltages will be different as torque is proportional to the square of the voltage.

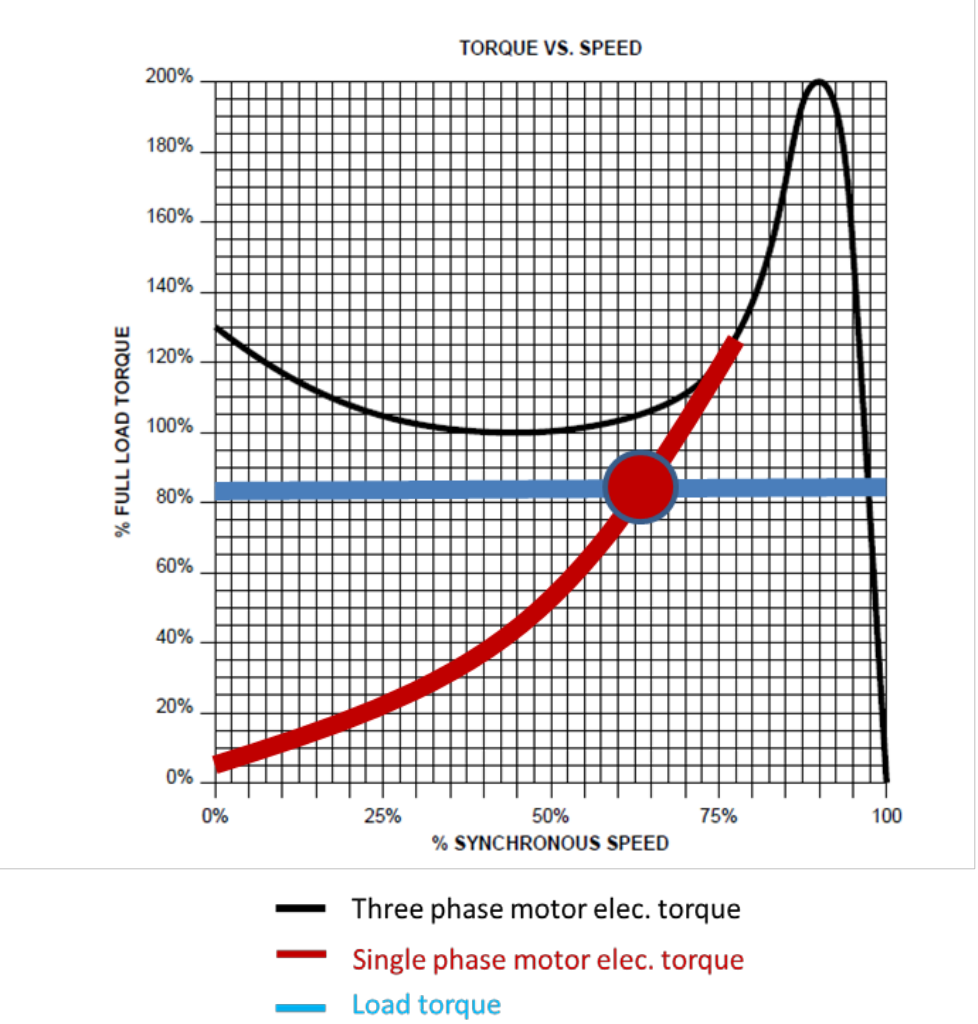


**Figure 17: Torque-Speed Curve for 3-Phase vs. 1-Phase Motors**

Figure 18 shows simulation results from an electromagnetic transient simulation of a 5kW single-phase induction motor driving a residential air conditioner. The inertia constant (H) is set to 0.048 seconds. Voltage is depressed at the terminals of the machine, as seen in $V_{as}$ and $V_t$, for 100 ms. Speed is pulled down very strongly due to a unidirectional negative electromagnetic torque (te). The immediate negative transient torque approaches eight times rated torque, and current drawn by the stalled motor is five times normal load current.

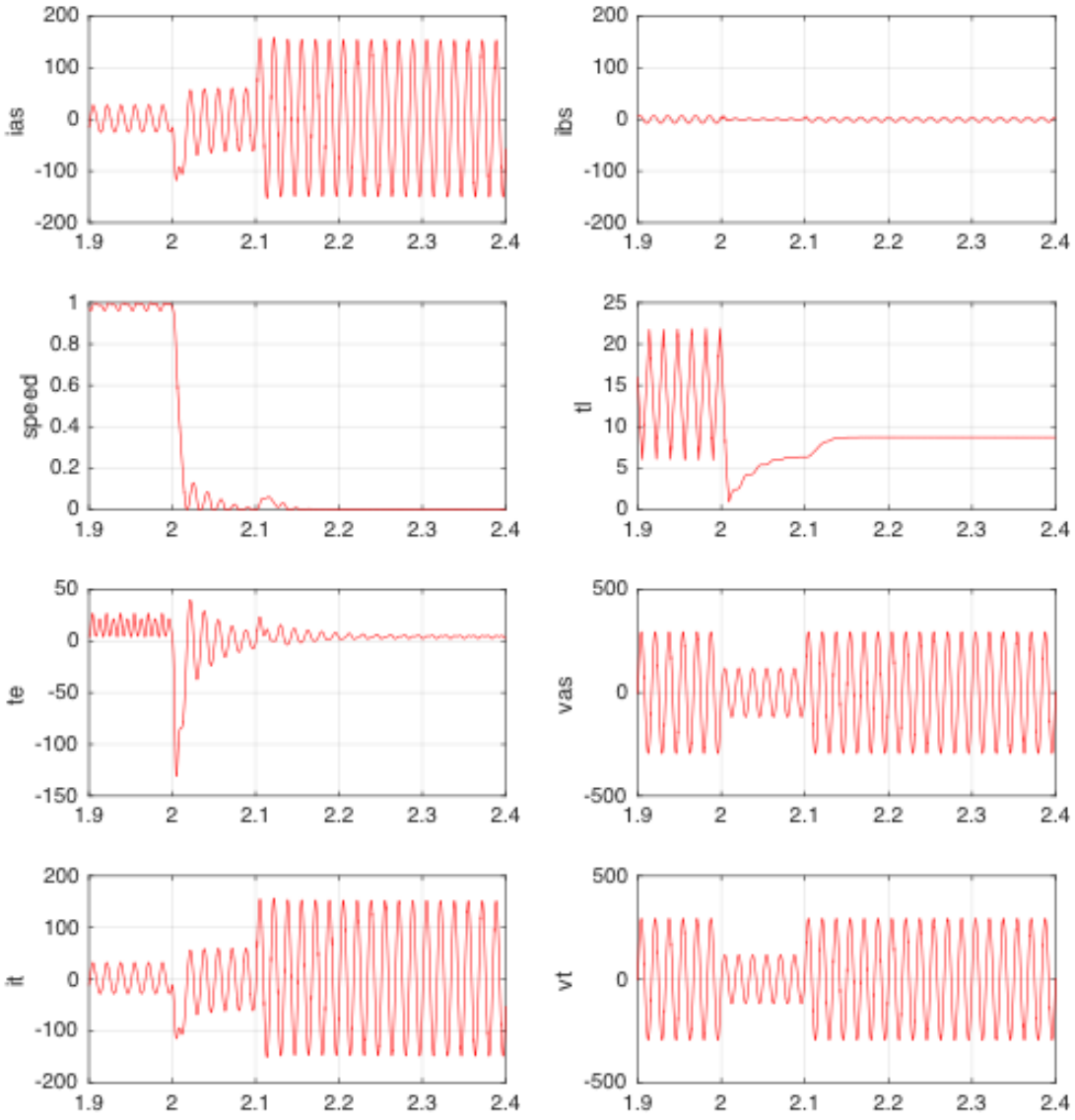


**Figure 18: Electromagnetic Simulation of Voltage Dip for 5kW Single-Phase Motor**

Time domain simulations show the electrical behavior of stalling very clearly, as shown in Figure 19. When a voltage sag sufficient to initiate motor stalling is exhibited on the machine, active and reactive power drawn by the motor are significantly increased. In the example shown, active power increases by 4 times its operating level and reactive power by approximately 10 times.

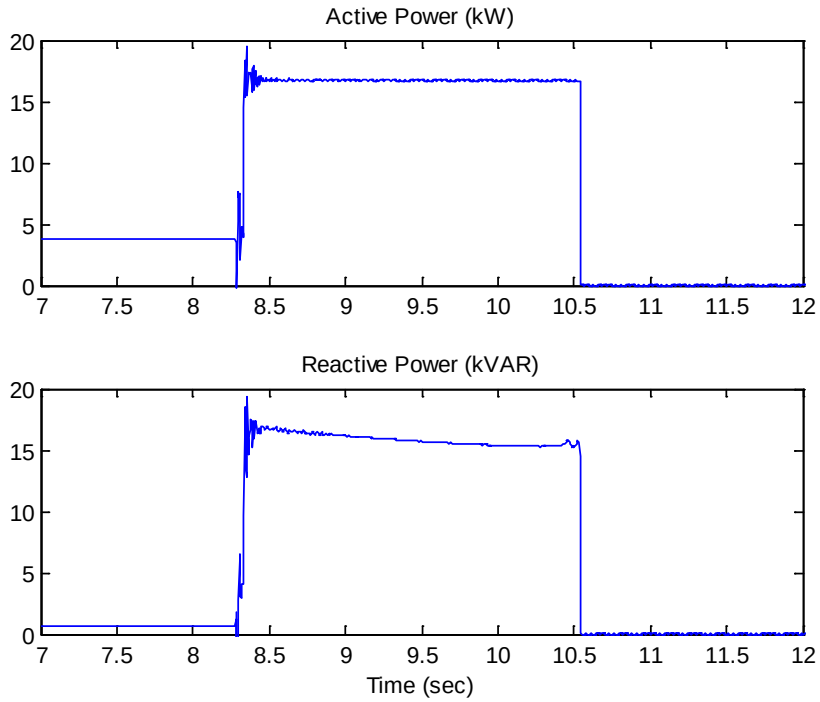


**Figure 19: Power Consumption during Single Phase Air Conditioner Stalling**

As mentioned, there is a strong sensitivity of single phase induction motor loading and stalling to ambient temperature. As the ambient temperature rises, the compressor motor is loaded to higher levels, as shown in Figure 20. Similarly, the stall voltage also rises in line with this loading. Increased loading on the machine leads to higher likelihood of stalling based on the torque-speed characteristic described above. There is less room for deceleration prior to the motor torque falling below the load torque, which leads to stalled conditions.

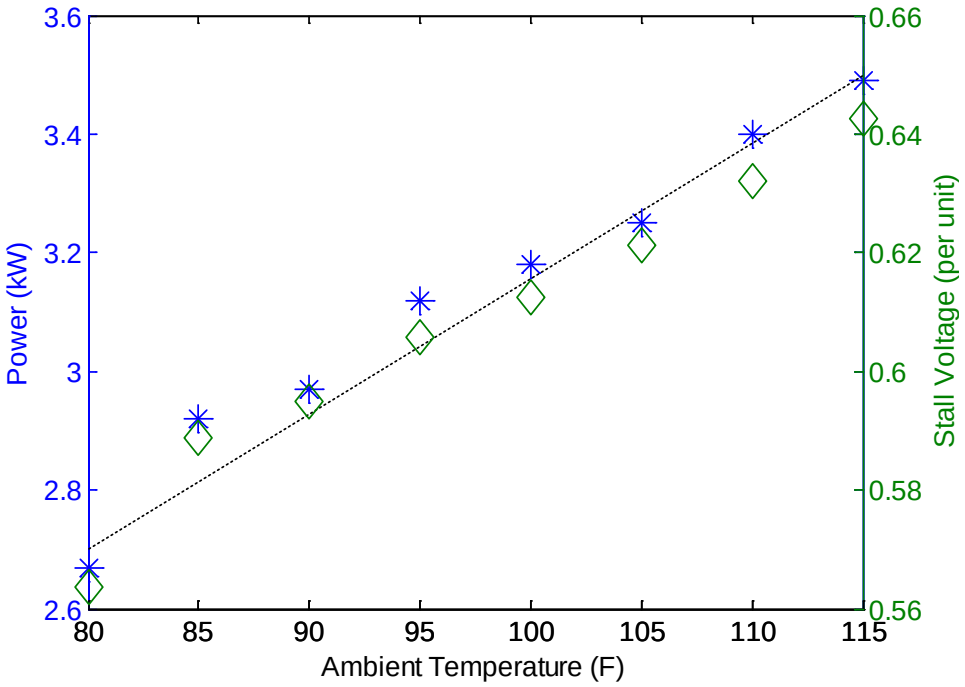


**Figure 20: Temperature Sensitivity on Consumption and Stall Voltage**

Air conditioner compressor motors have internal thermal overload (TOL) protection switches protecting the motor against high current that can damage the motor windings. Unlike motor starting, where high current persists for only a short time, the thermal protection mainly protects against sustained high currents present during stalling. The TOL is located in the motor winding circuit, and connected to the starting winding (S), running winding (R), and common wire (C) as shown in Figure 21[11]. TOL protection generally contains some form of bimetal strip with a trip mechanism; when the bimetal strips are heated by the motor current, they bend and activate the trip mechanism depending on the current set point of the thermostat. As the switch cools, it will reestablish electrical connection, enabling the motor to restart.

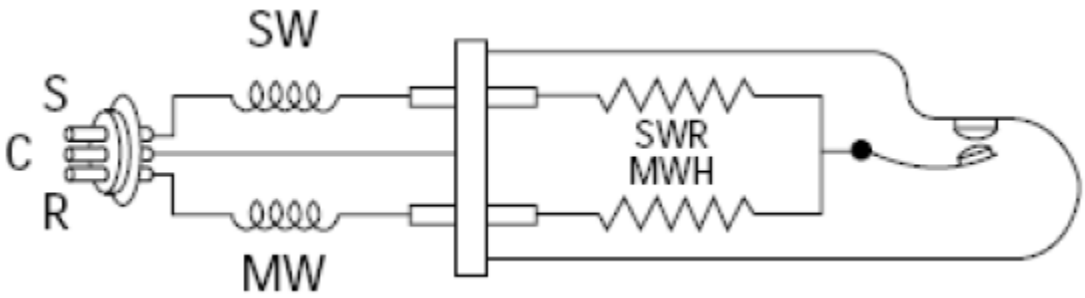


**Figure 21: Compressor Motor Thermal Overload Protection Switch**

## Power Electronic Loads

Power electronic loads are increasingly becoming popular at all levels of the end-use load spectrum, from large motor drives to small consumer electronics. This section provides a short description of the primary power electronic load types.

### Variable Frequency Drives (VFD) and Electronically Commutated Motors (ECM)

Variable Frequency Drives (VFD) are variable-speed drive technology applied to standard alternating-current induction or synchronous motors. VFDs manipulate the frequency of their output by rectifying the AC input and recreating an AC output using pulse-width modulation (PWM). Speed control is driven by the PWM controller, and can achieve full torque across a range of motor speeds. These inverter-based motors are increasingly used in commercial buildings for circulating pumps, fans, and other types of AC motor load. Figure 22 shows a VFD tested in the laboratory used to control a motor.

VFDs behave as a constant power load with power factor near unity for positive sequence fundamental frequency. However, power factor is actually around 0.75 RMS because of harmonics generated by the power electronics (Figure 22). They tend to trip at 60-70% voltage on internal undervoltage protection. Figure 23 shows the active and reactive power performance of the VFD for a voltage ramp test. Prior to the unit tripping offline due to low voltage around 70% of nominal, the active power exhibits a near constant power consumption.

For short duration voltage sags, VFDs will typically hit a current limit. This helps the motor ride through the voltage reduction. For unbalanced faults, the VFD will operate at a partial load due to the voltage reduction on the faulted phase. In testing, VFDs were found to ride through faults of up to 2 seconds but will likely trip on voltage recovery during motor reacceleration.

[11] https://www.wecc.biz/Reliability/WECC%20Air%20Conditioner%20Motor%20Model%20Test%20Report--%20Final.pdf

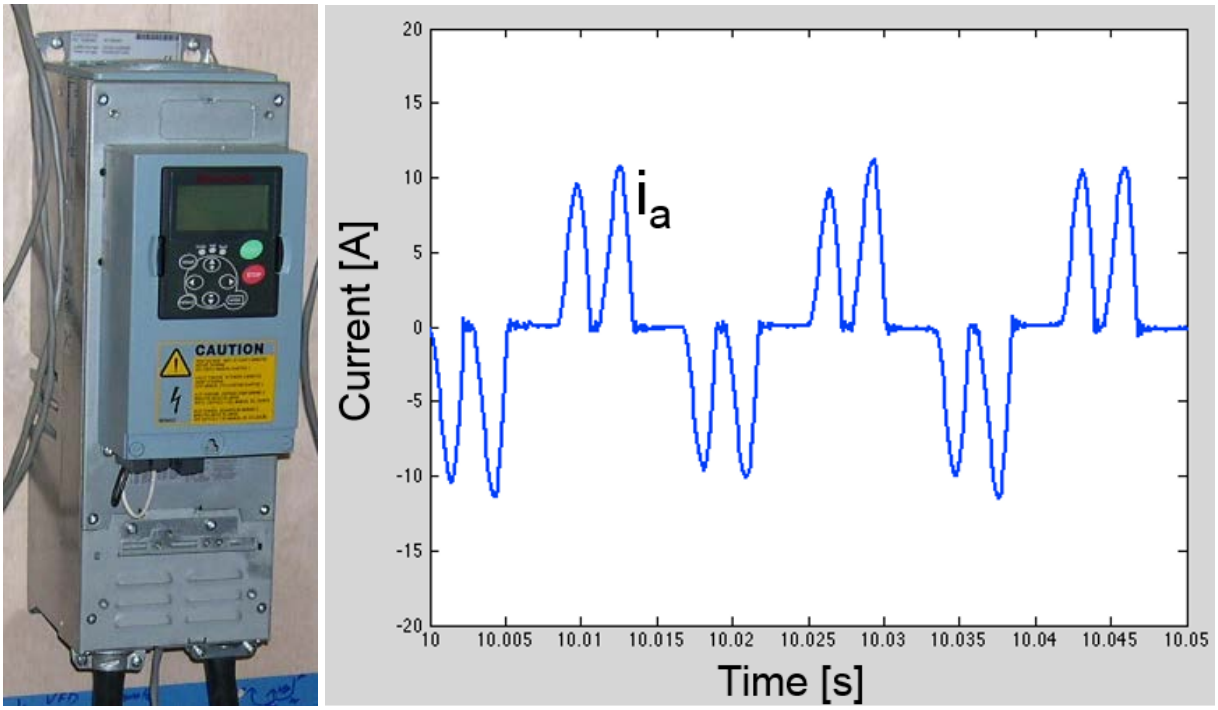


**Figure 22: Variable Frequency Drive and Harmonics**

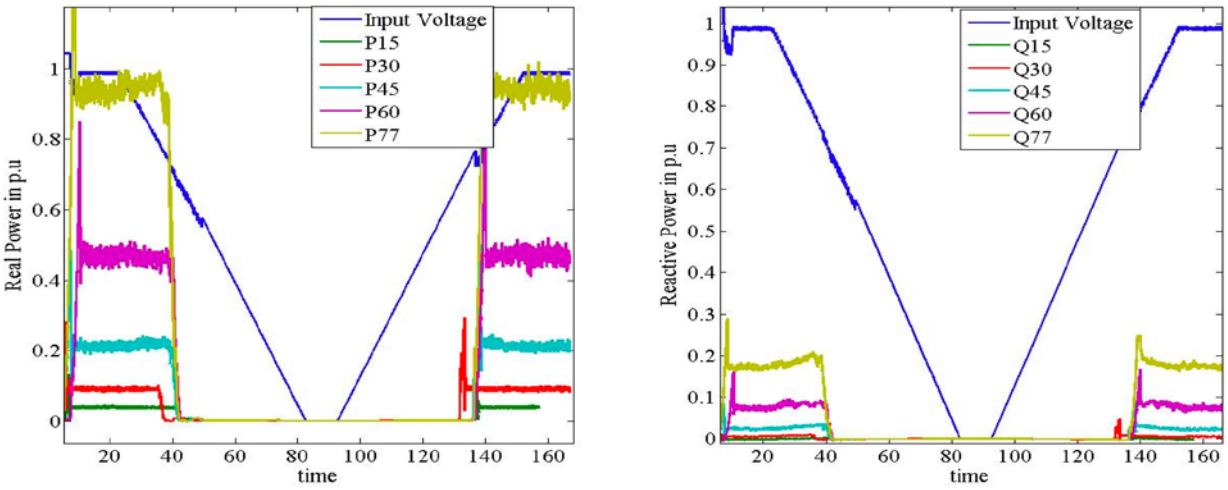


**Figure 23: Variable Frequency Drive Performance**

Electronically Commutated Motors (ECM) are variable-speed DC motors that provide high performance for various applications ranging from motors in furnaces, air handlers, condensing units, and other products. These inverter-based motors have high performance, efficiency, and reliability. An ECM is a direct-current motor with a permanent magnet rotor and series of windings on the stator. Power electronics control the commutation of the stator and therefore the speed and torque of the machine to maintain the set point requirement (e.g., constant air flow). These motors have efficiencies of up to 80%, making them advantageous for applications requiring these efficiencies and performance.

### Small Electronic Loads

Consider the average loads in a residential or small commercial office building. The majority of these loads, aside from fluorescent lighting, have some form of electronic inverter in front of them that converts the AC waveform to a DC circuit to serve the load. These loads come in all shapes and size, including, for example:

- Consumer Electronics: Plasma and LED televisions, cell phones and tablets, clocks, radios, etc.
- Appliances: High efficiency appliances such as refrigerators, washing machines, etc.
- Office Equipment: Printers, copy machines, servers, etc.

In general, most of these small motor or inverter-based loads are simply a rectification of an AC waveform to a DC waveform through power electronic converters. The controls in these rectifiers are generally a constant lower-power, higher steady-state efficiency load when in operation. From the grid dynamics standpoint, these loads may have a serious effect on overall grid support as they continue to proliferate. Laboratory testing of these loads has shown that they generally operate at or very near unity power factor (at least +/- 0.98 pf) for the fundamental frequency component.

## Lighting Loads

Various lighting loads exist on the grid today, and each has a different electrical characteristic. These different lighting technologies are described here briefly for background.

The incandescent light bulb is the oldest form of lighting technology consisting of a filament surrounded by a vacuum or inert gas. Light is produced when electrical current heats the metal filament until it illuminates. The bulb itself is simply a constant impedance load carrying current through a conductor. This simple design is disappearing, however, due to its low efficacy as compared with other lighting technologies. Typical lighting efficacies are shown in Table 3 for reference.

**Table 3: Lighting Technology Efficiencies[12]**

| Technology | Efficiency [Lumens/Watt] |
|---|---|
| Incandescent Lighting | 12-18 |
| Fluorescent Lighting | 60 |
| Compact Fluorescent Lighting | 80-100 |
| Standard 120V LED Lighting | 50-90 |

Fluorescent lighting produces fluorescence from a low pressure gas-discharge lamp to produce visible light. Electrical current in the gas excites mercury vapor, producing ultraviolent (UV) light, which is converted to visible light when it hits a phosphor coating on the inside of the bulb. Fluorescent lamps require an electrical ballast, or current limiting device, to regulate the current through the lamp. Compact fluorescent lighting (CFL) uses the same technology on the same size scale as popular incandescent lighting, and has been used as an energy-saving alternative for residential lighting. Both contain the electrical ballast, which drives the characteristic of the load to be constant current.

[12] Efficacy values shown are pulled from common ratings found across multiple manufacturers; found by web search and meant as illustrative reference only.

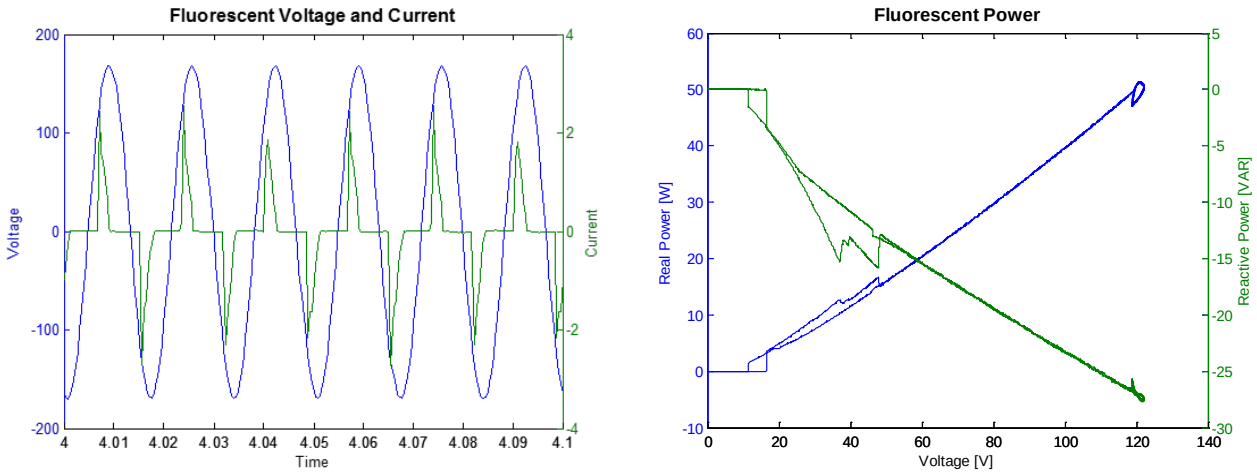


**Figure 24: Fluorescent Lighting Characteristic Response**

LED lights use a light-emitting diode (LED), which is a semiconductor device that produces visible light when sufficient electrical current is passed through it. LED lights are a power electronic-based technology that provides significantly higher energy efficiency (energy usage) while producing the same amount of lumens. LEDs, based on their electrical characteristic of the LED itself, are supplied by a constant current source

# Load Composition Data Development

Many factors are included in developing a representative load model useful for dynamic simulations. This section describes a number of these factors and how they are taken into consideration for creating the load model parameters.

## End-Use Load Surveys – Understanding End-Uses

Any dynamic load model used for dynamic simulations must be based on some judgment of the composition of the load for which is being modeled. The information used in that judgement ranges widely based on modeling practices and data available to the modeler. This section provides insights into some of the more comprehensive load composition and model parameter derivations that have been performed in the industry.

End-use load surveys are useful for gaining insight into the types of loads and breakdown of those loads for various end-use customers. This type of analysis provides additional insight into the end-uses, complementing the classification of loads (e.g., commercial, residential, industrial, etc.) commonly used for billing purposes. Figure 25 shows an example of end-use survey results collected for New England, developed in 2014, sponsored by Lawrence Berkeley National Laboratory[13] (LBNL). While the largest individual component of the load is lighting (fluorescent), note that there are multiple sections including machine drives, refrigeration, ventilation, cooling, heating, and small consumer products that are likely driven by motor loads.

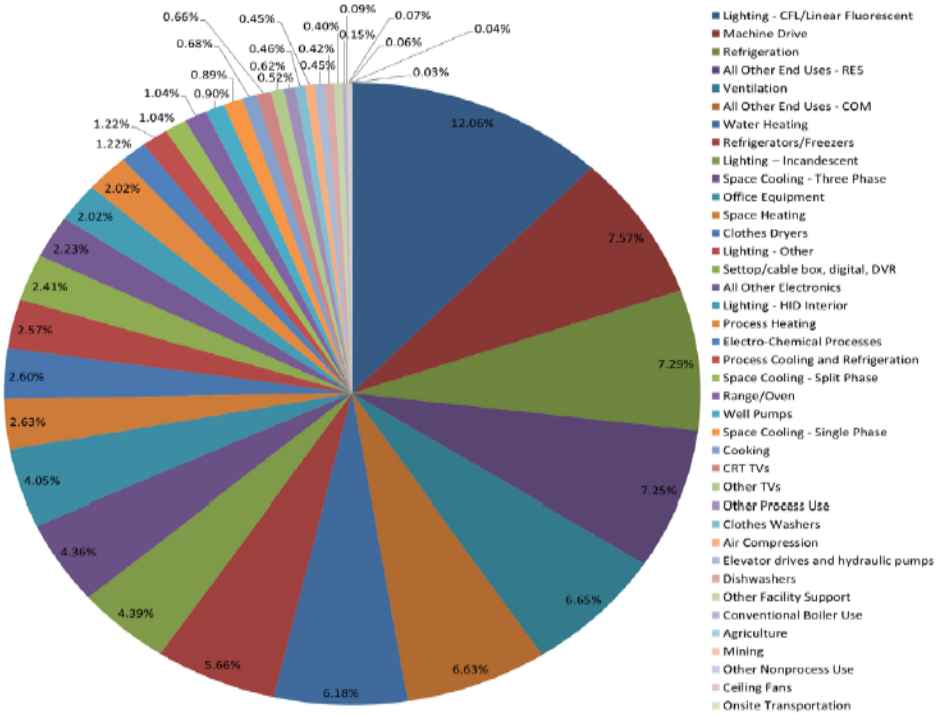


**Figure 25: New England End-Use Load Survey Results – Summer Peak [Source: NPCC]**

The California Energy Commission (CEC) also performed an extensive end-use survey, the California Commercial End-Use Survey (CEUS)[14], with select larger California utilities. This survey sampled 2,800 commercial facilities across California primarily to support demand forecasting activities for the state, market monitoring, and energy

[13] W. Gifford, et al., "End-Use Data Development for Power System Load Model in New England – Methodology and Results," Lawrence Berkeley National Laboratory, April 2014.

[14] *California Commercial End-Use Survey*, Report: CEC-400-2006-005, California Energy Commission, March 2006.

efficiency opportunities. The study captured detailed information relating the facilities themselves and the end-use equipment within these facilities, and also generated historical energy consumption profiles. Estimates of electric and gas usage in terms of magnitude and composition percentages were generated by this assessment. Figure 26 shows the breakdown of commercial end-use loads from this study.

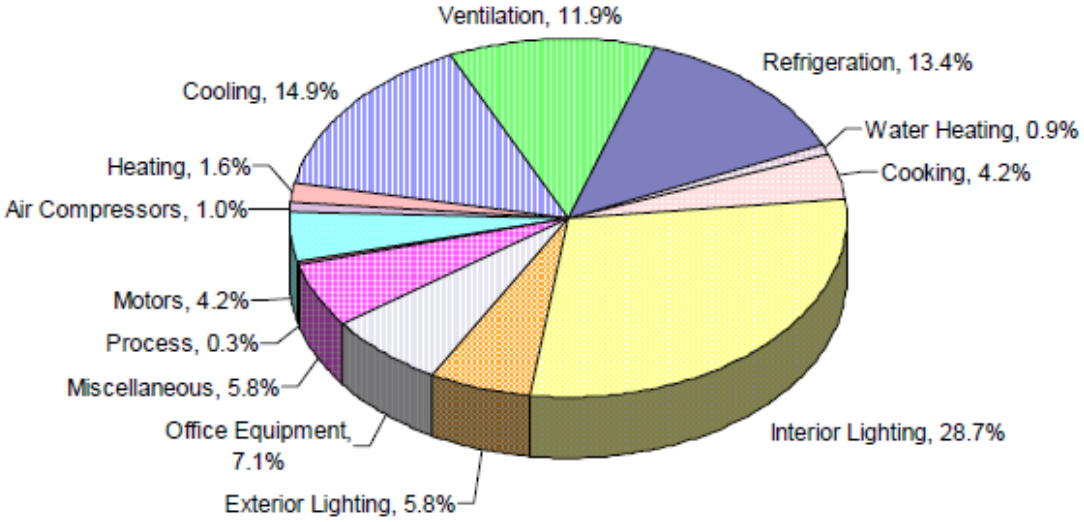


**Figure 26: Commercial Electric End-Use Load Composition [Source: CEC]**

The CEC also compiled data related to peak power consumption and annual energy consumption based on load breakdown for residential and commercial customers (Figure 27). The results are very indicative of the importance of developing accurate and representative load composition data for power system studies. Figure 27 clearly shows how air conditioning for residential and commercial loads are a substantial component of the peak load while relatively small with respect to annual consumption, representing a high percentage of load during peak conditions.

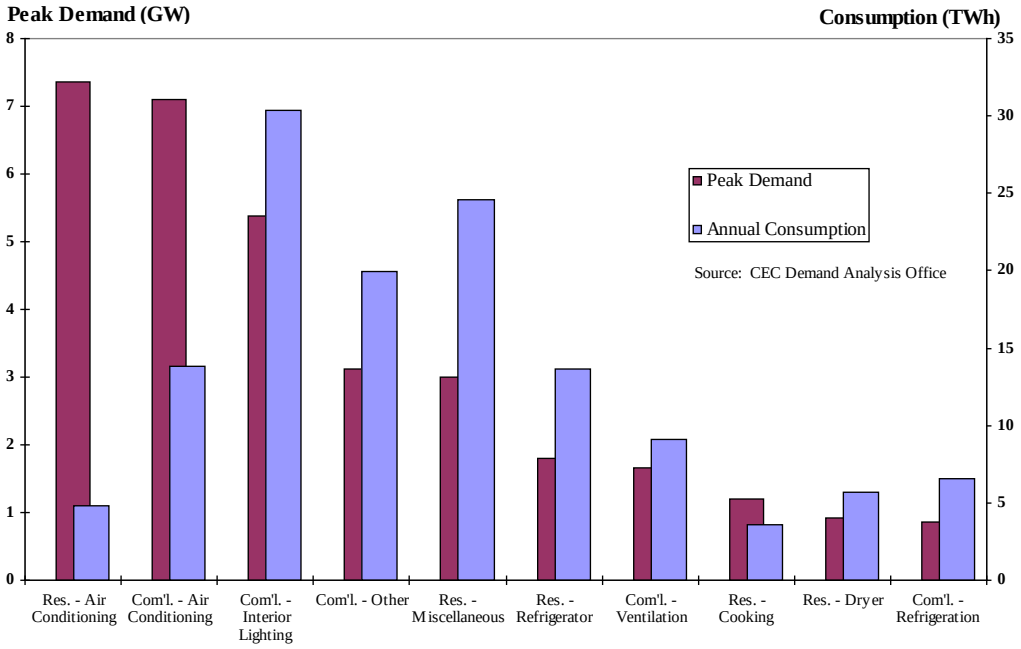


**Figure 27: Summer Peak Demand in California [Source: CEC]**

## Rules of Association

The ultimate objective is to decompose the aggregate system load into load components that can be used by a dynamic load model in stability programs. A commonly used process for decomposing the loads into usable model parameters is the "Rules of Association (RoA)". The RoA serve as a link between composition data available (end-use surveys, billing data, etc.) and needing fractional model parameters based on the model used. The model parameters are derived base on some type of RoA that each entity develops based on the expected allocation of motor and load types to the categorization of loads derived from the data. Figure 28 shows (1) the load classification breakdown for New England, and (2) the load composition model parameters derived from this process. While the data on the left is collected from the raw data, it must be translated to the fractional parameters used in the Composite Load Model. In this case, it is expected that for the peak summer conditions, approximately 25% of the load is single-phase air conditioners[15].

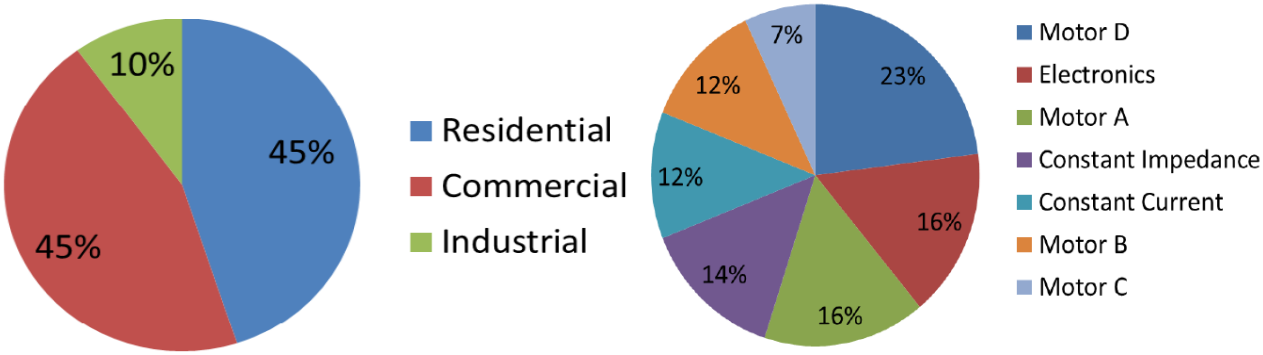


**Figure 28: New England Sector Breakdown and CMLD Parameters [Source: NPCC]**

The link between the left and right figures in Figure 28 is the RoA. These rules are generally based on engineering judgment and knowledge and experience of researching and understanding end-use loads rather than rigorous research. The RoA rules can be illustrated as a matrix of fractional values of how the end-use or load classification data can be broken down to the load model parameters. The rows of the matrix are based on the granularity of the data available (types of loads, classification of loads, etc.) while the columns represent the fractional model parameters.

Figure 29 shows a table from the New England load composition work funded by LBNL. In this example, data is shown for Grocery and Health end-use loads. The Composite Load Model is used in this case; hence the columns match the CMLD model parameters. As an example, let us review a couple entries in the RoA matrix:

- Grocery Ventilation is assigned as 30% power electronic loads and 70% Motor B (ventilation and air-handler fans).
- Grocery Motors are assumed to have more (30%) small-scale compressors such as typical rooftop air-conditioners while Health motors are assumed to be predominantly more fans (Motor B-50%) and pumps (Motor C-50%) used for ventilation and water circulation, respectively.

[15] This can be determined at any granularity level (e.g., region, zone, owner, bus, etc.) and depends on the resolution of the end-use load data collected.

| Building Type | End Use | Electronic | Motor-A | Motor-B | Motor-C | Motor-D | ZIP Ip | ZIP Iq | ZIP Zp (G) | ZIP Zq (B) |
|---|---|---|---|---|---|---|---|---|---|---|
| Grocery | Heating | | 0.70 | | | 0.20 | | | 0.10 | 0.02 |
| | Cooling | | 1.00 | | | 0.00 | | | | |
| | Vent | 0.30 | | 0.70 | | | | | | |
| | Water Heating | | | | | | | | 1.00 | 0.15 |
| | Cooking | 0.20 | | 0.20 | | | | | 0.60 | |
| | Refrigeration | 0.10 | 0.80 | | | 0.10 | | | | |
| | Exterior Lighting | | | | | | 1.00 | -0.36 | | 0.06 |
| | Interior Lighting | | | | | | 1.00 | -0.36 | | 0.06 |
| | Office Equipment | 1.00 | | | | | | | | |
| | Miscellaneous | | | 0.50 | 0.50 | | | | | |
| | Process | | | 0.50 | 0.50 | | | | | |
| | Motors | | 0.30 | 0.40 | 0.30 | | | | | |
| | Air Compression | | 1.00 | | | | | | | |
| Health | Heating | | 0.75 | | | 0.15 | | | 0.10 | 0.02 |
| | Cooling | | 1.00 | | | | | | | |
| | Vent | 0.30 | | 0.70 | | | | | | |
| | Water Heating | | | | | | | | 1.00 | 0.15 |
| | Cooking | 0.20 | | 0.20 | | | | | 0.60 | |
| | Refrigeration | 0.20 | 0.70 | | | 0.10 | | | | |
| | Exterior Lighting | | | | | | 1.00 | -1.20 | | 0.20 |
| | Interior Lighting | | | | | | 1.00 | -1.20 | | 0.20 |
| | Office Equipment | 1.00 | | | | | | | | |
| | Miscellaneous | | | | | | | | 1.00 | |
| | Process | | | 0.50 | 0.50 | | | | | |
| | Motors | | | 0.50 | 0.50 | | | | | |
| | Air Compression | | 1.00 | | | | | | | |

**Figure 29: Rules of Association Matrix Example[16] [Source: LBNL]**

By applying the Rules of Association with the fractional load classification data (if available), the user of the model can derive the model parameters in terms of fractions of load composition. The protection parameters associated with the motor load(s) are based on representative controls and protection for each particular motor.

## Composition Sensitivities

The composition of the end-use load is dependent on many different factors that should be taken into account when deriving the load model composition parameters. Some examples of sensitivities include:

- **Season:** Season can affect a number of other factors including humidity, ambient temperature, time of peak, and percentage of air-conditioning.
- **Time of Day:** Research and end-use load surveys have shown that time of day has a significant impact on load composition and the types of loads online at a given time. For example, penetration of air-conditioner dependency on time as well as residential load pick-up in the morning and evening time drive changes in the load behavior. Figure 30 shows an example from the WECC Load Model Data Tool illustrating the impacts of time of day.

[16] W. Gifford, et al., "End-Use Data Development for Power System Load Model in New England – Methodology and Results," Lawrence Berkeley National Laboratory, April 2014.

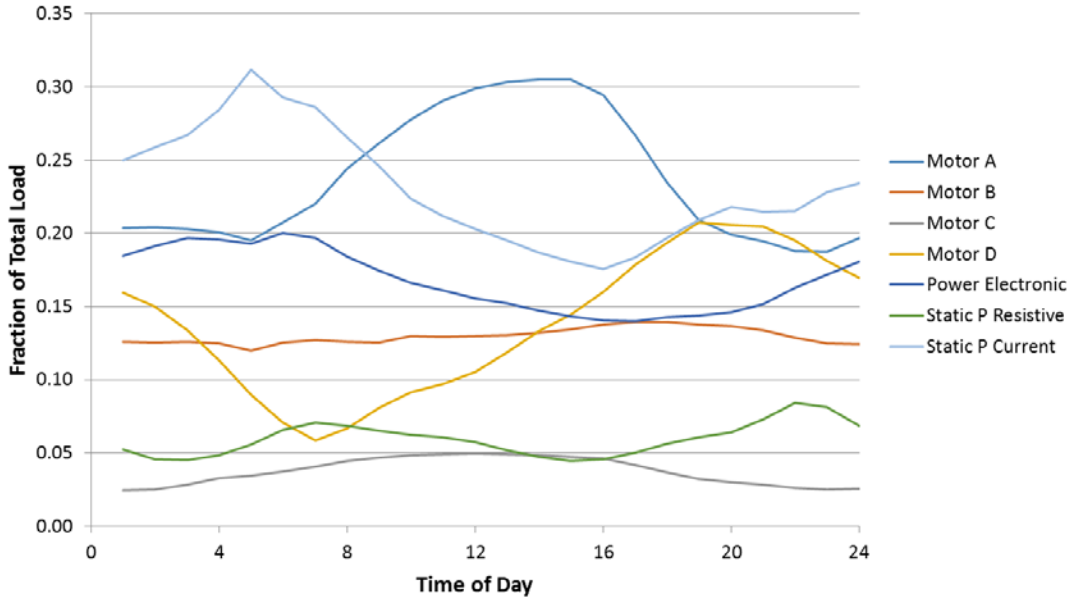


**Figure 30: Time of Day Analysis**

- **Climate Zone:** Climate zones have a major impact on load composition and types of end-use loads. For example, desert or high humidity environments have a higher likelihood for air-conditioning while temperature or coastal climates have a lower likelihood. Also, the stall or performance characteristics may vary by climate zone due to ambient conditions due to other factors.

- **Load Classification:** The classification of load on a given feeder, substation, region, or area has an impact on the end-use load composition in terms of all types of motor, power electronic, lighting, and static loads. Aggregate loads that are predominantly commercial will have much higher penetration of three-phase and/or single-phase compressor load compared to residential load. Industrial loads are often modeled explicitly because of their unique composition in terms of large three-phase compressor fan, and pumping loads.

- **Temperature:** Ambient temperature has a clear effect on load composition, particularly for residential load classes. Figure 31 shows two examples of load profile with respect to temperature, with a suburban (newer construction) residential feeder circuit on the left and a commercial feeder circuit on the right. Both the temperature profiles are the same (top plot) for the three days selected, and the active (middle) and reactive (lower) power consumptions are shown for each day. The plots each show three curves (red, green, blue) that represent three days with different ambient temperatures. They clearly show a strong correlation between peak load and temperature for the residential feeder while the commercial load does not exhibit that same correlation. This increase in peak load for hot conditions for residential load is attributed to the increased usage and power consumption of residential air conditioners. For example, residential load can double between the 75 degree and 103 degree days, while commercial load increases by approximately 30%. This observation, along with many similar situations, validates the statement that 40-60% of total summer peak load for similar residential feeders is air conditioning load.

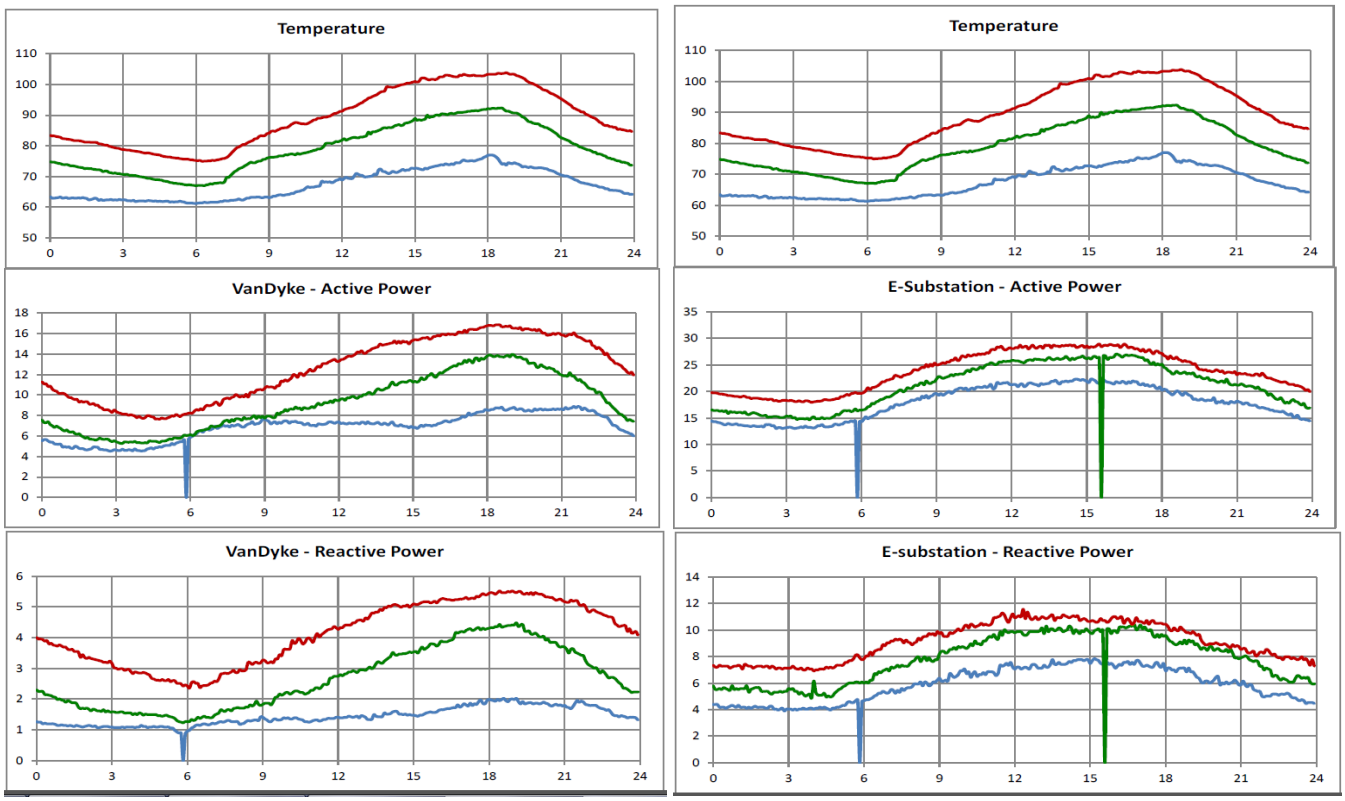


**Figure 31: Load (Residential and Commercial) Responses to Temperature**

# Field Measurements

Capturing actual data from system events in the field is an essential component of benchmarking and validating the models created. This section highlights installation of field equipment used to capture load response.

## Distribution System Monitoring

Phasor measurement units (PMUs) and other high resolution disturbance monitoring equipment have captured transient behavior at the transmission-level; however, limited information has generally been available to study the load response. One reason for this is the lack of high-resolution, longer-term recordings at the distribution system. Protective relays and fault recorders capture high-resolution data pre-, during-, and post-fault but these recordings are generally not configured to capturing longer-term dynamics simply due to practical reasons such as data storage. Furthermore, relatively no measurements are collected "down the feeder" out on the distribution system for residential or mixed-commercial feeders. While power quality metering may be installed for key industrial customers, this type of monitoring is generally not captured at these other types of feeders again due to practical reasons of not needing that type of data unless a specific issue is raised.

However, with the growing understanding of Fault-Induced Delayed Voltage Recovery (FIDVR)[17], recording devices have been installed at the distribution level at end-use load customers to capture these dynamics. Southern California Edison (SCE) has installed power quality monitors[18] on residential transformers, as shown in Figure 32. These devices are installed in pad-mounted residential transformers on the secondary 240 V side, recording residential loads' aggregate behavior. For example, multiple households are served off this transformer, and the PQube device captures the aggregate response of these residences by measuring line-to-ground voltage and line current serving this aggregate load.

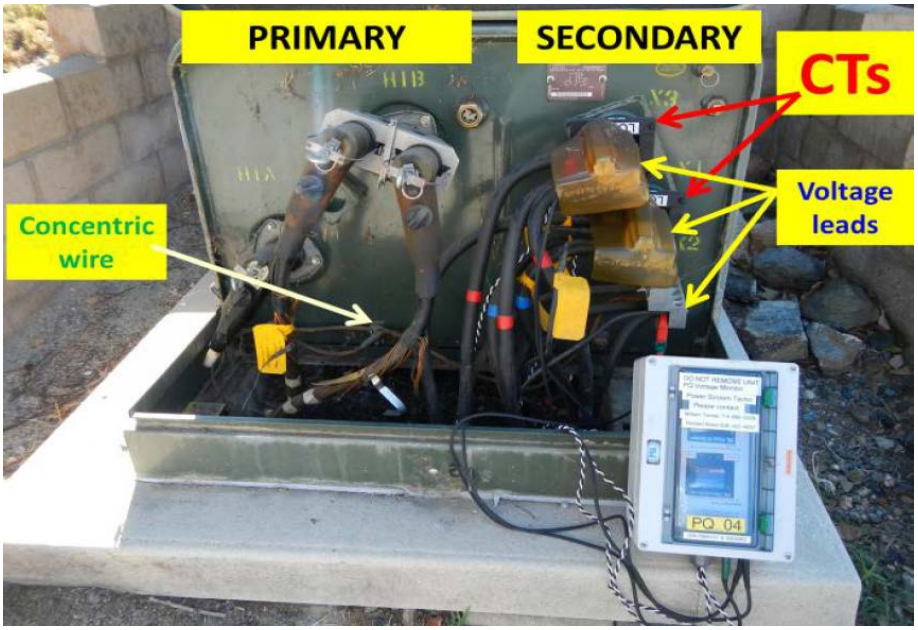


**Figure 32: PQube Meter Installation at Residential Transformer**

One specific application of these devices was to capture the end-use load response within the SCE Valley system distribution circuits, which serves approximately 1,500 MW of peak load mainly consisting of residential and small

[17] R. Bravo, R. Yinger, S. Robles, J. Eto, "FIDVR in Distribution Circuits," 2013 IEEE Power and Energy Society Meeting, Vancouver, BC, pp. 1-5, 2013.

[18] Power Sensor Ltd, PQube®, Online. Available: http://www.powersensorsltd.com/PQube

commercial load. Figure 33 shows a diagram of the 500/115kV network and the load serving 12kV and 33kV buses. It also shows the diversity of the power quality meter installations on different phases and at different locations on the distribution feeders.

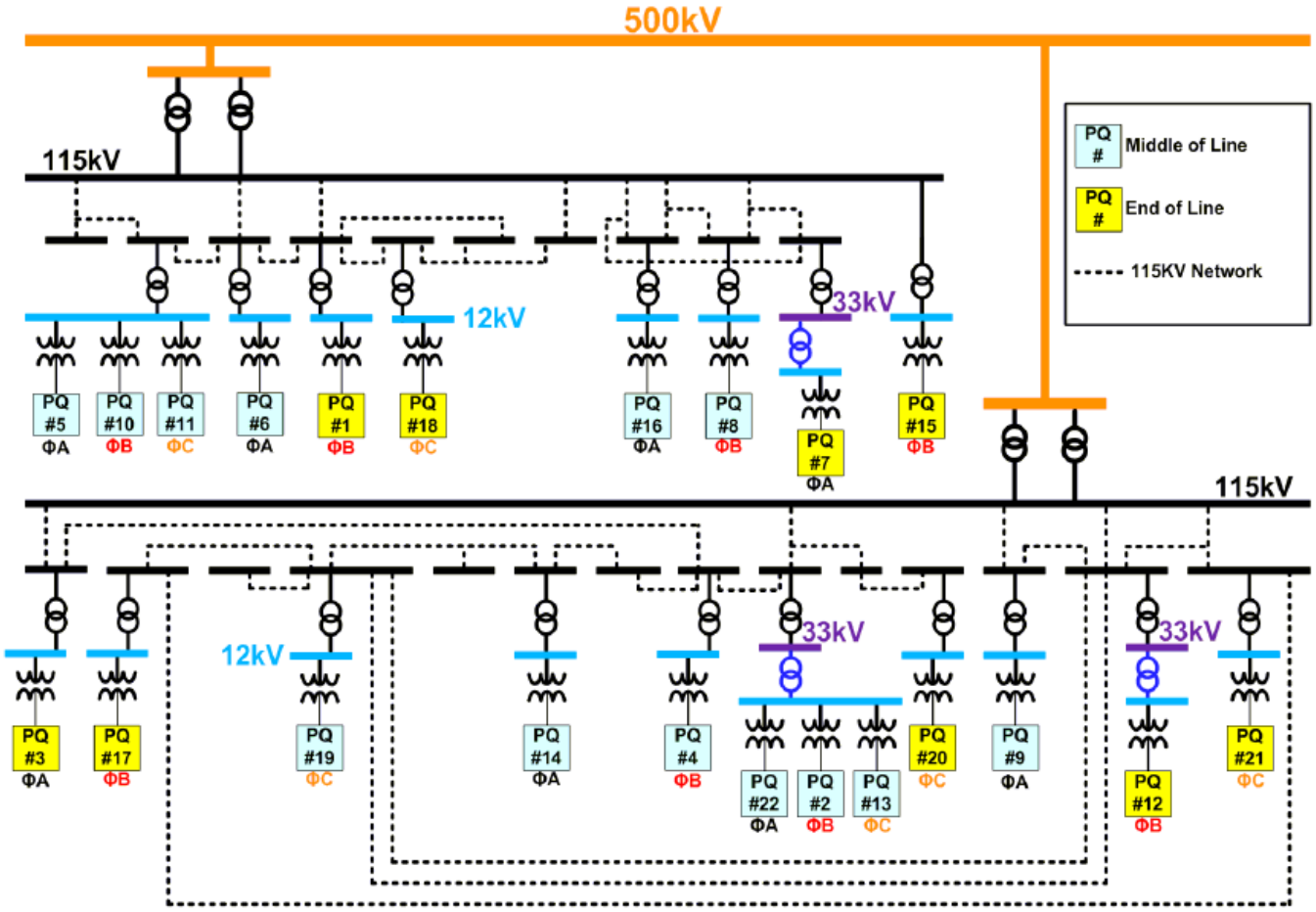


**Figure 33: SCE Valley Distribution Network PQ Monitoring**

The power quality meters were configured to capture events with the following trigger settings:

- Undervoltage trigger at 80% nominal voltage
- Overvoltage trigger at 110% nominal voltage
- Capture RMS readings
- Capture sinusoidal waveform readings

Many events have been captured since this monitoring system was installed. Figure 34 illustrates the value of capturing the end-use load response in addition to the transmission level response. As the figure shows, the 500kV PMU readings showed a quick recovery of system voltage at that level (following return of the PMU recording); similarly the 115kV voltage also recovered very quickly, with some FIDVR-like response in the voltage and a slight overshoot. However, the PQ monitors installed at the distribution system captured a drastically different voltage recovery for this same event, exhibiting severe FIDVR characteristic with overshoots near 115% and delayed voltage recovery up to 15+ seconds. In addition, the active and reactive power ("P & Q") are also shown on the same plot, illustrating the effects of motor stalling and tripping. This increased visibility into the effects of load response help better understand and model this behavior in simulation.

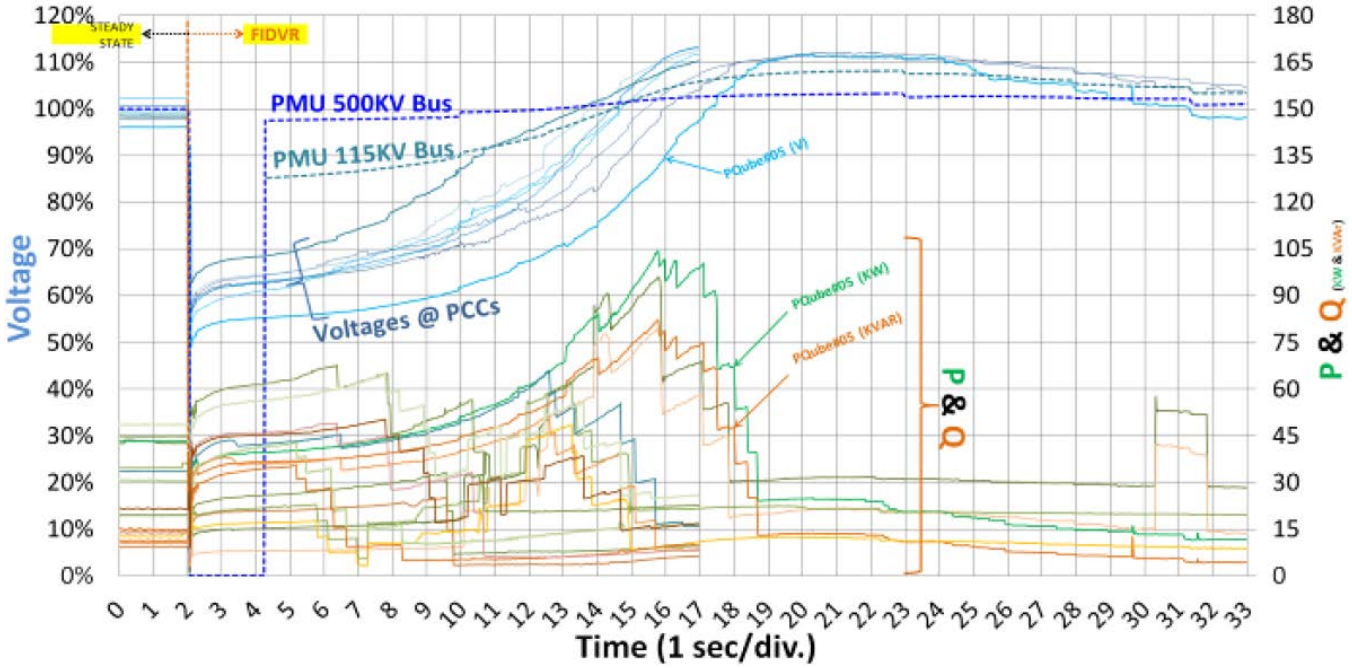


**Figure 34: Sample Event Captured at all Voltage Levels**

# Composite Load Modeling Guidance

This section is meant to provide guidance and information around the composite load model. The composite load model is considered the state-of-the-art in dynamic load modeling, enabling representation of three phase and single-phase induction motors, power electronic load, static load, distributed generation, and the distribution equivalent network. It also allows for modeling of the protection systems around each component useful for representing end-use load dropping due to system conditions.

The composite load model is implemented in most commonly used software platforms such as GE PSLF, PTI PSS®E, PowerWorld, and PowerTech DSATools. Implementation of the model may be slightly different, but the principles and parameters are generally the same.

Figure 35 shows the overall structure of the composite load model; the major components of the model include:

5. Definition of load composition
6. Substation transformer (LTC) and distribution feeder equivalent impedance
7. Substation and distributed feeder shunt compensation
8. 3-phase motor loads (3) with built-in protection
9. 1-phase motor loads (1) with built-in protection
10. Power electronic loads
11. Static representation of loads
12. Load shedding – UFLS, UVLS
13. Distributed generation resources

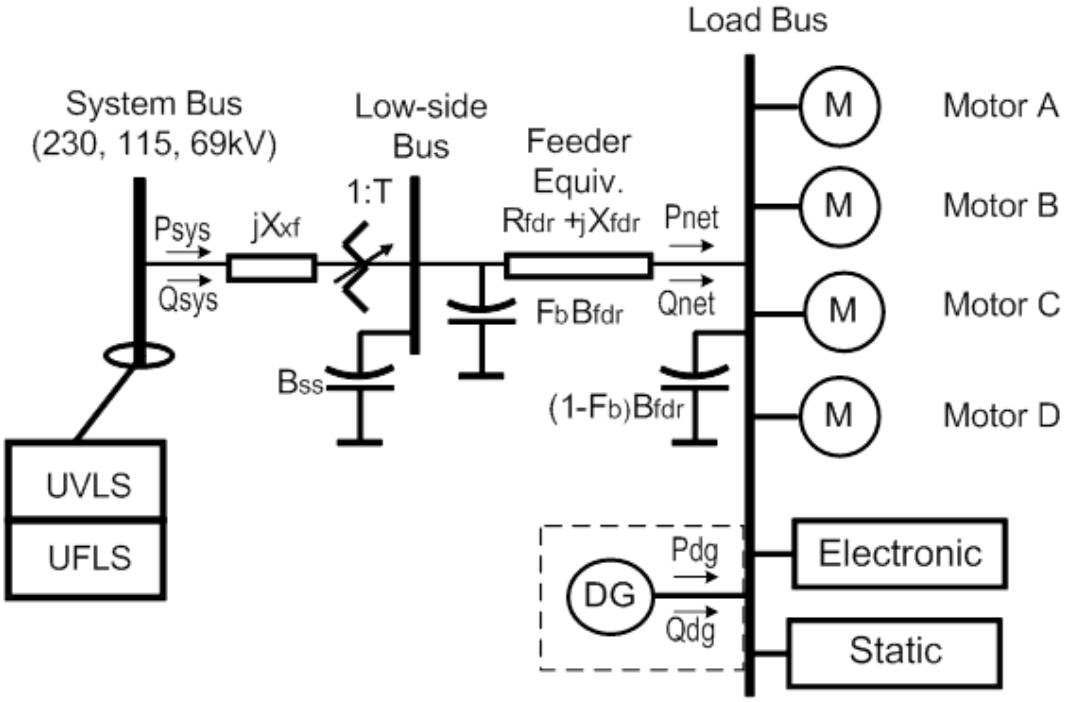


**Figure 35: Composite Load Model Structure (CMPLDW/CMLD)**

Figure 36 shows "default" parameters for the distribution equivalent, transformer, and shunt compensation elements of the model. A safe assumption is an 8% transformer impedance (on transformer MVA base) with loading factor of 110-140% of rated. Under-load tap changing[19] (ULTC) will depend on utility practices; however, assuming ULTC action, a tap range of ± 10% with a control delay of 30 seconds and tap change delay of 5 seconds is reasonable[20]. Distribution impedance voltage drop is generally between 4-6% from the substation to the end of the feeder (load bus), with a reactance-to-resistance (X/R) ratio of 1.5 approximately 1.0-1.5[21]. Some implementations of the composite load model assume no shunt compensation (B1 = B2 = 0) and account for this by assigning the static load component with a capacitive (negative) power factor[22]. Regardless of these settings, the load bus voltage magnitude is assumed to be greater than or equal to 0.95 pu; in the event that voltage is less than 0.95 pu, the equivalent distribution network impedance is reduced to attain this voltage[23].

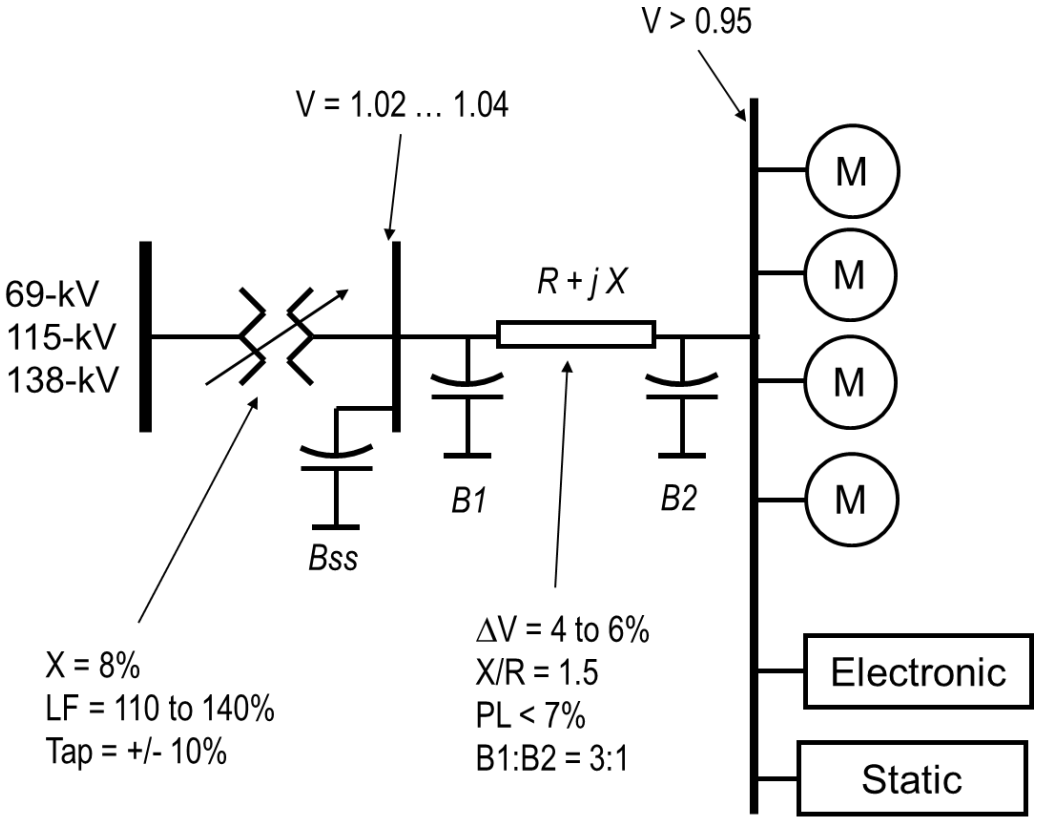


**Figure 36: Distribution Equivalent Data**

## Composite Load Model Elements

This section describes the various elements of the composite load model to provide background information for those using the model. More detailed information related to each parameter is provided in Appendix A.

[19] The transformer is modeled with a fixed tap on both the high and low side with a variable tap on the low side of the transformer. LTC action is controlled by a flag in the parameters. $V_{max}$ and $V_{min}$ define the control band in which the LTC will try to operate in voltage falls outside that band for $T_{control}$ amount of time.

[20] Again, utility practices vary and therefore "default" settings may vary as well.

[21] This is dependent on the distribution system electrical characteristics; however, these values are provided as a "default" feeder impedance.

[22] The parameter Fb used for allocating shunt compensation is no longer necessary and causes numerical issues in the software implentations. Newer versions of the composite load model now represent the feeder shunt compensation at the load bus only.

[23] Far-end (load bus) voltage too low can result in simulation initialization issues or errors.

## Three-Phase Induction Motor Models

Motor A represents three-phase induction motors with low inertia (H = 0.1 sec) driving constant torque loads. This represents motors commonly found in commercial/industrial air conditioning compressors and refrigeration systems. The model represents two forms of compressor motors, both special design motors (not NEMA B):

- Smaller 5-15 HP compressor motors – typical of rooftop air conditioning units commonly found at grocery stores, consumer products stores, and malls
- Larger 200-500 HP compressor motors – typical of large commercial buildings' central cooling systems

The composite load model distinguishes between large and small 3-phase compressor motors in order to represent their different protection characteristics. Based on laboratory testing and insights from building design and motor protection experts, it is projected that the majority of large 3-phase compressor motors will trip at around 65% voltage in 100 ms by EMS action or other sensitive undervoltage protection, and will remain disconnected once tripped and require manual restart. To represent this in the composite load model, 20% of motor A will trip at 65% voltage in 100 ms and not reconnect. This protection characteristic is generally represented by parameters "Ftr1A", "Vtr1A", "Ttr1A", "Vrc1A" and "Trc1A" in the composite load model, shown in Table 4 below. Similarly, the majority of small 10-25 HP compressors disconnect due to basic contactor dropout at around 50% voltage in about 20 ms. The contactors then reconnect once the voltage recovers to about 65% in about 100 ms as the contactors reclose. To represent this in the composite load model, 75% of motor A will trip at 50% voltage in 20 ms and reconnect in 100 ms once the voltage recovers to 65%. This protection characteristic is represented by parameters "Ftr2A", "Vtr2A", "Ttr2A", "Vrc2A", and "Trc2A" in Table 4 below. The remaining 5% of Motor A not modeled with protection is expected to ride through disturbances without tripping[24].

Motor B represents three-phase induction motors with high inertia (H = 0.25-1.0 sec) driving loads whose torque is proportional to speed squared. This represents motors commonly found in commercial ventilation fans and air-handling systems. The model is representative of 5-25 HP fan motors, which are usually NEMA B design motors. Similar to Motor A, the undervoltage tripping and restart capabilities are driven by the idea that a building EMS system would automatically attempt restart upon voltage recovery since there is no apparent reason to keep the equipment out of service. For motor B, the trip settings represent staggered tripping due to contactor dropout such that load tripping experiencing common instantaneous voltage will not necessarily have identical trip settings. Stagger tripping is accomplished by tripping 30% of motor B once voltage drops to 55% for 20 ms (represented by "Ftr1B", "Vtr1B", "Ttr1B" in Table 4) and tripping an additional 30% of motor B once the voltage drops to 50% for 20 ms (represented by "Ftr2B", "Vtr2B", "Ttr2B"). Staggered reconnection also occurs as the contactors reclose. 30% Motor B will reconnect when the voltage recovers to 60% for 50 ms and another 30% will reconnect when voltage recovers to 65% for 50 ms. This is represented by "Vrc1B", "Trc1B", "Vrc2B", and "Trc2B" in Table 4. The staggered tripping also more accurately represents aggregate load performance based on engineering judgment of large aggregates of load. It is possible that future installations of this type of load would be replaced by Electronically Commutated Motors (ECM); however, this is still a relatively low penetration at this time.

Motor C represents three-phase induction motors with low inertia (H = 0.1-0.2 sec) driving loads whose torque is proportional to speed squared. This represents motors commonly found in commercial water circulation pumps in central cooling systems. As with motor B, staggered tripping is accomplished by using two sets of protection parameters. The model is representative of 5-25 HP pump motors, which are usually NEMA B design motors. For this type of load, it is possible that future trends may lead to this load being replaced with Variable Frequency Drives (VFD); however, this is still a relatively low penetration at this time.

[24] This is predominantly due to numerical purposes in the models – fraction of motor tripping cannot equal 100% for Motor A 3-phase compressor motors due to motor starting issues if all the motor is tripped in the model.

The motor models have the following parameters:

**Table 4: Industrial Motor Load Parameters**

| Parameter | Description | Motor A Value | Motor B Value | Motor C Value |
|---|---|---|---|---|
| Lfm | Loading Factor [pu] | 0.75 | 0.75 | 0.75 |
| Rs | Stator Resistance [pu] | 0.04 | 0.03 | 0.03 |
| Ls | Stator Reactance [pu] | 1.8 | 1.8 | 1.8 |
| L' | Transient Reactance [pu] | 0.12 | 0.19 | 0.19 |
| L'' | Sub-transient Reactance [pu] | 0.104 | 0.14 | 0.14 |
| $T_0$' | Transient OC Time Const [sec] | 0.095 | 0.2 | 0.2 |
| $T_0$'' | Sub-transient OC Time Const [sec] | 0.0021 | 0.0026 | 0.0026 |
| H | Inertia Constant [sec] | 0.1 | 0.5 | 0.1 |
| Etrq | Torque Speed Exponent* | 0 | 2 | 2 |
| Vtr1 | Undervoltage Relay Trip 1 $V_{mag}$ [pu] | 0.65 | 0.55 | 0.58 |
| Ttr1 | Undervoltage Relay Trip 1 Time [sec] | 0.1 | 0.02 | 0.03 |
| Ftr1 | Fraction of Motors w/ UV Trip 1 [pu] | 0.2 | 0.3 | 0.2 |
| Vrc1 | UV Reclose 1 $V_{mag}$ [pu] | 0.1 | 0.65 | 0.68 |
| Trc1 | UV Reclose 1 Time [sec] | 9999 | 0.05 | 0.05 |
| Vtr2 | Undervoltage Relay Trip 2 $V_{mag}$ [pu] | 0.5 | 0.5 | 0.53 |
| Ttr2 | Undervoltage Relay Trip 2 Time [sec] | 0.02 | 0.025 | 0.03 |
| Ftr2 | Fraction of Motors w/ UV Trip 2 [pu] | 0.75 | 0.3 | 0.3 |
| Vrc2 | UV Reclose 2 $V_{mag}$ [pu] | 0.65 | 0.6 | 0.62 |
| Trc2 | UV Reclose 2 Time [sec] | 0.1 | 0.05 | 0.05 |

*Load Torque: $TL = T0 * \omega^{Etrq}$

The three-phase models represented in the composite load model use existing three-phase motor models (e.g., *motorw* or *CIM6BL*). Either a "one-cage" or "two-cage" model can be represented. Default parameters used in the composite load model use a "two-cage" representation, which provides a higher starting torque at low current. This provides greater robustness in the model performance for severe fault conditions. These motor models are intended to represent aggregations of many motors dispersed through the distribution system where no detailed information on the actual characteristics of the individual motors is known. For this reason, the 3-phase motor

model parameters used in the composite load model are generally not modified for sensitivity analysis. Figure 37 shows the steady state equivalent impedance circuit of the three-phase motor models. This circuit is used to initialize the motor model in software programs. Based on the terminal voltage and active power load level, the slip of the motor and the reactive power consumption can be determined. For dynamic simulations, a set of algebraic and differential equations are used to represent the motor. These algebraic and differential equations are derived from both the steady state circuit representation and from the well-established knowledge of the operation physics of the motor.

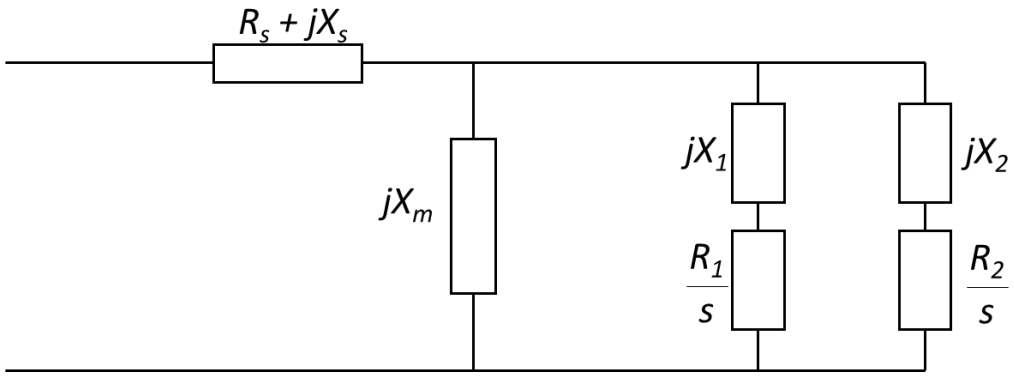


**Figure 37: Three-Phase Induction Motor Model**

## Single-Phase Air Conditioner Model – Motor D

The single-phase air conditioner model in the composite load model is a "performance model" derived from laboratory testing of the behavior of these loads. Figure 38 shows the performance characteristics for active and reactive power. The model uses algebraic equations to represent the motor power consumption in terms of terminal voltage. The model has two distinct operating conditions in which the motor can perform. These include "RUN" and "STALL" states defined by *Vstall* and *Tstall* parameters in the model. When the terminal voltage of the motor model experience a voltage magnitude below *Vstall* threshold for *Tstall* duration, the motor switches from the RUN state to the STALL state and the algebraic representation of the motor "switches over". In the STALL state, the motor consumes large amounts of current due to locked rotor conditions, particularly once the terminal voltage has recovered. For the conditions where voltage is less than *Vstall* but *Tstall* duration has not been exceeded, the model should follow the RUN state and continue onto the lower voltage STALL state to accommodate a smooth transition between states.

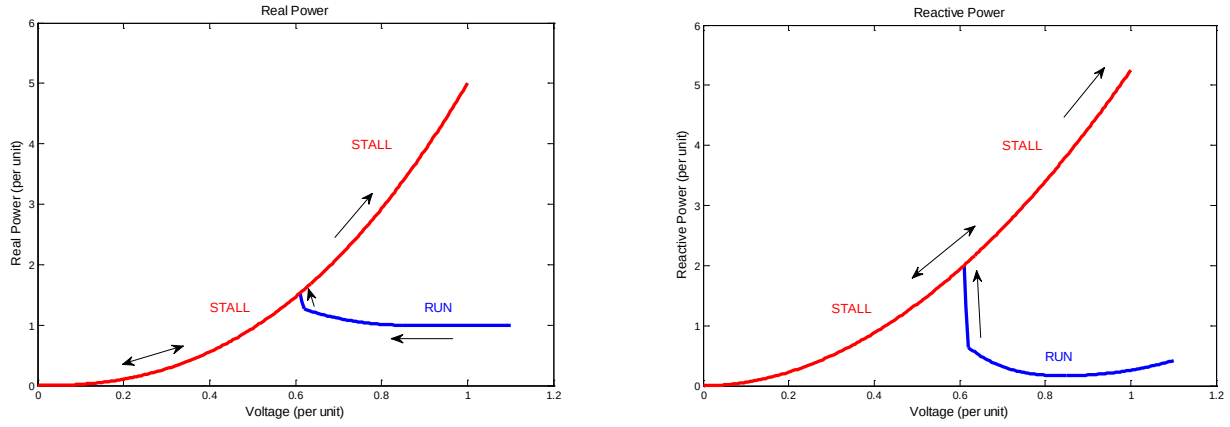


**Figure 38: Single-Phase Air Conditioner Performance Model Characteristic**

Once in the STALL state, the motor remains stalled until the thermal relay protection function trips the motor offline. The thermal relay model implemented for the single-phase air conditioners represents the aggregate behavior of these loads using a linear tripping mechanism. $T_{th}$ represents the Motor D motor heating time

constant, which is the time constant associated with the thermal overload protection of the motors that physically trips the unit offline. $K_{th}$ represents a fraction of the connected motors in the model and $\theta_{TRIP1}$ and $\theta_{TRIP2}$ are the per unit temperature levels where tripping is initiated and completed along a linear scale.

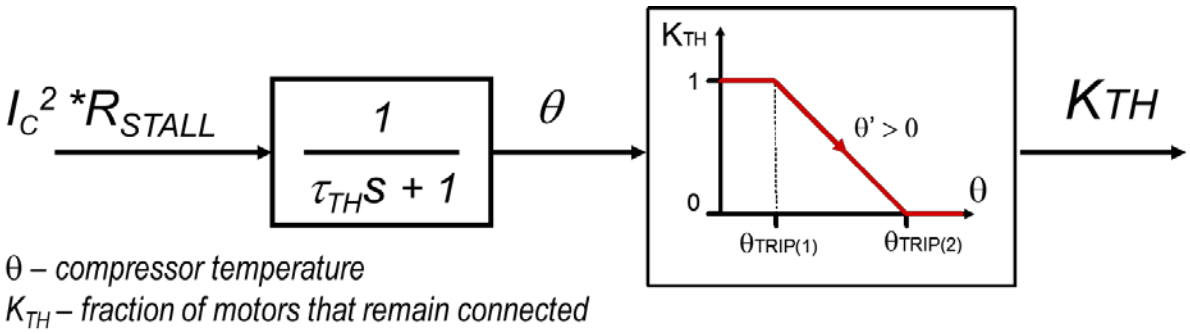


**Figure 39: Thermal Relay Model**

Figure 40 shows an example of a voltage dip to 55% for a 3-cycle fault. Stalling occurs and high current is drawn from the load. This current remains for approximately 2.5 seconds until the per unit temperature in the model surpasses the trip levels based on the motor heating time constant setting.

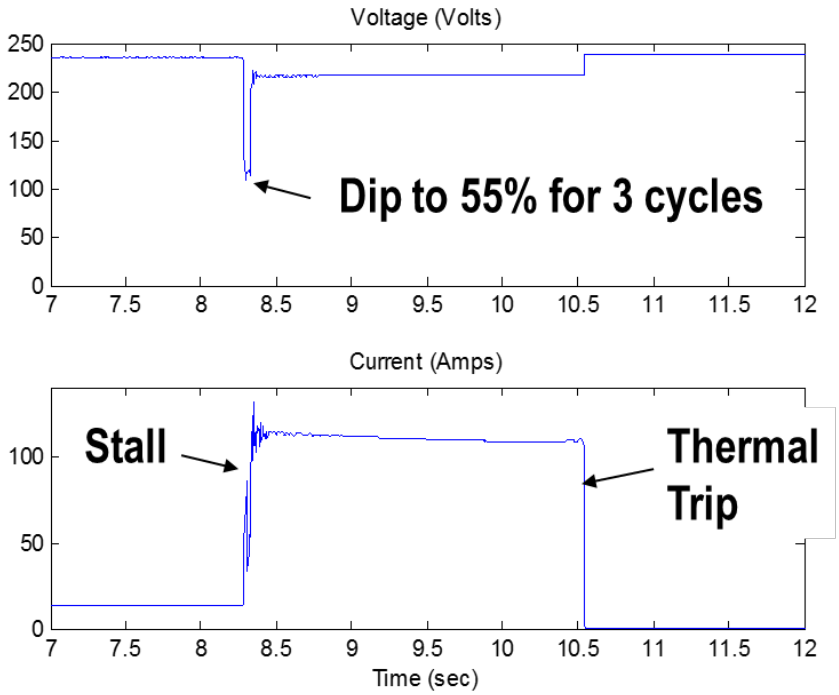


**Figure 40: Testing of Thermal Relay Tripping – Voltage & Current**

Figure 41 shows the reaction in terms of motor current (top) and compressor pressure (bottom). While running, the pressure is approximately 190 psi. Upon locked rotor stalled conditions, the pressure immediately begins to fall. At t = 18 seconds, the thermal relay trips the motor from the circuit and compressor pressure continues to decline. At t = 60 seconds, the thermal relay allows the compressor motor to reclose and the motor attempts to restart. However, there is insufficient starting torque and the motor cannot restart. The thermal relay will again trip the motor and pressure continues to fall. At some point, there will be sufficient starting torque to overcome the compressor pressure and the motor will be able to successfully restart assuming strong system voltage.

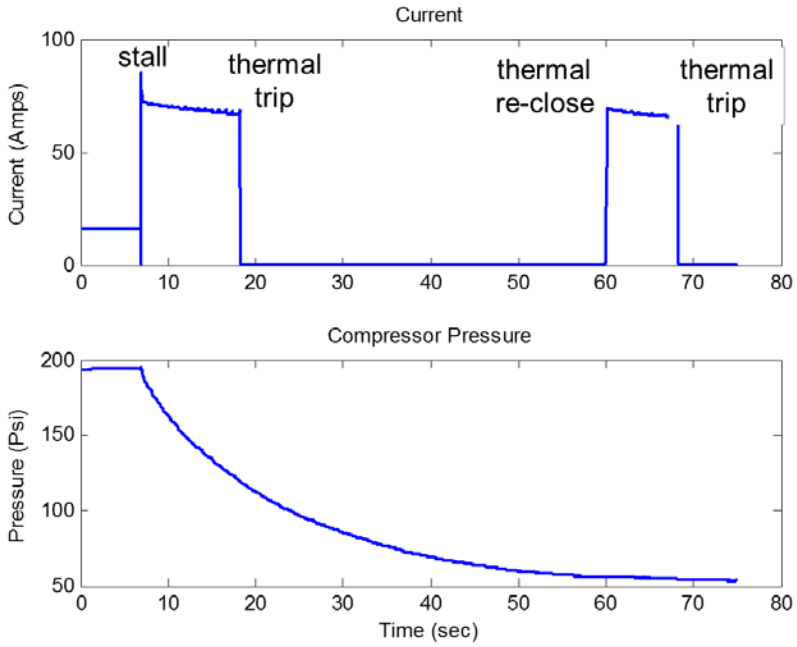


**Figure 41: Thermal Relay and Compressor Pressure Testing**

Different manufacturers of thermal cutout relays may have different characteristics in terms of tripping time with respect to motor current. Figure 42 shows testing of various air-conditioners and the thermal trip times with respect to current. A curve is fitted to the results to get an average or expected performance of a generic thermal relay.

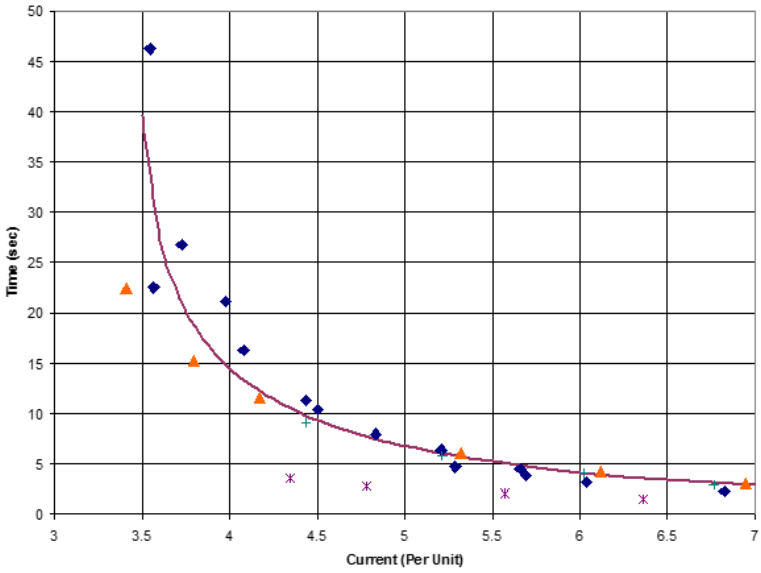


**Figure 42: Thermal Relay Characteristic Testing Results**

## Power Electronic Load Representation

The power electronic (inverter-based or electronically coupled) load component of the model represents an aggregate effect of power electronic loads. The model assumes constant active and reactive power until voltage $V_{d1}$. The active and reactive power are reduced linearly to 0 consumption between voltages $V_{d1}$ and $V_{d2}$. Below voltage $V_{d2}$, load is 0.0. This load type is generally assumed to have unity (1.0) power factor, with voltage breakpoints Vd1 ~ 0.7 pu and Vd2 ~ 0.5 pu to capture load diversity of the end-use equipment.

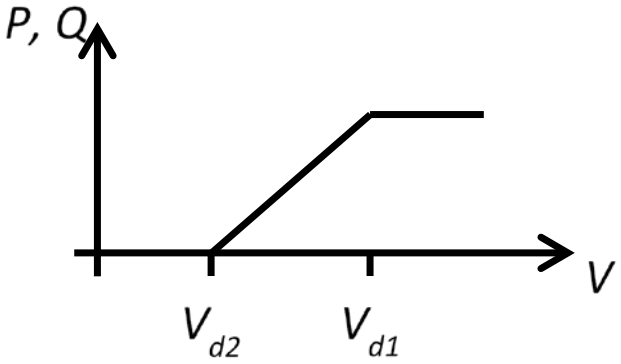


**Figure 43: Power Electronic Load Tripping Characteristic**

### Static Load Representation

The static load is represented using the polynomial representation shown below, which captures the active and reactive power sensitivity to voltage and frequency.

$$P = P_0 * \left(P_{1c} * \left(\frac{V}{V_0}\right)^{P_{1e}} + P_{2c} * \left(\frac{V}{V_0}\right)^{P_{2e}}\right) * \left(1 + P_{frq} * D_f\right)$$
$$Q = Q_0 * \left(Q_{1c} * \left(\frac{V}{V_0}\right)^{Q_{1e}} + Q_{2c} * \left(\frac{V}{V_0}\right)^{Q_{2e}}\right) * \left(1 + Q_{frq} * D_f\right)$$

The power factor of the static load component is explicitly specified in the dynamic record, and the reactive power component is calculated using $Q_0 = P_0 * \tan(\cos^{-1}(PF_s))$. The initial condition active power consumption is calculated by $P_0 = P_{load} * (1 - F_{mA} - F_{mB} - F_{mC} - F_{mD} - F_{el})$. The difference between 1.0 and the coefficients ($\{P_{1c}, P_{2c}\}$, $\{Q_{1c}, Q_{2c}\}$) is modeled as constant power load (exponent of 0). Commonly used static load parameters using the following assumptions, where $P_{1c}$ and $P_{2c}$ are approximately a 50/50 split.

$$P = P_0 * \left(P_{1c} * \left(\frac{V}{V_0}\right)^{2} + P_{2c} * \left(\frac{V}{V_0}\right)^{1}\right) * (1 + 0)$$
$$Q = Q_0 * \left(-0.5 * \left(\frac{V}{V_0}\right)^{2} + 1.5 * \left(\frac{V}{V_0}\right)^{1}\right) * \left(1 - D_f\right)$$

The static load representation should represent the other types of loads that are not explicitly modeled by the other load components such as motor load, power electronic load, etc. These types of loads include lighting, small electrical household and commercial loads, and other types of offhand loads. The static load characteristic selected should be based on some aggregate testing or laboratory testing of these loads to identify reasonable parameters.

## Initialization of Composite Load Model

The initialization process for the composite load model is as follows[25]:

1. Total load active (P) and reactive (Q) power quantities and bus voltage (V) are acquired from load flow.
2. The low-side substation bus and load bus are added to the admittance (Y) matrix[26].

[25] http://www.pnl.gov/main/publications/external/technical_reports/PNNL-16916.pdf
[26] This is done is some software platforms while in others only the system bus is included in the Y matrix.

3. The transformer, feeder branch, and substation capacitors are also added to the Y matrix[27].
4. Low-side bus voltages are computed based on specified electrical impedances.
5. LTC taps are adjusted to put the low-side bus voltage near midpoint of control range.
6. Required load bus shunt compensation is estimated using static load reactive ($Q_{static}$) and estimated motor reactive ($Q_{motor}$) power.
7. The substation end shunt compensation is set based on allocation.
8. Far-end (load bus) voltages are computed.
9. If load bus voltage is $0.94 < V < 1.05$, feeder reactance is adjusted to maintain acceptable voltage; feeder resistance is also adjusted to maintain the same X/R ratio.
10. The required far-end active (P) and reactive (Q) power are computed to match high side real (P) and reactive (Q) power, accounting for losses in the transformer, feeder, and shunts.
11. Motor models and static load models are initialized.
12. Load end feeder compensation is set to match required reactive (Q) power flow at far-end.

[27] This is done is some software platforms while in others only the system bus is included in the Y matrix.

# Data Management

Load modeling is a complex subject, further exacerbated by the complexity of data management for system studies. The total system demand and composition of the end-use loads is changing continuous – year to year, season to season, day to day, minute to minute. Each end-use customer has a different composition that must be aggregated up to a level used for system analysis. Therefore, modelers must find ways to simplify the data management process. This section highlights the work done by the Western Electricity Coordinating Council (WECC) on developing processes for building composite load models for a given base case, and describes some of the tools used in the model creation process.

## WECC Climate Zones

WECC has decided to classify its loads based on a set of criteria that consist of geography and feeder or load type. The network is broken down into a set of climate zones that capture the geographic diversity of the loads, which is used to adjust the percentages of motor loads, for example. Figure 44 shows the relative geographic boundaries of the 10 climate zones defined within WECC. Table 5 provides a representative city for which each climate zone is trying to mirror. For example, the NWC (Northwest Coast) captures a wet, temperate climate like Seattle, WA while DSW (Desert Southwest) captures a dry, arid, desert-like climate similar to Phoenix, AZ. These locations have significantly different characteristics in terms of load composition (air conditioners, for example) and seasons.

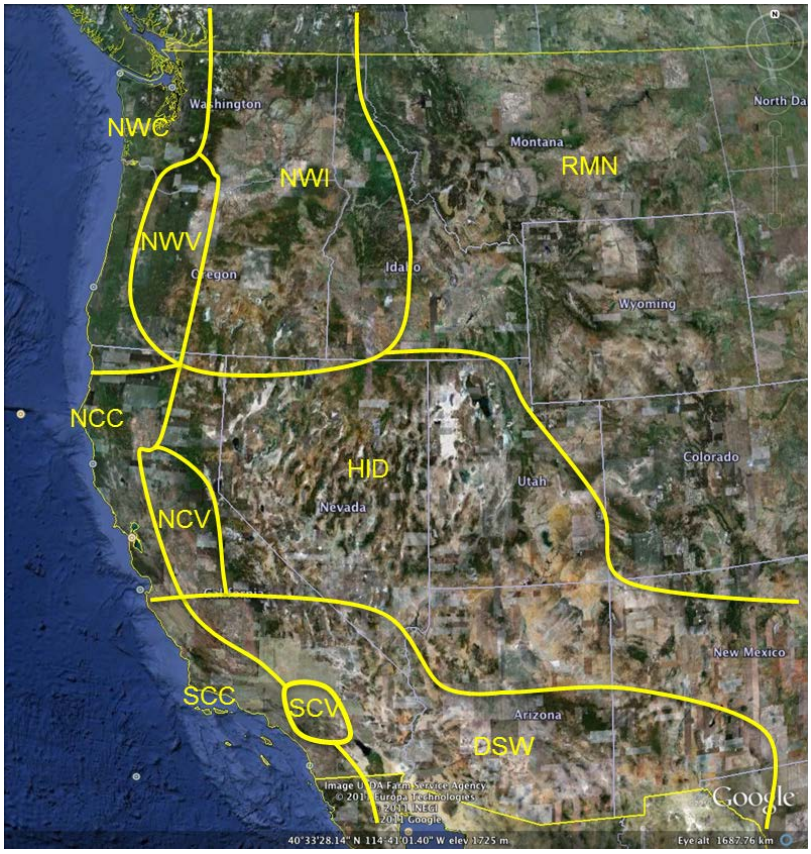


**Figure 44: Map of WECC Climate Zones**

| Table 5: WECC Climate Zone Representation | | |
|---|---|---|
| **ID** | **Climate Zone** | **Representative City** |
| NWC | Northwest Coast | Seattle, WA; Vancouver, BC |
| NWV | Northwest Valley | Portland, OR |
| NWI | Northwest Inland | Boise, ID; Tri-Cities, WA; Spokane, WA |
| RMN | Rocky Mountain North | Calgary, Canada; MT; WY |
| NCC | Northern California Coast | San Francisco, CA |
| NCV | Northern California Valley | Sacramento, CA |
| NCI | Northern California Inland | Fresno, CA |
| SCC | Southern California Coast | Los Angeles, CA; San Diego, CA |
| SCV | Southern California Valley | Los Angeles, CA; San Diego, CA |
| SCI | Southern California Inland | Los Angeles, CA; San Diego, CA |
| DSW | Desert Southwest | Phoenix, AZ; Riverside, CA |
| HID | High Inland Desert | Salt Lake City, UT; Denver, CO |

Feeder type also has a significant impact on the composition of the load, and must be accounted for at some level to differentiate the load types. Feeders can generally be categorized based on the customers being served. This may change based on areas. For example, one area may find a need to identify server farms as a unique load classifier while others may need to differentiate agricultural load. Regardless, WECC adopted three distinct classes of load: Residential (RES), Commercial (COM), and Rural Agricultural (RAG). A fourth classification is Mixed (MIX), which is a default of the various types of loads as shown in Table 6.

| Table 6: WECC Climate Zone Representation | | | | | |
|---|---|---|---|---|---|
| **ID** | **Feeder Type** | **Residential Load** | **Commercial Load** | **Industrial Load** | **Agricultural Load** |
| RES | Residential | 80% | 20% | 0% | 0% |
| COM | Commercial | 20% | 80% | 0% | 0% |
| MIX | Mixed | 40% | 40% | 20% | 0% |
| RAG | Rural Agricultural | 40% | 40% | 10% | 10% |

WECC uses the Long ID (LID) load identifier to classify the load type. The LID consists of: <3-character climate zone>_<3-character load class>_<(optional) 7-character industrial load ID>. For example, commercial load in the Desert Southwest would have a LID = “DSW_COM”.

Industrial loads are also separated from the aforementioned load types due to their specific application to key (relatively large) loads in the power flow model. Table 7 shows examples of different industrial load types and their composition of induction motor and power electronic load. Any remaining percentage is accounted for as static load.

**Table 7: Industrial Loads**

| ID | Load Type | % MA | % MB | %MC | %MD | %PEL |
|---|---|---|---|---|---|---|
| IND_PCH | Petro-Chemical Plant | 15 | 25 | 40 | 0 | 15 |
| IND_ASM | Aluminum Smelter | 10 | 0 | 0 | 0 | 0 |
| IND_SML | Steel Mill | 20 | 25 | 30 | 0 | 20 |
| IND_SCD | Semiconductor Plant | 10 | 35 | 10 | 0 | 40 |
| IND_SRF | Server Farm | 25 | 10 | 5 | 0 | 60 |
| IND_OTH | Industrial – Other | 20 | 25 | 30 | 0 | 20 |
| PPA | Power Plant Aux Load | 5 | 50 | 25 | 0 | 15 |

## Load Model Data Tool

The Load Model Data Tool (LMDT) has been developed by PNNL in cooperation with Bonneville Power Administration (BPA) and WECC modeling and validation working group (MVWG). The LMDT is a standalone Windows application and it helps to generate composite load model parameters taking into account climate zone and seasonal information, operating hour and feeder type. The LMDT reads in the necessary long identifier (LID) information, and supplements that with the base case power flow conditions and supplemental load shape data to generate the dynamics records in GE PSLF and Siemens PTI PSS®E format. The LMDT application has been released under an open-source license and can be downloaded at: https://svn.pnl.gov/LoadTool

The first version of the tool (LMDT 1.0) was released in 2013. The first version of the tool is a relatively simple application (Figure 45), it does not have built-in load model database and it requires to generate composite load data using external tools (e.g. WECC composite load spreadsheet). The LMDT 1.0 is still maintained and available for downloading on the LMDT web site. Recently, the PSLF19 format and long ID support has been added to the LMDT 1.0.

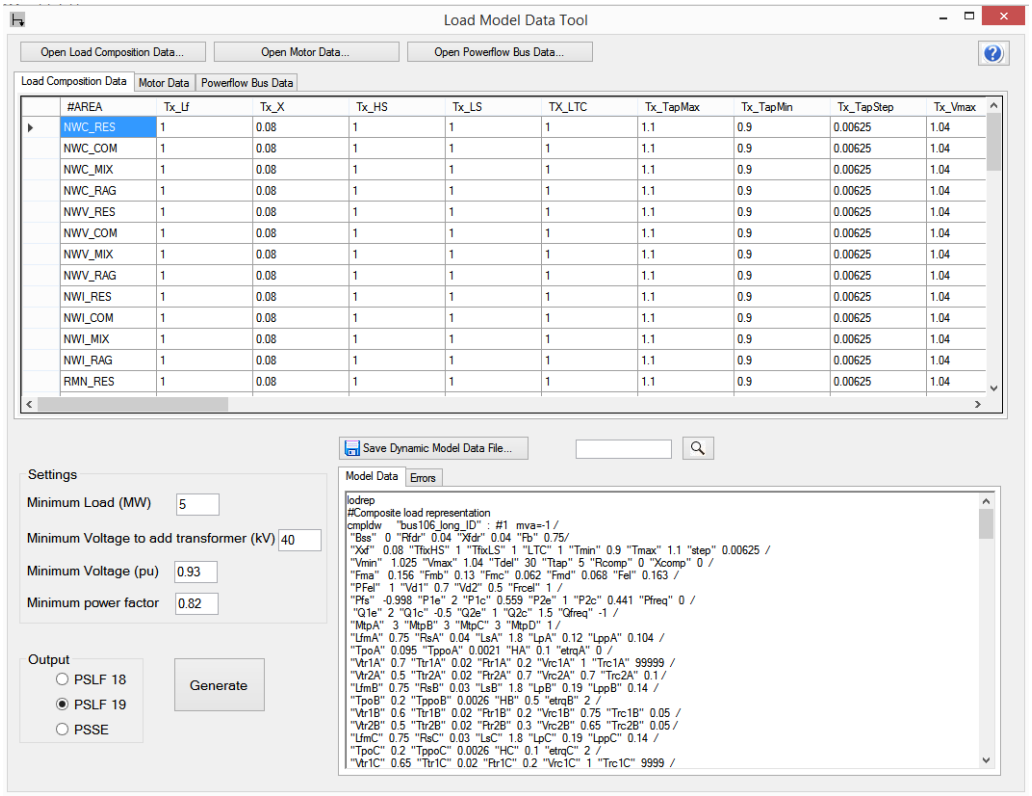


**Figure 45: LMDT 1.0 Main Graphical User Interface (GUI)**

New version of the tool (LMDT 2.0) was released in 2016. The LMDT 2.0 has a built-in database of load models for different climate zones and also has an advanced analytical and visualization capabilities (Figure 46).

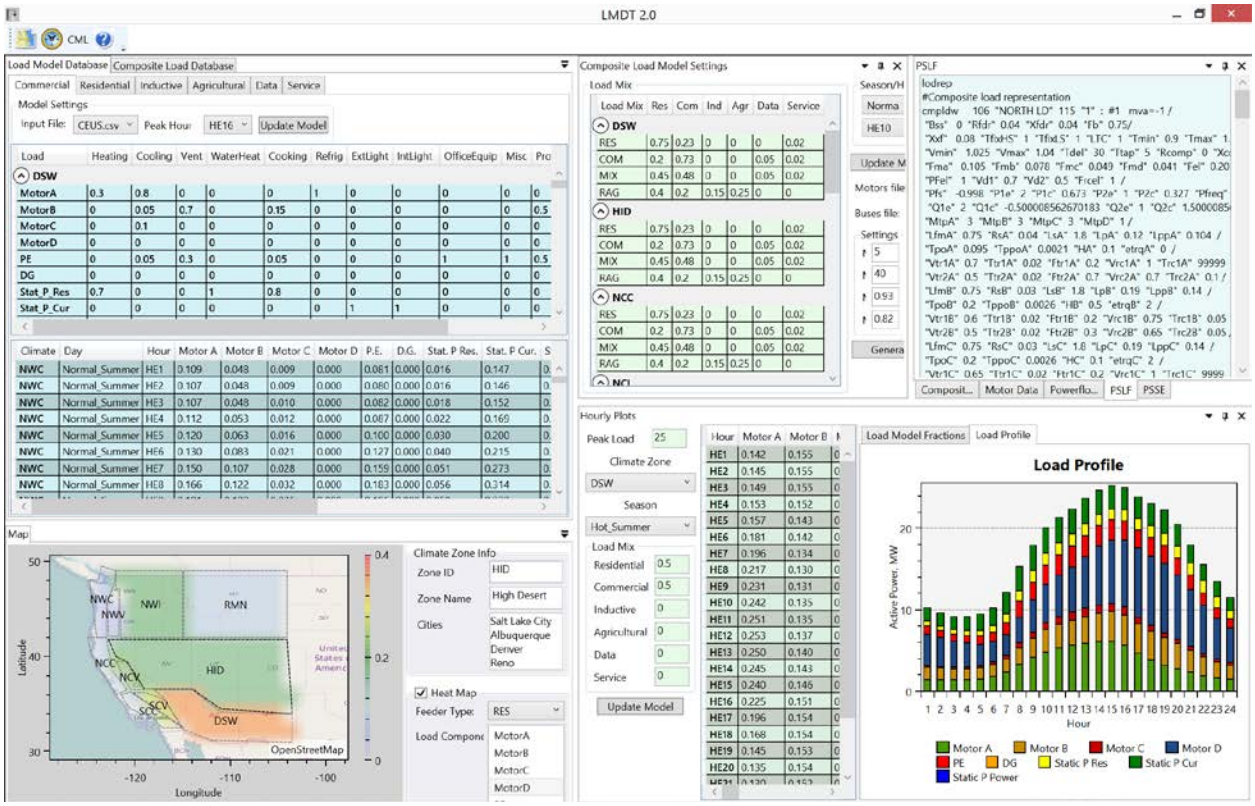


**Figure 46: LMDT 2.0 Main Graphical User Interface (GUI)**

**Load Model Creation Process using LMDT 1.0**

The following process is used for generating the dynamic load model records used in planning and operational studies within the Western Interconnection.

1. Each Transmission Planner (or preparer of load data) populates the LIDs (PSLF19 has a dedicated field for the load climate zone information) for their respective load, capturing the load type and climate zone. Typically this is done once for each load, and used in all future cases.
2. WECC utilizes the Composite Load Model Spreadsheet to look up the climate zone definitions for a given power flow case based upon the hour of day and season represented. The spreadsheet produces a calculated sheet with feeder information, proportion of various motor types in each climate zone, etc., to a .csv file.
3. WECC runs an automation program in GE PSLF (.epcl script) that reads the completed power flow case to generate a spreadsheet of necessary information including load size, voltage, and climate zone for each bus.
4. WECC runs a tool to create the composite load model records, which are part of the dynamics data file. The tool outputs composite load records in GE PSLF or PTI PSS®E format, and read three files to do so[28]:
   a. .csv file from spreadsheet tool (step 2).
   b. .csv file output from .epcl program (step 3).
   c. .csv file with predefined motor definitions (predetermined).

**Load Model Creation Process using LMDT 2.0**

To create composite load dynamics records the following steps need to be done:

- Step 1: Select season
- Step 2: Select operating hour
- Step 3 (*optional*): Specify percentage of different type of loads connected to the feeders:
  - RES – residential feeder
  - COM – commercial feeder
  - MIX – mixed use feeder
  - RAG – rural feeder
- Step 4: Click "Update Model" button

[28] More details can be found in the LMDT 1.0 user's manual available at: https://svn.pnl.gov/LoadTool

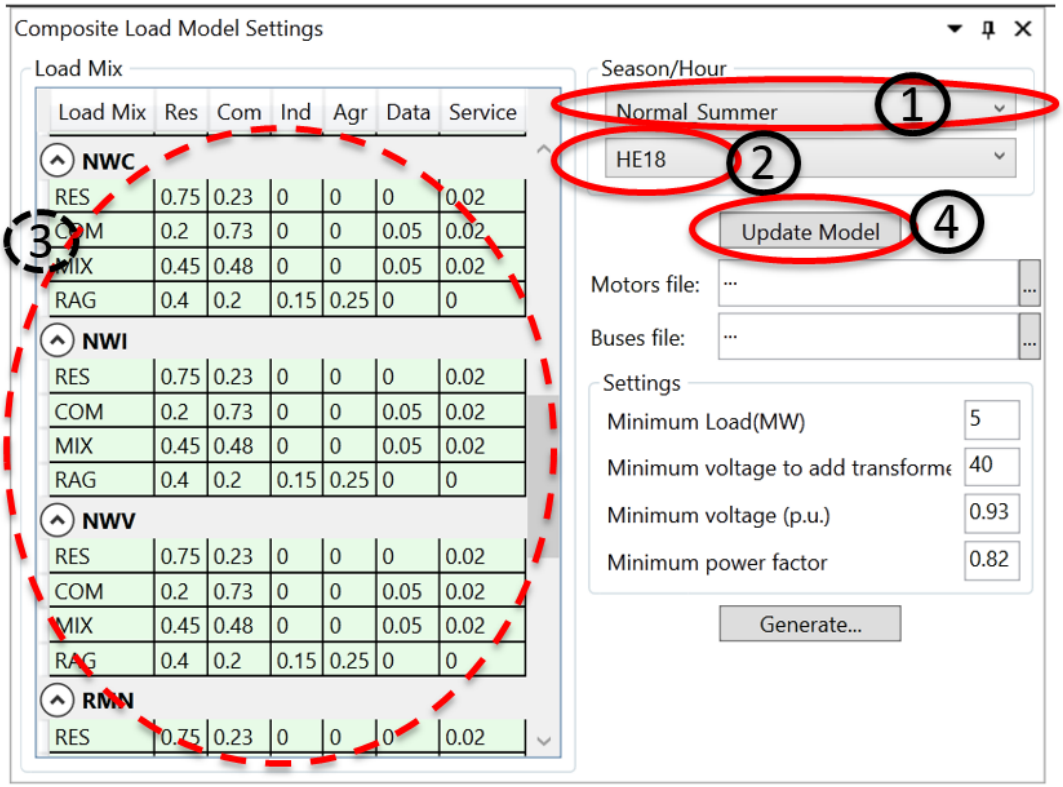


**Figure 47: Composite Load Model Creation (Steps 1-4)**

- Step 5: Select file with "Motor" information
- Step 6: Select file with "Power Flow" information
- Step 7 (*optional*): Specify additional settings

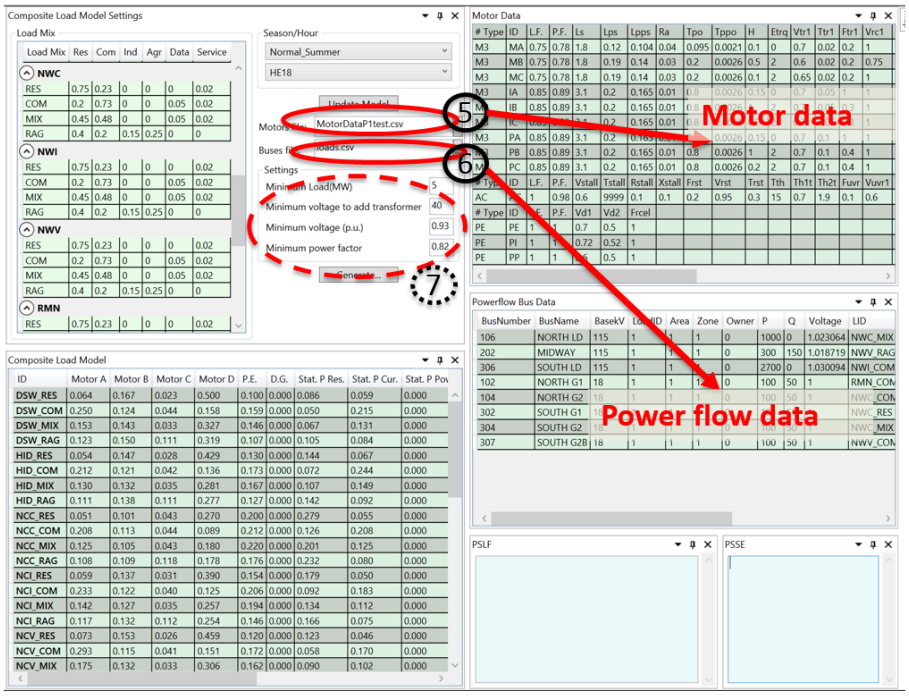


**Figure 48: Composite Load Model Creation (Steps 5-7)**

- Step 8: Click "Generate" button
- Step 9: Copy and add composite load model dynamic records to the dynamic records file

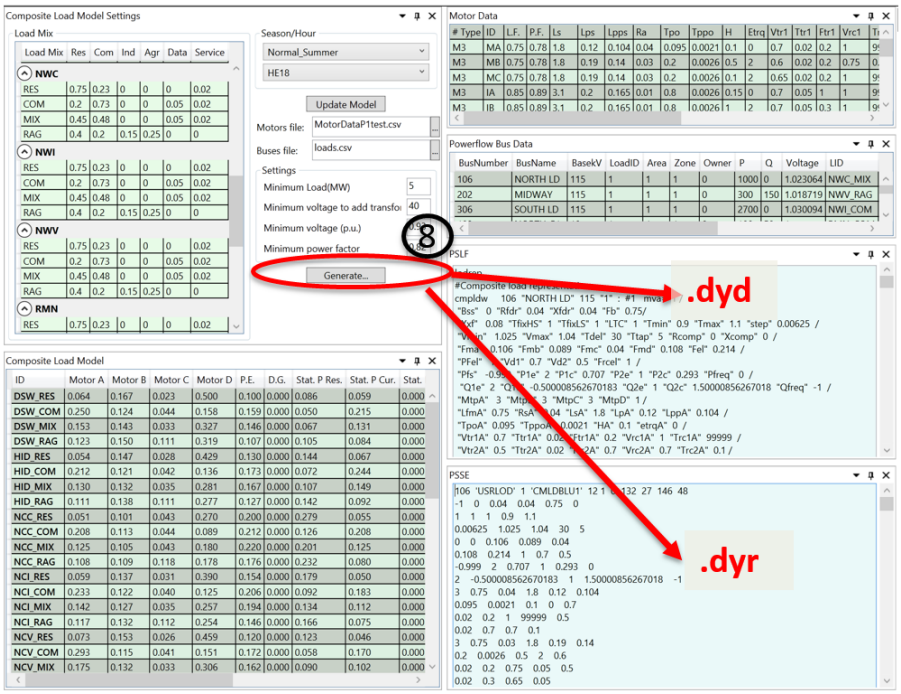


**Figure 49: Composite Load Model Creation (Steps 8-9)**

**LMDT 2.0 analytical and visualization capabilities**

Climate zone information, season and load mix need to be specified to generate the load profile and load model fractions. Figure 50 shows the load profile that is used for generating the composite load models (NWC climate zone, Normal summer season). This shape was based on research conducted by PNNL[29], exploring the composition of the load for different times in the day. This information is used to generate a set of load model fractions, as shown in Figure 51. These fractions are used to allocate the various load types into the composite load Model.

[29] Chassin D., Zhang Y., Etingov P., Kirkham H., Li X., et al. "Load Composition Modeling and Tools", PNNL-24453. Pacific Northwest National Laboratory, Richland, WA, July, 2015.

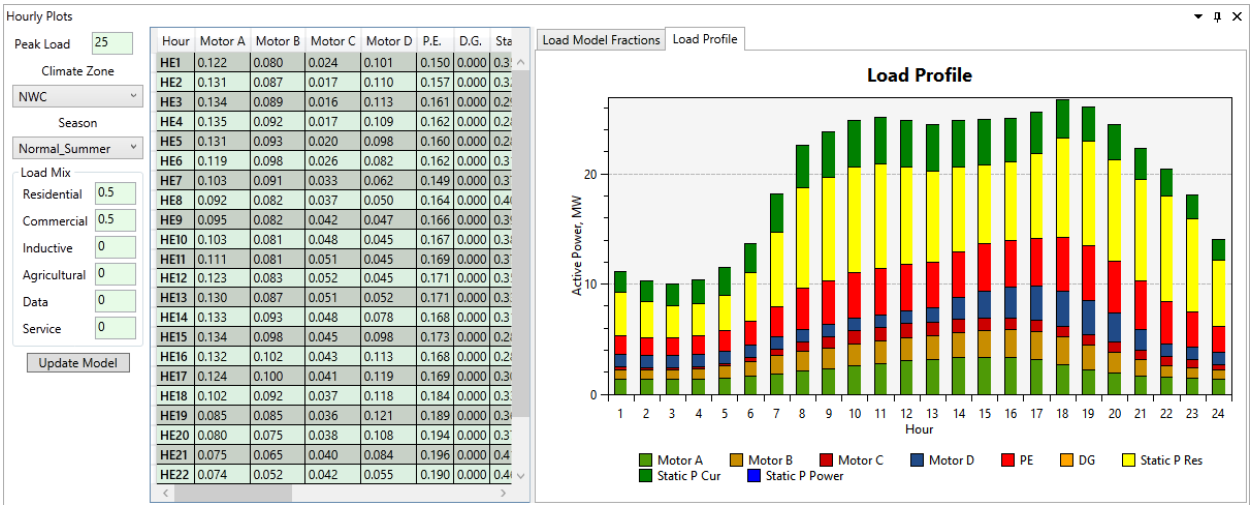


**Figure 50: Load Profile Screen**

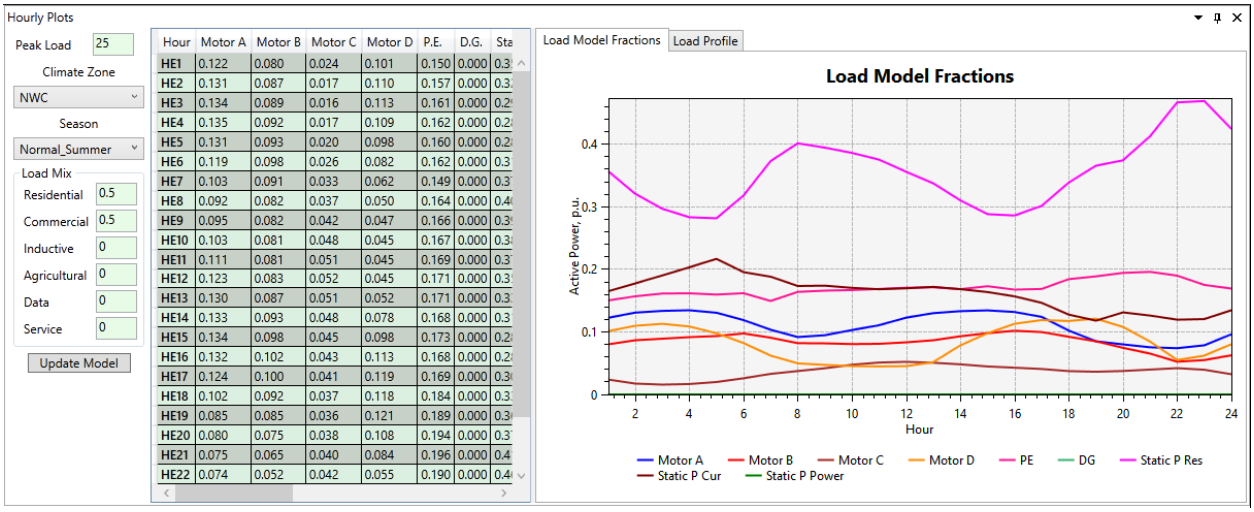


**Figure 51: Load Model Fractions**

The LMDT 2.0 also contains a map that displays climate zone information. Dependence of different composite load parameters on the geographical location can be also displayed using a heat map plot. Figure 52 shows an example of Motor D (Residential feeder) parameter distribution over different climate zone (geographical regions) at hour ending by 11.

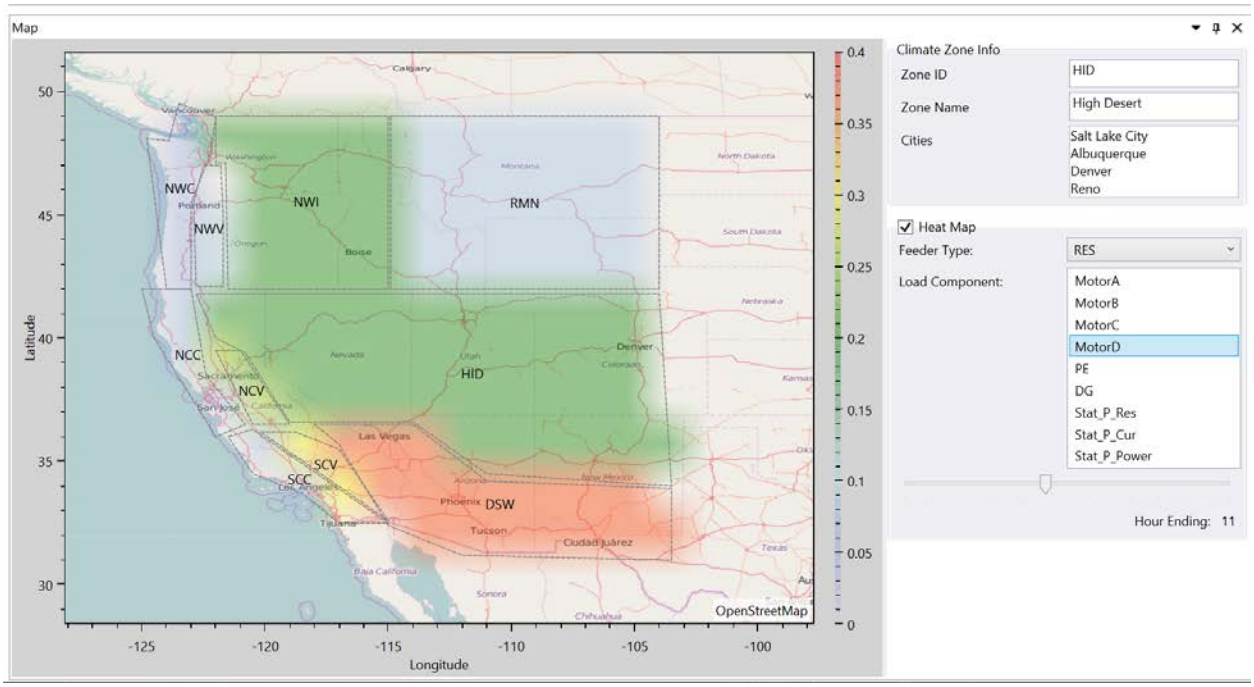


**Figure 52: Map Visualization Screen**

### Load Model Creation Process

The following process is used for generating the dynamic load model records used in planning and operational studies within the Western Interconnection.

1. Each Transmission Planner (or preparer of load data) populates the LIDs for their respective load, capturing the load type and climate zone. Typically this is done once for each load, and used in all future cases.
2. WECC utilizes the Load Model Data Tool to look up the climate zone definitions for a given power flow case based upon the hour of day and season represented. The spreadsheet produces a calculated sheet with feeder information, proportion of various motor types in each climate zone, etc., to a .csv file.
3. WECC runs an automation program in GE PSLF (.epcl script) that reads the completed power flow case to generate a spreadsheet of necessary information including load size, voltage, and climate zone for each bus.
4. WECC runs a tool to create the composite load model records, which are part of the dynamics data file. The tool outputs composite load records in GE PSLF or PTI PSS®E format, and read three files to do so:
   a. .csv file from spreadsheet tool (step 2).
   b. .csv file output from .epcl program (step 3).
   c. .csv file with predefined motor definitions (predetermined).

## "Default" Data Sets

Appendix A provides a detailed description of the various parameters and also provides a "default" value for each parameter. The values greyed out are not expected to change, and therefore can be held constant across sensitivity runs. The NERC Load Modeling Task Force (LMTF) is developing default data sets that can be used as a starting reference point for developing robust data sets for the composite load model across North America.

## Benchmarking Software Vendors

An array of software platforms are widely used by transmission planers across the utility industry in North America. Benchmarking the performance of each software is important to ensure uniform and accurate implementation of load model applied to transmission planning studies, and also helps identify errors to improve the model performance. The NERC LMTF has been working with software vendors[30] to benchmark their tools. The process consisted of three steps:

- Determine and prepare the test case;
- Determine and prepare contingencies/events; and
- Determine variables to compare.

For the load model benchmarking purposes focusing on performance of the load model itself, complicated larger networks can be reduced to a small system under test. This single load infinite machine is used in conjunction with playback models in the software platforms to play in a set of test events or contingencies.

In real power systems, the aggregate load has a clearly observable dependency on system frequency. The load model should represent the frequency sensitivity of loads for disturbance events involving large imbalances in generation and load. When system frequency drops during a frequency response event, the electric machinery will experience high flux density, thereby causing higher magnetizing currents. Fewer things can be compared between software platforms. At a frequency lower than the rated frequency, the motor speed will be decreased, locked-rotor torque will be increased, and power factor will be decreased. Figure 53 shows a simulated frequency event to 59.55 Hz; Figure 54 shows the benchmark results for under frequency event. Notice that the Motor A speed deviations are similar between software; however, the electrical torque experiences some numerical issues in one platform.

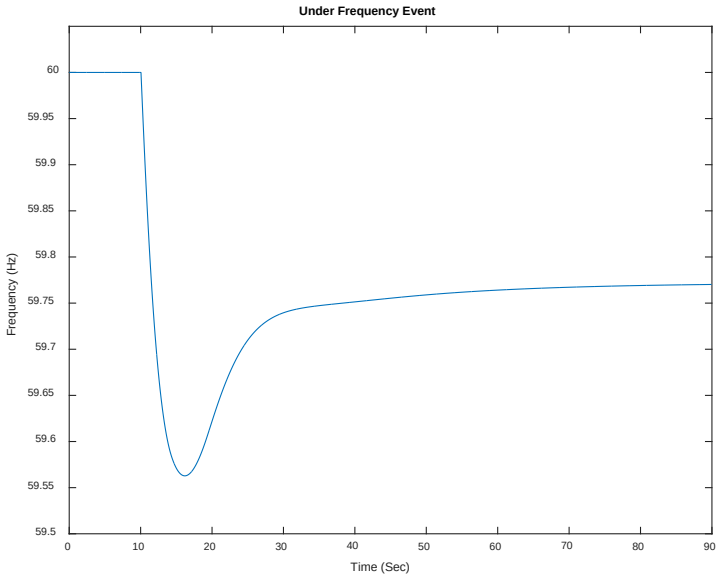


**Figure 53: Underfrequency Test**

[30] Notably, GE PSLF, Siemens PTI PSS®E, PowerWorld and Powertech.

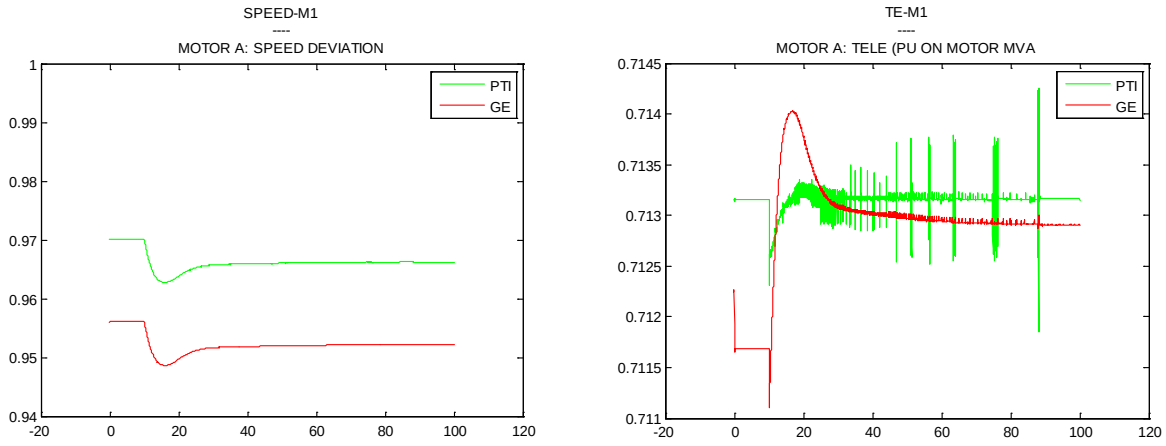


**Figure 54: Benchmarking Software Platforms for Underfrequency Event**

The load model should realistically impact the damping of inter-area oscillations, as has been observed in real large-scale events. The load model also should represent the voltage sensitivity of loads for reasonable voltage oscillations and deviations in the transmission grid such as those experienced during voltage swings. Figure 55 shows the oscillation test with different oscillation frequencies throughout the test. Figure 56 shows the results. Notice the anomalous behavior of Motor A performance during higher frequency oscillations.

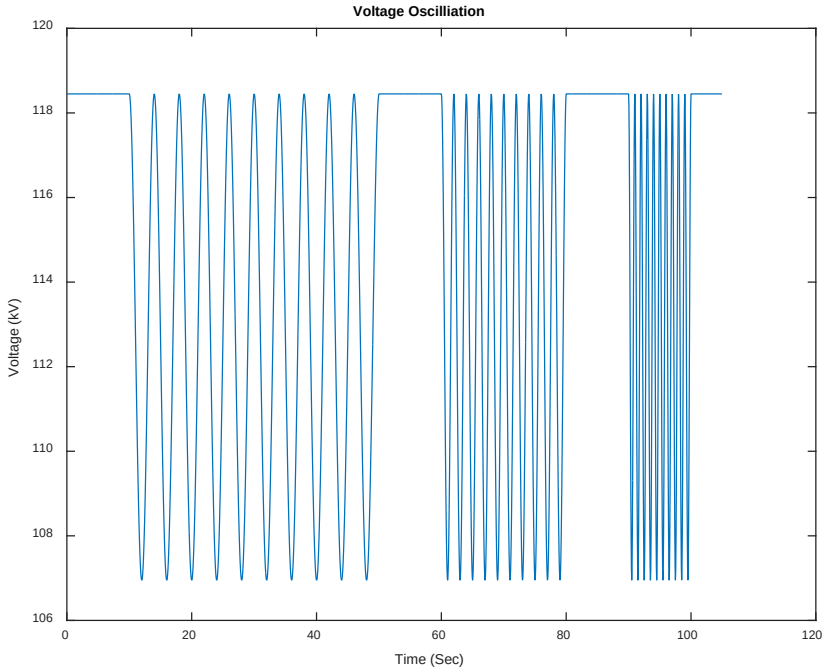


**Figure 55: Oscillation Test**

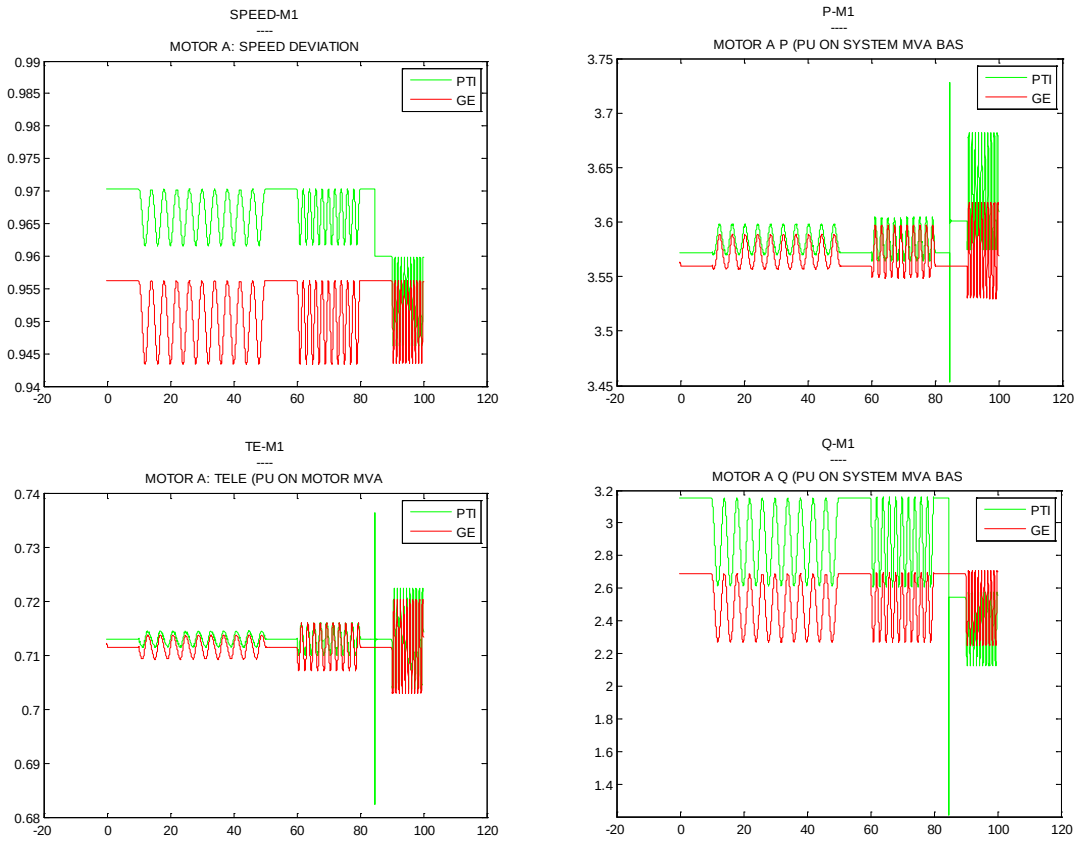


**Figure 56: Benchmarking Software Platforms for Oscillation Event**

The load model should capture the impact that motor load has on voltage recovery following faults in the transmission grid and large voltage deviations. Load performance can be different when voltage ramps slowly down to zero and back to normal voltage. Another test is a prolonged voltage excursion to marginally low level for a relatively long time. Voltage sag to 90% of normal voltage can happened in real life when system outages occur. Voltage drops to 75% will put single phase motor load at the edge of stalling. Figure 57 shows the voltage events; Figure 58 shows the results for the voltage ramp test while Figure 59 shows the results for the sag test. Notice the relative match in performance for overall active and reactive power ($P_{load}$, $Q_{load}$) as well as Motor B performance.

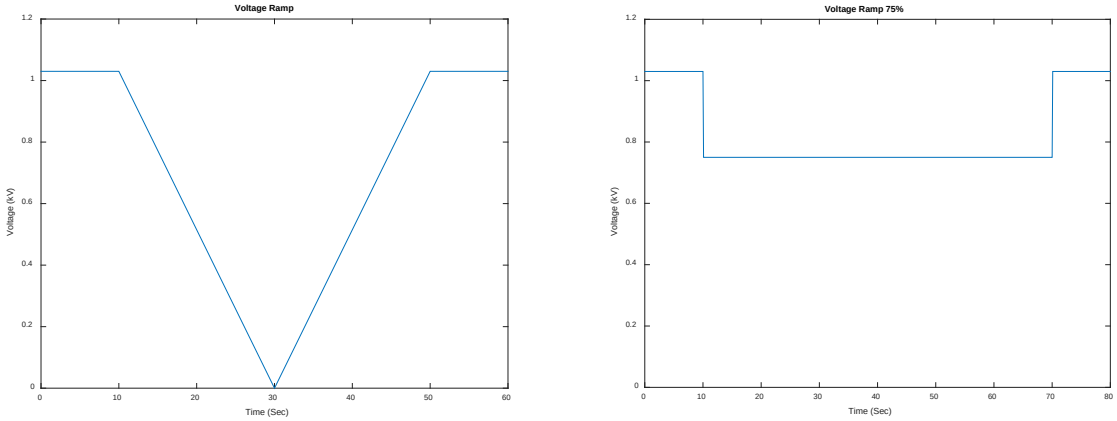


**Figure 57: Voltage Ramp and Voltage Sag Tests**

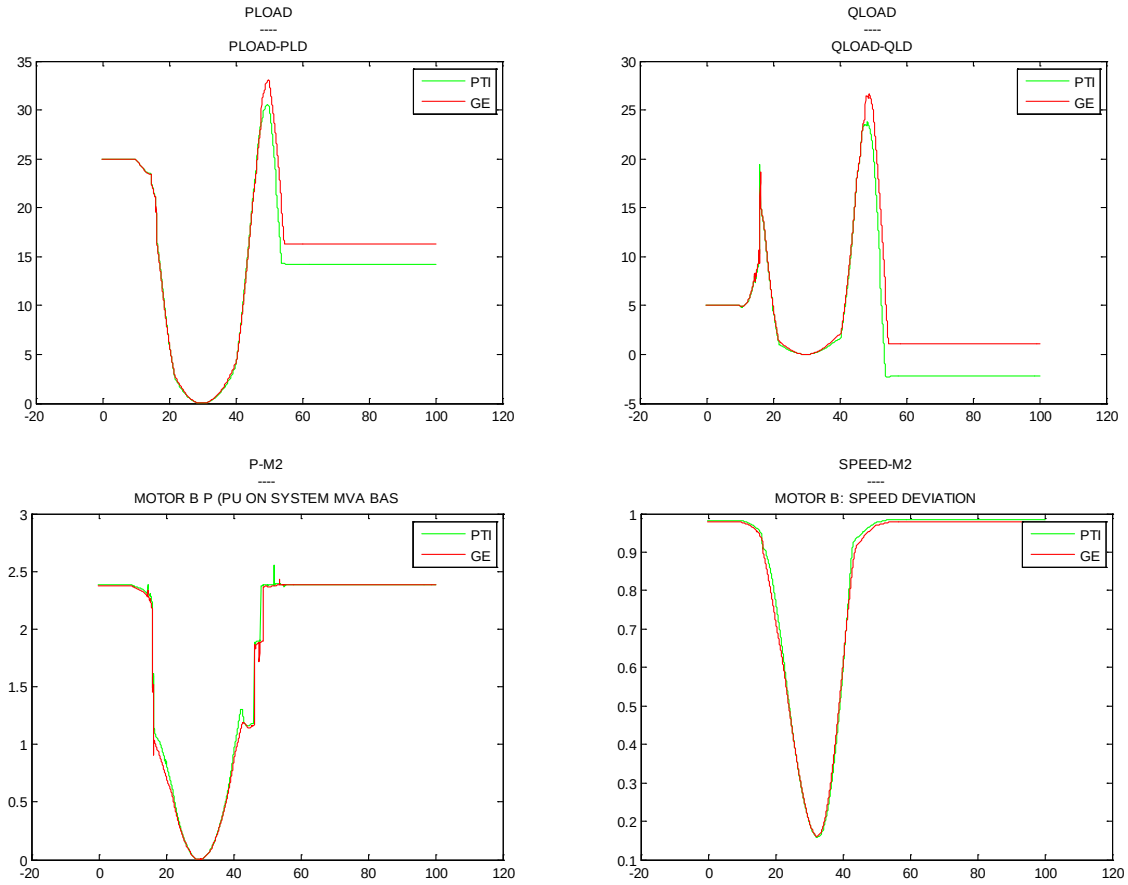


**Figure 58: Benchmarking Software Platforms for Voltage Ramp Event**

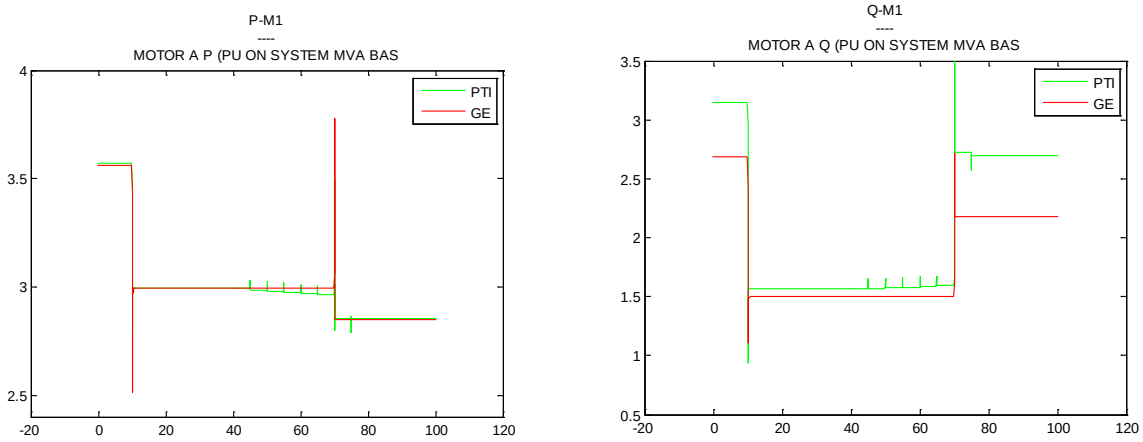


**Figure 59: Benchmarking Software Platforms for Voltage Sag**

Different load compositions can result in different model response to the variation of system frequency and voltage. This is fundamentally due to the changing dynamic load characteristics as the load composition changes. Below is an example of different load models tested.

- All Load Components Present, Phase 1 Implementation (no stalling)
- All Components Present, Phase 2 Implementation (stalling)
- 100% Motor A – 3-Phase Compressor Motor

- 100% Motor B – 3-Phase Fan Motor
- 100% Motor D – 1-Phase Compressor Motor, Phase 1
- 100% Motor D – 1-Phase Compressor Motor, Phase 2

Voltage, frequency, motor speed, torques, active and reactive power are generally useful variables to compare, but more detail variables monitored will explore more detailed issues internal to the software calculations, and will help to resolve issues working with the vendor. Below are some variables monitored in the benchmarking analysis between software platforms.

- High side bus voltage magnitude
- Low side bus voltage magnitude
- Load bus voltage magnitude
- Load – Total real power
- Load – Total reactive power
- Transformer Tap Position
- Motor A: Real power
- Motor A: Reactive power
- Motor A: Trip-reclose factor
- Motor A: Speed
- Motor A: Electrical torque
- Motor B: Real power
- Motor B: Reactive power
- Motor B: Trip-reclose factor
- Motor B: Speed
- Motor B: Electrical Torque
- Motor C: Real power
- Motor C: Reactive power
- Motor C: Trip-reclose factor
- Motor C: Speed
- Motor C: Electrical Torque
- Motor D: Real power
- Motor D: Reactive power
- Motor D: Fraction of motors not tripped by U/V relay
- Motor D: KthA non-restartable compressor motor A fraction not tripped by thermal protection
- Static load real part
- Static load reactive part
- Electronic load real part
- Electronic load reactive part

## Load Model Validation Studies

The need for accurate load models was predominantly driven by the determination that the dynamic load model representation in the Western Interconnection was not able to accurately represent the inter-area dynamics of the grid for major system events. The August 4, 2000 oscillation event provides an illustration of the early validation studies to develop the composite load model that could model induction motor loads. At that time, the MOTORW model was available, representing either a two-cage or one-cage induction machine for part of a constant-power load at a given bus. Figure 60 shows the August 4, 2000 event actual versus simulated response using the MOTORW model at that time; this plot includes many other model modifications to match actual with simulated response. Clearly, there are major discrepancies between the voltage magnitude oscillation frequency and damping ratio.

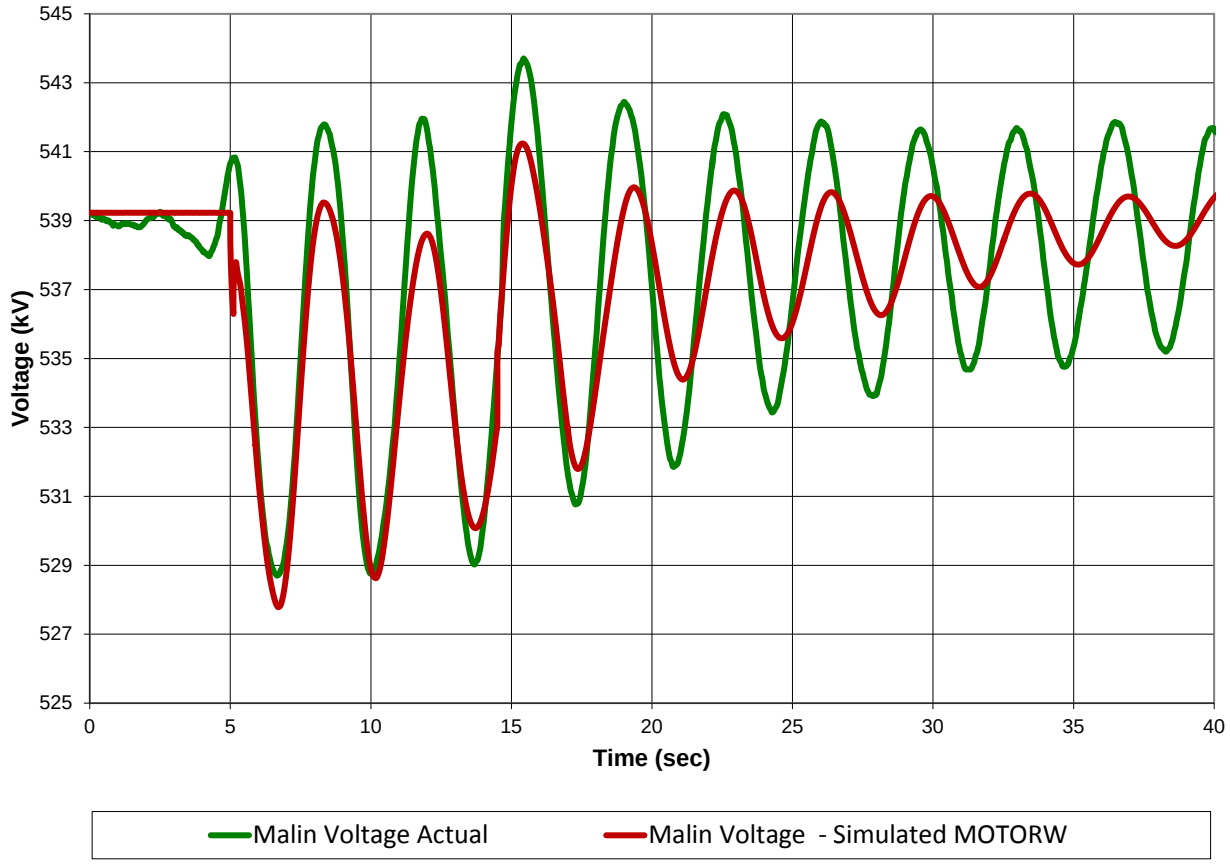


**Figure 60: August 4, 2000 WECC Oscillation Event – Interim Model**

Results from this testing developed the recommendation in the West that the dynamic load model should include 20-30% of induction motor loads at non-industrial load busses across the WSCC system for loads greater than 5 MW for heavy summer operating conditions. Sensitivity studies with respect to higher induction motor percentage could be performed for critical cases. This led to a load survey to determine the load composition across the WSCC system on a regional basis.

After development and testing of the CMPLDW model in GE PSLF, the composite load model was used to validate the event and use as a benchmark case. The CMPLDW model was tuned to the expected conditions based on the interim model assumptions and the simulations were rerun with that model. Figure 61 shows the results of applying the CMPLDW model compared with actual voltage on the system. Notice the stark difference between Figure 60 and 61 in terms of accuracy. Oscillation frequency matches very closely and the oscillation damping ratio also is improved. Notice that the initial testing of the CMPLDW model was not to recreate a delayed voltage

recovery case; rather, it was tested to recreate a large oscillation case. The effect of induction motor loads on the system affect the asymptotic stability of the system and must accurately be accounted for when studying interconnection-wide events that can affect large areas of the system.

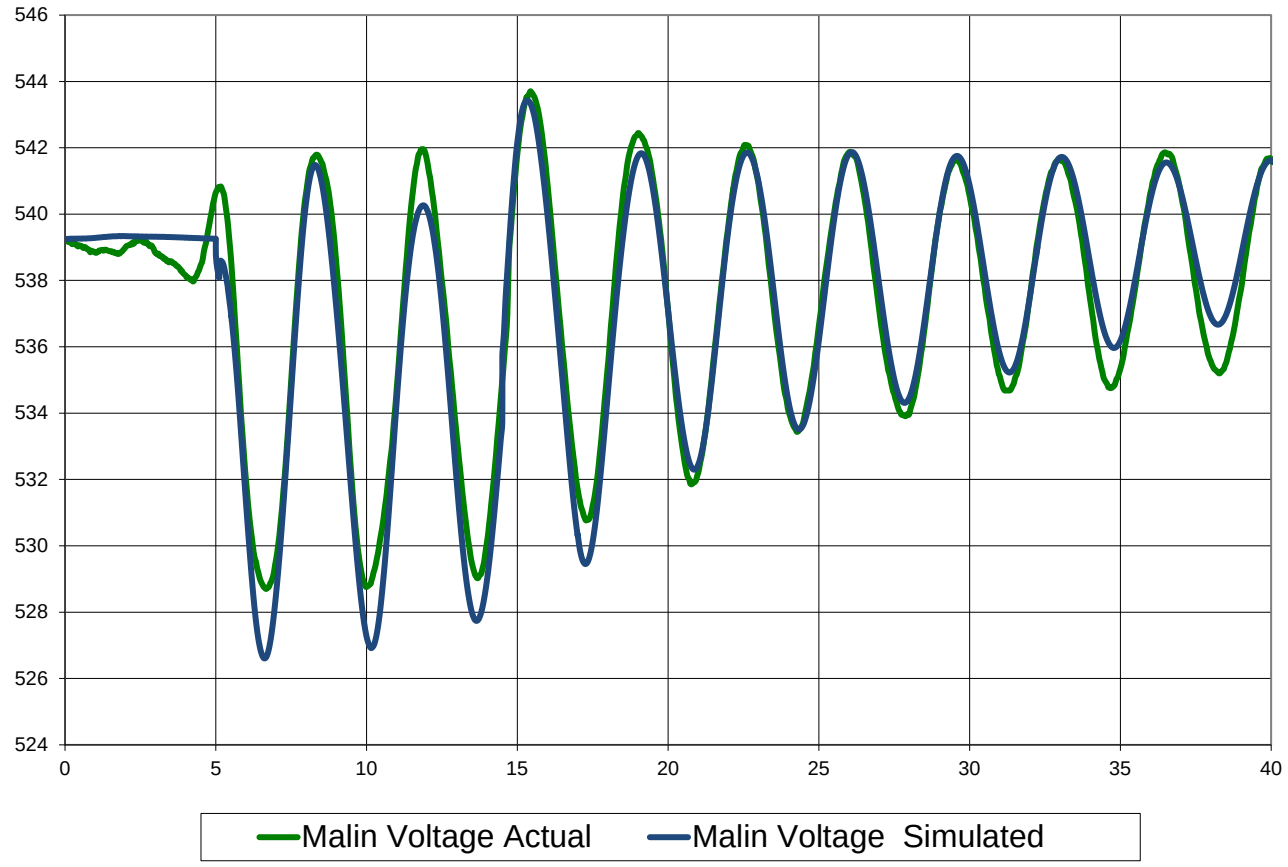


**Figure 61: August 4, 2000 WECC Oscillation Event – CMPLDW Model**

Southern California Edison was able to capture a number of FIDVR events on their system, including one event captured on the 500kV system using Phasor Measurement Units. This provided a very useful event for validating the model performance for delayed voltage recovery events. Figure 62 shows the actual PMU data as compared with 1) the standard motor model (MOTORW) and 2) the new CMPLDW motor model that included stalling effects. Note how the delayed recovery is not represented with the old motor model; the composite load model was able to recreate the event closely by tuning the model to a given set of parameters and protection settings including the single-phase motor stalling characteristic.

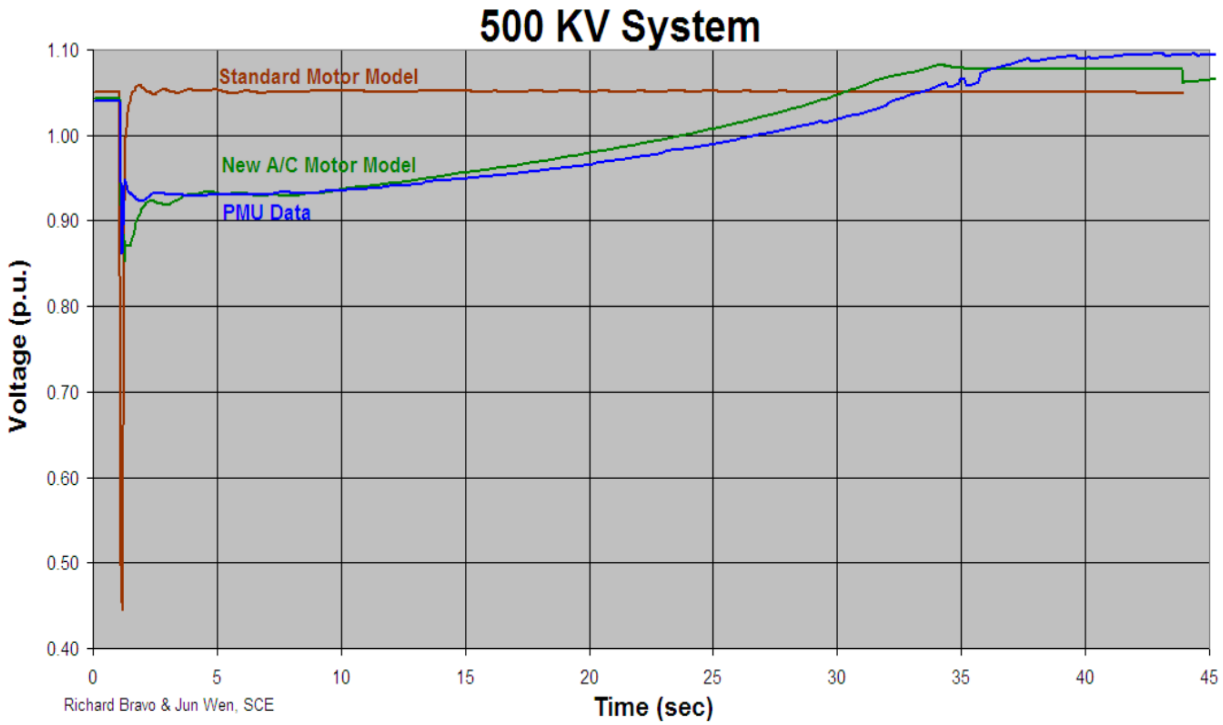


**Figure 62: Model Benchmarking for Fault in SCE Territory using PMU Data**

American Electric Power (AEP) was also able to capture FIDVR events on their system with PMU data and was able to closely match the transient voltage responses of the events using the dynamic load model. Figure 63 shows a multiple fault event that resulted in some delayed recovery. UVLS operations also occurred following fault clearing. Figure 64 shows a second FIDVR event at a different location. Default CMLD parameters were adjusted to match these events. For the events captured so far, CMLD model changes to the default model parameters to get a more exact fit included A-B-C-D-E percentage and the D-component thermal protection parameter adjustments. Most other CMLD parameters did not need to be changed. AEP continues to expand its PMU coverage to be in position to collect future events.

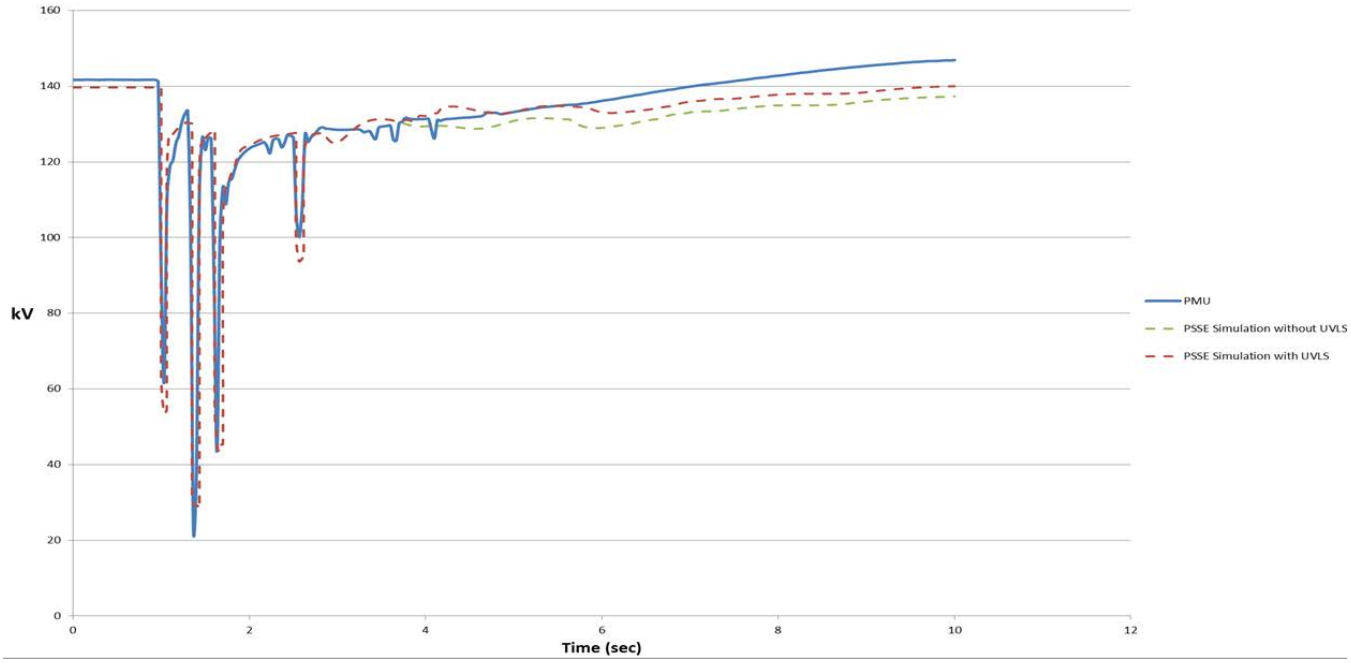


**Figure 63: Load Model Parameter Validation for AEP Fault Event 1 using PMU Data**

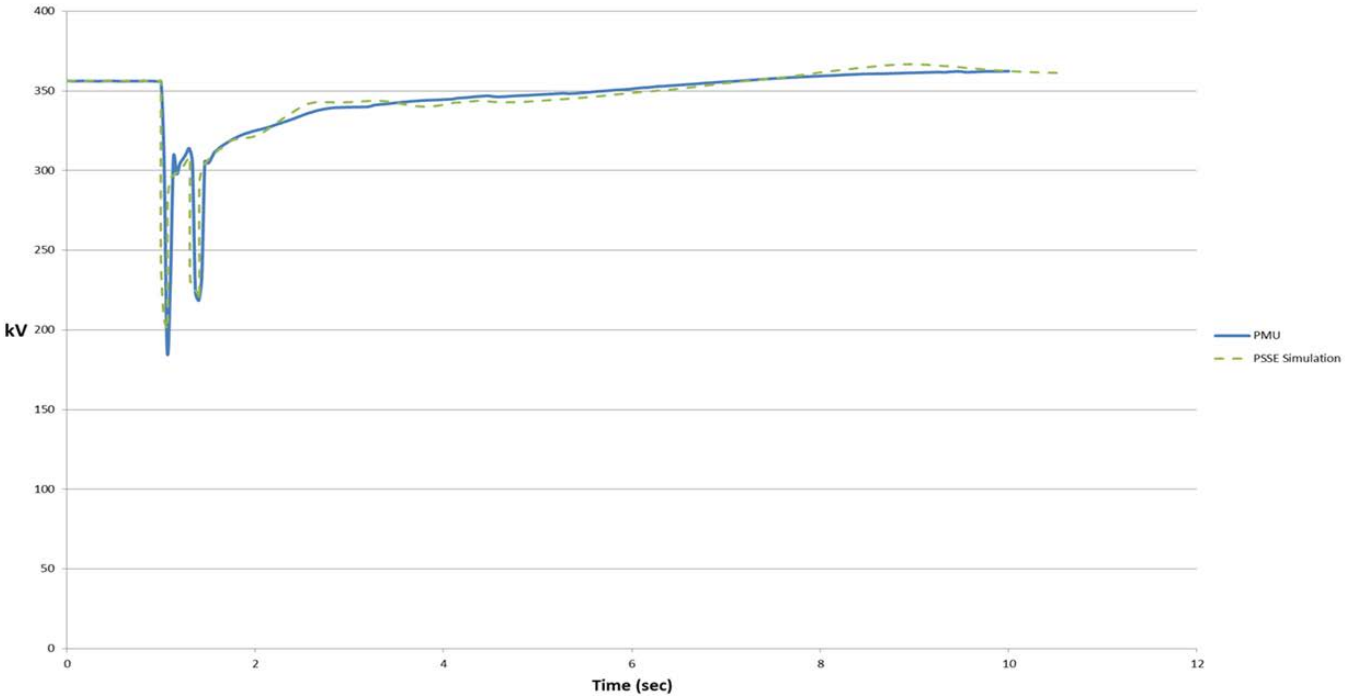


**Figure 64: Load Model Parameter Validation for AEP Fault Event 2 using PMU Data**

## Phased Implementation

WECC is using a phased approach for approving use of the composite load model for compliance with NERC Reliability Standards and WECC Regional Reliability Standards. The phased approach allows utilities to gain confidence in the model and understand the sensitivities of its parameters on their respective systems. The phased approach consists of:

- Phase 1 – Single-phase air conditioner stalling is disabled by setting the $T_{stall}$ parameter to a large value (e.g., $T_{stall}$ = 9999).
- Phase 2 – Better understanding the reliability implications of delayed voltage recovery due to air conditioner stalling, developing appropriate reliability metrics for delayed voltage recovery, and improving identified deficiencies in the composite load model.

WECC approved adoption of Phase 1 in 2014 and member utilities are now using the composite load model for system planning and seasonal operating limit studies. WECC is continuing efforts to improve the composite load model for Phase 2 adoption.

## Sensitivity Analysis and System Impact Assessment

To fully understand how the load response impacts system stability, sensitivity analysis must be performed for various system impact assessments. Sensitivities identify (1) load parameters which have an impact on transient behavior, and (2) system conditions that may develop potential problems using the given load model. These complementary sensitivities provide a more comprehensive understanding of whether the load has a substantive impact on grid reliability and ensures a more robust planning process.

Based on utility experience, the following parameters within the composite load model are recommended for sensitivity analysis:

- Load Composition Fractions (FmA, FmB, FmC, FmD, Fel)
- Voltage protection tripping levels and times (Vtr1, Ttr1, Vtr2, Ttr2)
- Protection reclosing levels and times (Vrc1, Trc1, Vrc2, Trc2)
- Single-phase motor stall voltage and time (Vstall, Tstall)
- Single-phase motor restart time (Trestart)
- Single-phase motor restart voltage and fraction of phase motors capable of restart (Frst, Vrst)
- Single-phase motor voltage tripping and reclosing ( UVtr1, Ttr1, Vc1off, Vc2off, Vc1on, Vc2on)
- Single-phase motor tripping thermal cutout time constant (Tth)

With respect to the system, the following sensitivities may be considered:

- Generation dispatch and unit statuses
- Dynamic reactive support dispatch and statuses
- Transmission system topology
- Load power factor
- Stress levels and interface flows
- Pre-contingency voltages
- Status of in-service series and shunt reactive devices

Figure 65 shows system performance to a large number of sensitivity studies for a given set of critical 3-phase fault contingencies in the load center being studied. Visualizing these sensitivities allows the Transmission Planner to understand the envelope of expected performance and drill down to any contingencies of risk that do not meet transient response criteria or cause abnormal system behavior. In this example, the transient voltage response is not a major issue (voltage recovers to reasonable levels quickly post-fault); however, it is clear that overvoltage may be an issue for certain operating conditions or load model parameters. In these studies, a relatively large number of load tripping occurs based on the model parameter settings, resulting in overvoltages greater than 1.2 pu for short durations. Automatic switched shunt capacitor controls begin operating to bring the voltage back to within normal limits.

Figure 66 shows the impact on system performance for single-phase fault contingencies both for normal clearing and delayed clearing. The studies show that single-phase faults with normal clearing do not pose a risk of motor stalling and load loss. Delayed clearing single-phase faults show some oscillatory behavior and slightly delayed voltage recovery; however, the responses are all reasonable for the studied contingencies.

Performing large batch studies under varied operating conditions and parameter values provides these types of insights into the key contributors to voltage and stability risks as well as a broad understanding of system strength for the areas studied with the dynamic load model.

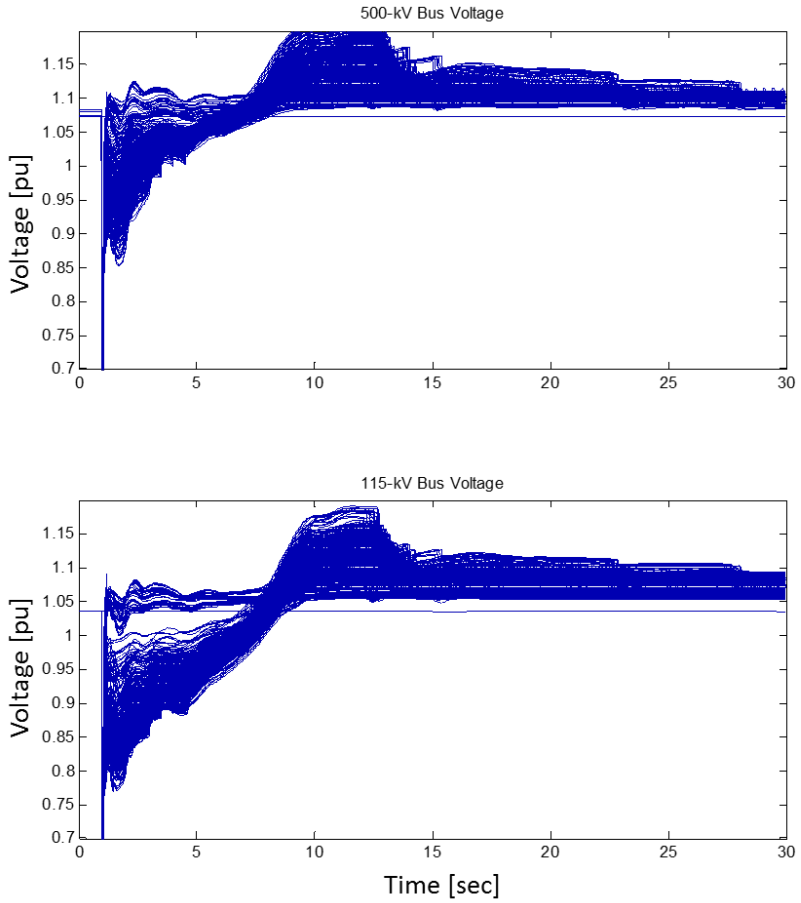


**Figure 65: Voltage Performance for Three-Phase, Normally Cleared Fault**

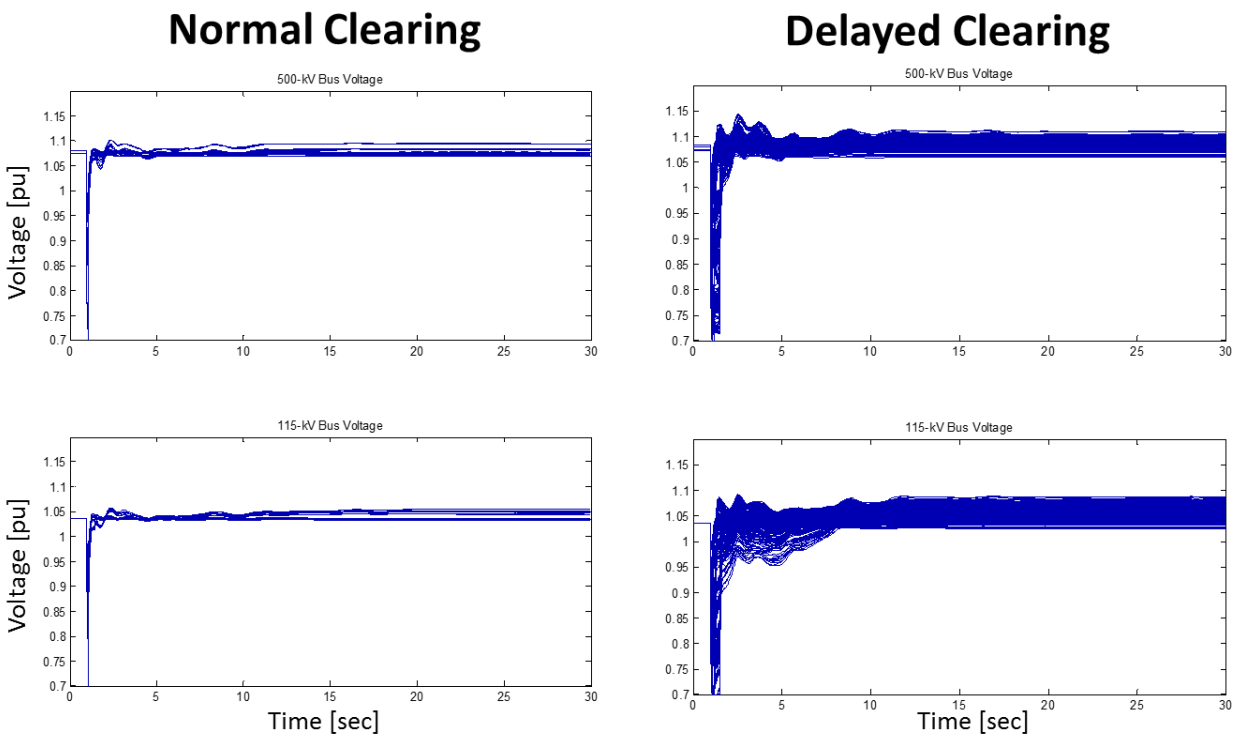


**Figure 66: Single-Phase Fault with Normal and Delayed Clearing**

The impact the induction motor load is having on system performance requires understanding of the sensitivities of key parameters. Figure 67 shows system stability analysis for varying penetrations of single-phase induction motor load with a fixed set of assumptions regarding protection, tripping, and stalling mechanisms.

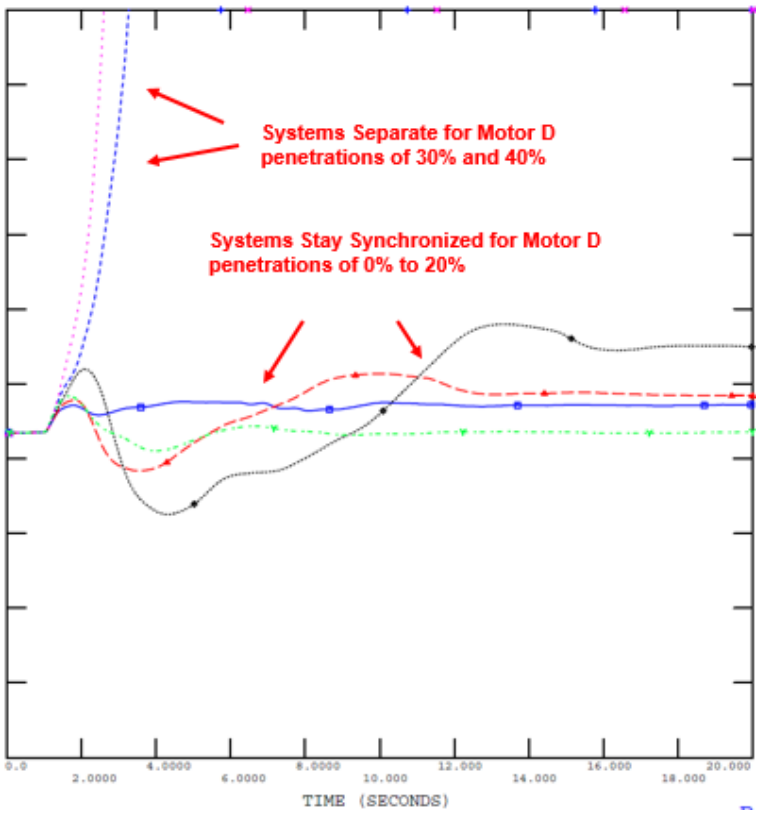


**Figure 67: Stability Assessment for Varying Levels of Motor D**

To quantify the performance of voltage response more completely some entities have developed metrics that can be applied to actual system measurements or simulation results. Figure 68 illustrate a set of detailed measures used by Southern California Edison to better assess the aspects of voltage recovery using the Phase 2 Composite Load Model including the single-phase air-conditioner motor stalling effect. In addition to the performance metrics, the number of buses with stalled load is tracked (for simulation results) to determine the electrical and geographic impact of motor stalling on the transient voltage response.

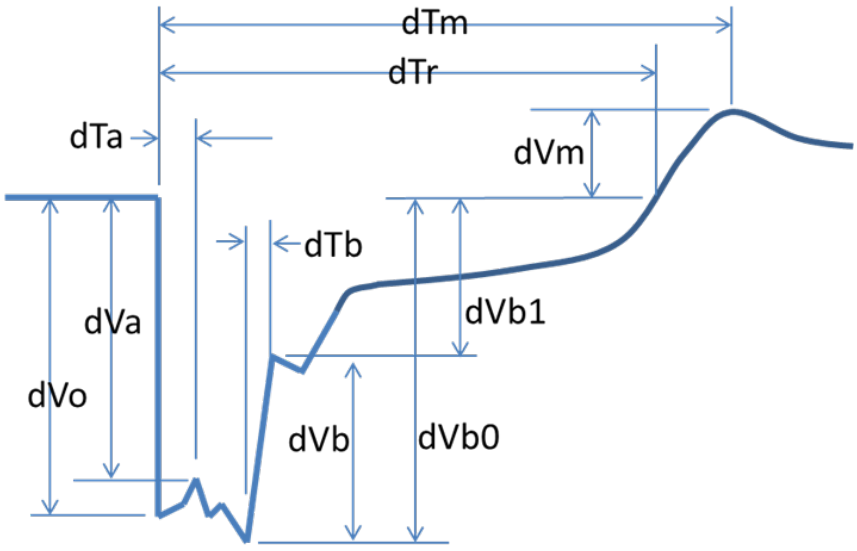


| Variable | Variable Description |
|---|---|
| dVo (%) | First sample voltage dip |
| dVa (%) | Persistence voltage dip |
| dTa (cycl) | Persistence time |
| dVb0 (%) | Lowest value of dVb in % |
| dVb1 (%) | Highest value of dVb in % |
| dVb (kV) | dVb in KV |
| dTb (cycl) | Time from lowest to highest dVb |
| dVm (%) | Peak voltage overshooting |
| dTr (sec) | Time to reach initial volt level |
| dTm (sec) | Time to reach maximum voltage |

**Figure 68: Phase 2 Composite Load Model Performance Metric**

# Modeling Improvements – Next Steps

This section identifies future or current work related to modeling improvements of the various composite load model components. While some improvement analysis and studies have been completed, these modifications have not yet been made to the software programs. Therefore, they are captured under this section rather than the model or end-use load characteristic sections for reference.

## Single-Phase Induction Motor Model

The single-phase induction motor model is currently represented by a performance model using algebraic equations to represent the consumption of power as well as the transition from run to stall state. However, this is known to be an approximation and recent studies and laboratory testing have uncovered modifications to the Motor D model that will be considered in future revisions to the model. These are discussed here for reference.

### Point-on-Wave Sensitivity

Original laboratory testing of single-phase air-conditioner motors applied the voltage sags at the voltage zero crossing. These tests led to the development of the initial stall characteristics used in the performance model. However, subsequent laboratory testing and 3-phase modeling explored the sensitivity that point-on-wave effects have on single-phase induction motor stalling. Figure 69 shows simulated motor speed (right) based on the point of the voltage waveform where the instantaneous sag is applied. At the voltage zero crossing (blue), the motor exhibits the most dramatic speed reduction and stalls. At the 45° point (yellow), the motor slowly recovers and reaccelerates. At the voltage peak, the motor rides through the voltage sag with little issues. The red plot of motor speed (not shown in the voltage plot) shows the marginal point where the motor almost reaccelerates but ends up stalling with a longer time delay.

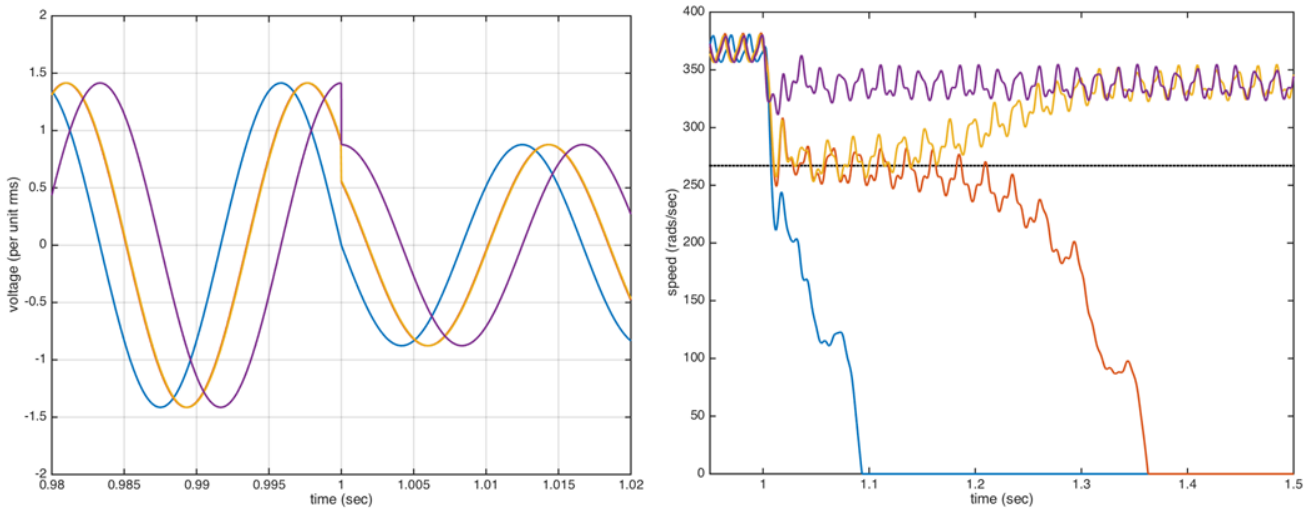


**Figure 69: Point-on-Wave Sensitivity Analysis**

Based on these types of tests, stall voltage versus voltage sag duration can be developed to better understand the sensitivity that point-on-wave effects have on stalling. Figure 70 clearly shows how the point-on-wave where the fault or voltage sag is instantiated affects the stall characteristic. When the sag is applied at the voltage zero crossing, the motor is more likely to stall for a given voltage sag duration (stall voltage level). Notice that at voltage peak, stall voltage drops drastically to about 0.46 pu for a voltage sag of 3 cycles. While this information is valuable for understanding the stall characteristic of these types of motors, it poses a challenge for modeling in positive sequence simulation tools. Since the characteristics are strongly dependent on a point-on-wave effect, this cannot be modeled in the positive sequence realm and simplifications would have to be made.

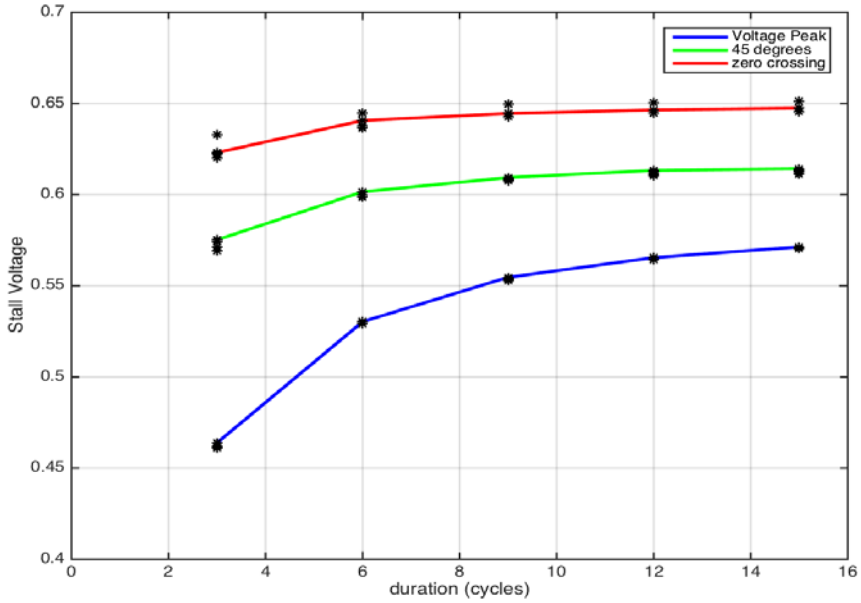


**Figure 70: Motor Stall Sensitivity of Point-on-Wave**

## Voltage Ramp Rate-of-Change Sensitivity

It is widely observed that stalling does not seem to be as severe based on field measurements compared with laboratory testing environments. One idea why this is the case is that simulation tools and lab tests have assumed an instantaneous rate of change of voltage for the voltage sags applied (this is the standard convention for positive sequence simulation tools). However, in the field there may be a very short ramping effect due to a number of factors including electromagnetic time delays, motor back feed, etc. The simulation tests were recreated using a short ramp to the voltage sag. The same voltage tests were performed using a short 1-cycle ramp in the voltage sag. Upon doing so, the stall characteristics all exhibited a relatively similar response in terms of stall voltage and duration as shown in Figure 71 (right). These characteristics are much more optimistic in terms of motor stalling (lower voltage for given sag duration) for the voltage peak and 45° point. In addition, the similarity in stall characteristics allows this to be modeled in positive sequence simulations.

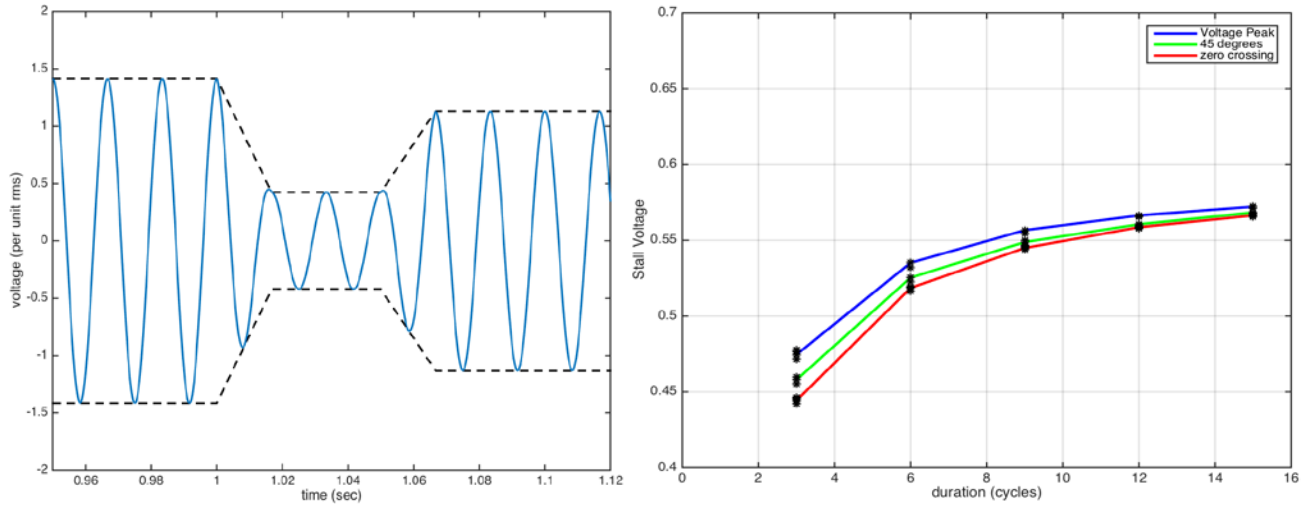


**Figure 71: Voltage Sag Rate-of-Change and Stall Characteristics**

# Dynamic Phasor Model

In contrast to a static performance-based model comprising a set of algebraic equations representing the stall and run states of the motor, a dynamic phasor model captures the rotor and flux dynamics of single-phase motor. This more detailed representation introduces motor variables associated with time-varying phasor quantities that do not require point-on-wave simulation, and it can be implemented in a positive-sequence simulator. The fundamental approach is displayed in Figure 72 below in which the system response is shown both with the fast oscillatory point-on-wave representation, and a slower amplitude-tracking (phasor) representation[31]. Similar to positive sequence models, use of the phasor dynamic model implicitly relies on an assumption that sub-cycle phenomenon is not critical to the outcome of the simulation[32].

The explicit dynamic representation of the dynamic phasor model is intended to improve the accuracy of FIDVR studies, better capturing the possibility of the spread of an event beyond the location of the initial fault. It also is used in traditional transient stability studies, accounting for the effect of single-phase motors on system oscillations.

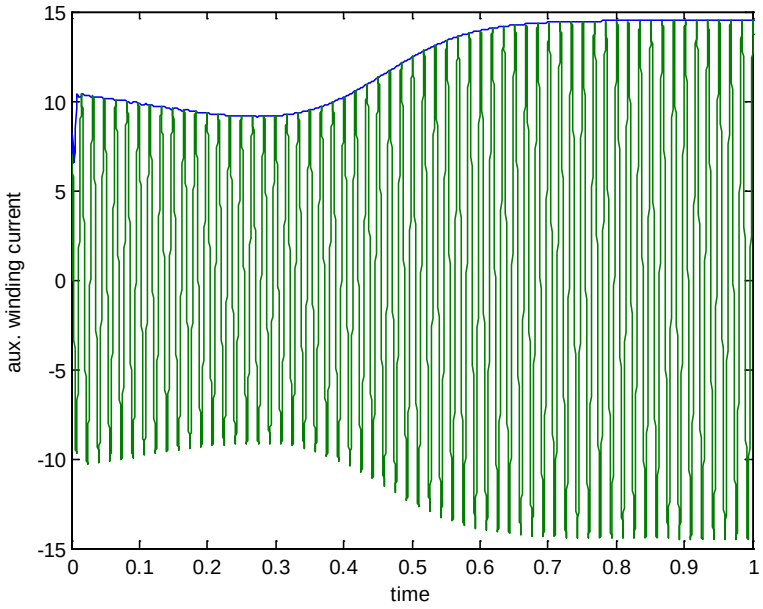


**Figure 72: Phasor Dynamics Model of Single Phase Induction Motor**

# Inverter-Based Generation

Ongoing research is exploring how to best incorporate distributed generation resources in the dynamic load models to capture those resources that are not explicitly modeled in the powerflow and dynamics cases. Fundamentally, there appears to be two distinguishable types of distributed resources at the distribution level that can be modeled in the dynamic load models separately:

1. **Utility-Scale Distributed Generation (UDG):** These resources generally include large 3-phase interconnections of distributed generation (DG) most commonly located at the distribution system bus and may also include significant commercial or industry installations at the distribution system.
2. **Retail Distributed Generation (RDG):** These resources generally include residential or small deployments of distributed energy resources. Predominantly, this focuses on rooftop solar PV installations.

[31] The differential/algebraic equations for the dynamic phasor model can be found at:
Lesieutre, B.C., D.N. Kosterev, and J. Undrill, "Phasor Modeling for Single Phase A/C/ Motors," IEEE PES General Meeting, 2008.
[32] As discussed in the section on Point-on-Wave Sensitivity.

Separating these resources in this way simplifies data management for the users and modelers of the dynamic load models while capturing the general behavior between these two types of distributed resources. It is expected that the large-scale DG may have more strict requirements on voltage control and ride-through capability as compared with the dispersed resources (particularly the older DG). However, if future requirements are more uniform than expected, these resources can have similar settings in the model or the model can be further reduced. In addition to the requirements, the location aspect is captured by having some of the DG connected at the head of the feeder (characteristic of large installations of solar PV farms) as well as at the load-end bus representing DG down the feeder. Figure 73 shows an example of the composite load model including both the commercial-type and rooftop residential-type DG resources.

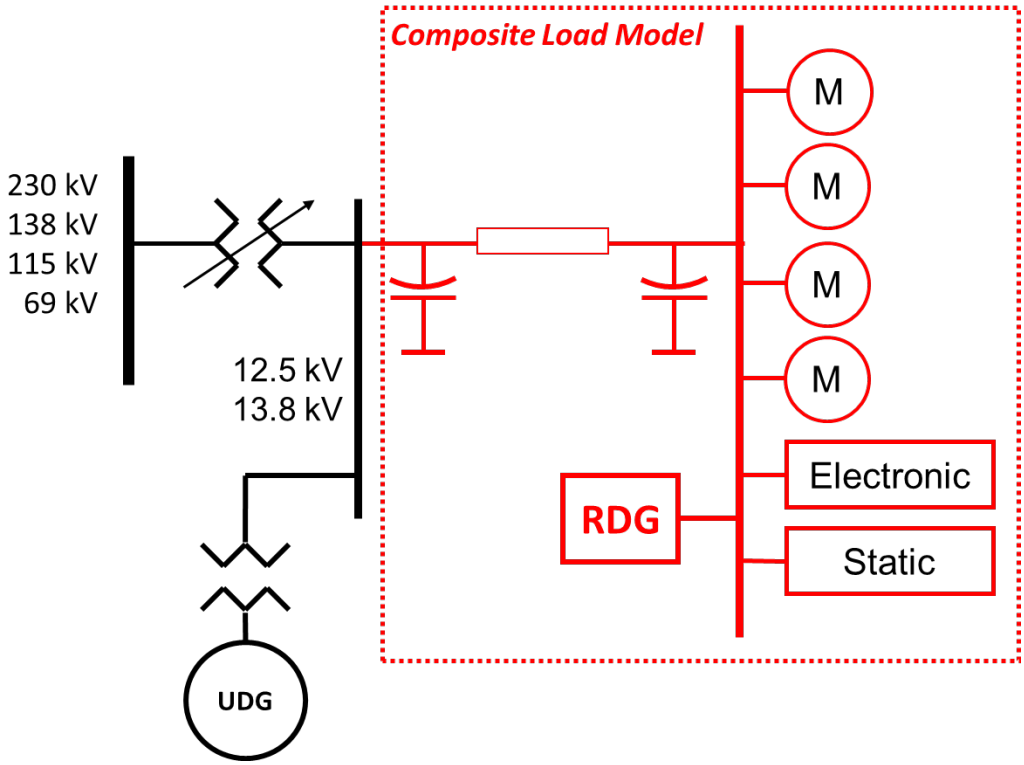


**Figure 73: Distributed Generation in Dynamic Load Models**

## Progressive Stalling and Tripping

While not all single phase motors on a feeder will stall if voltage depression is in the stall threshold range, all motors will stall/stop if voltage depression goes far below the threshold range. Single phase motors that do stall will not all stall simultaneously and motors driving reciprocating compressors are unlikely to restart. A significant fraction of air conditioner motors driving scroll compressors will reverse and reaccelerate running backwards. Older residential thermostats do not trip motors and the trend is for newer thermostats to trip motors promptly to ensure against backward rotation.

Based on this general information, the concept of blocks of load responding uniformly must be reconsidered. In the current deployment of the composite load model, the entire category of load (e.g., Motor D) changes state at the same instant (Run to Stall state). Stalling as a block is not realistic based on the diversity of load characteristics (different manufacturers, points on the feeder, A-B-C phase loading, etc.), and also makes sensitivity studies impractical.

In a progressive approach, the change of state for a given load category takes place over a time interval of, at least, a few simulation time steps based on the conditions presented to the load model. This allows the user to

study the sensitivity to the fraction of load that changes state. Figure 74 shows one approach[33] to a progressive stalling/tripping model that could be used. The fraction of stalled motors is dependent on a defined stall voltage (Vstall). In addition, the following calculations can be used to define the fractional value:

$$f_r = \frac{1 - S_{frac}}{1 + sT_{stall}}$$
$$f_{stalled} = \max((1 - f_r), f_{stalled})$$
$$f_r = \frac{i_{stalled}^2 - 1}{1 + sT_{therm}}$$

where $T_{stall}$ is the time constant associated with stalling, $S_{frac}$ is the fraction of motors that will stall at stall threshold voltage, $f_r$ is the fraction of motors that have not stalled and are still running, $f_{stalled}$ is the fraction of motors that have actually stalled, $T_{th}$ is the temperature of thermal cutouts in motors that have stalled, and $i_{stalled}$ is the current in motors that have stalled.

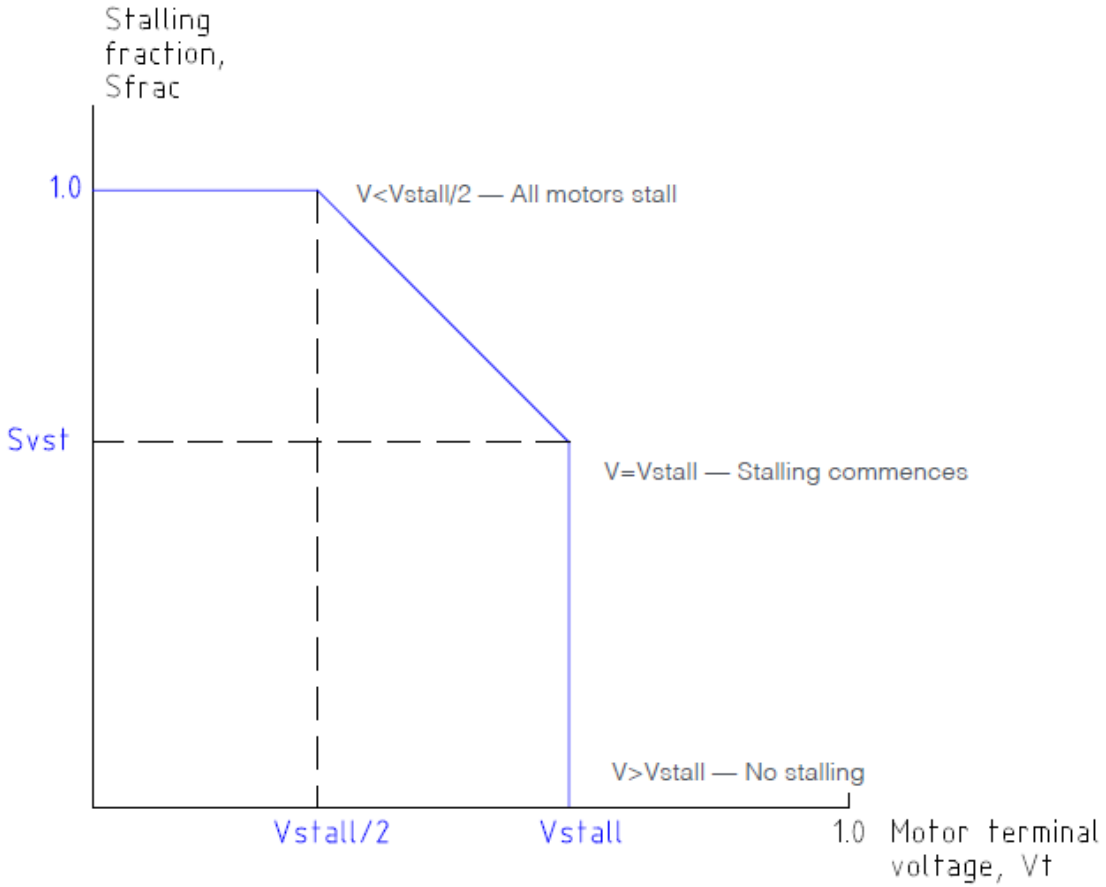


**Figure 74: Progressive Stalling Concept**

## Benchmarking with Electromagnetic Transient Models

Large scale grid simulator programs are presently positive sequence simulators which represent only a single phase of the power system network and elements with the assumption that all three phases are balanced. This assumption is essentially true when modeling the bulk transmission system. The program thus contains

[33] As conceptualized by Dr. John Undrill as an example of progressive stalling characteristic to be explored in more detail.

information only of the sinusoidal voltage/current magnitude and angle of a single phase at every time instant. Further, the time step of numerical integration is generally taken to be 4ms.

On the other hand, electromagnetic transient simulations represent all three phases of the network and elements and operate at a time step of micro seconds. This type of simulation thus contains information regarding potential unbalance between phases and very small changes and transitions. This difference between the two simulation procedures is illustrated in Figure 75 wherein the voltage at the terminals of a 100 kW three phase motor driving a pump was reduced to 0.5pu for 0.1s. The inertia constant of the motor is 0.3s.

The set of graphs on the left side are from an electromagnetic transient simulation while the graphs on the right side are from a positive sequence simulation. From the graphs of stator current (red color box), motor speed (green color box) and motor electrical torque (magenta color box) it is apparent that the positive sequence simulation, while showing the same general trend of the response, is unable to capture the detailed response at the instant of disturbance.

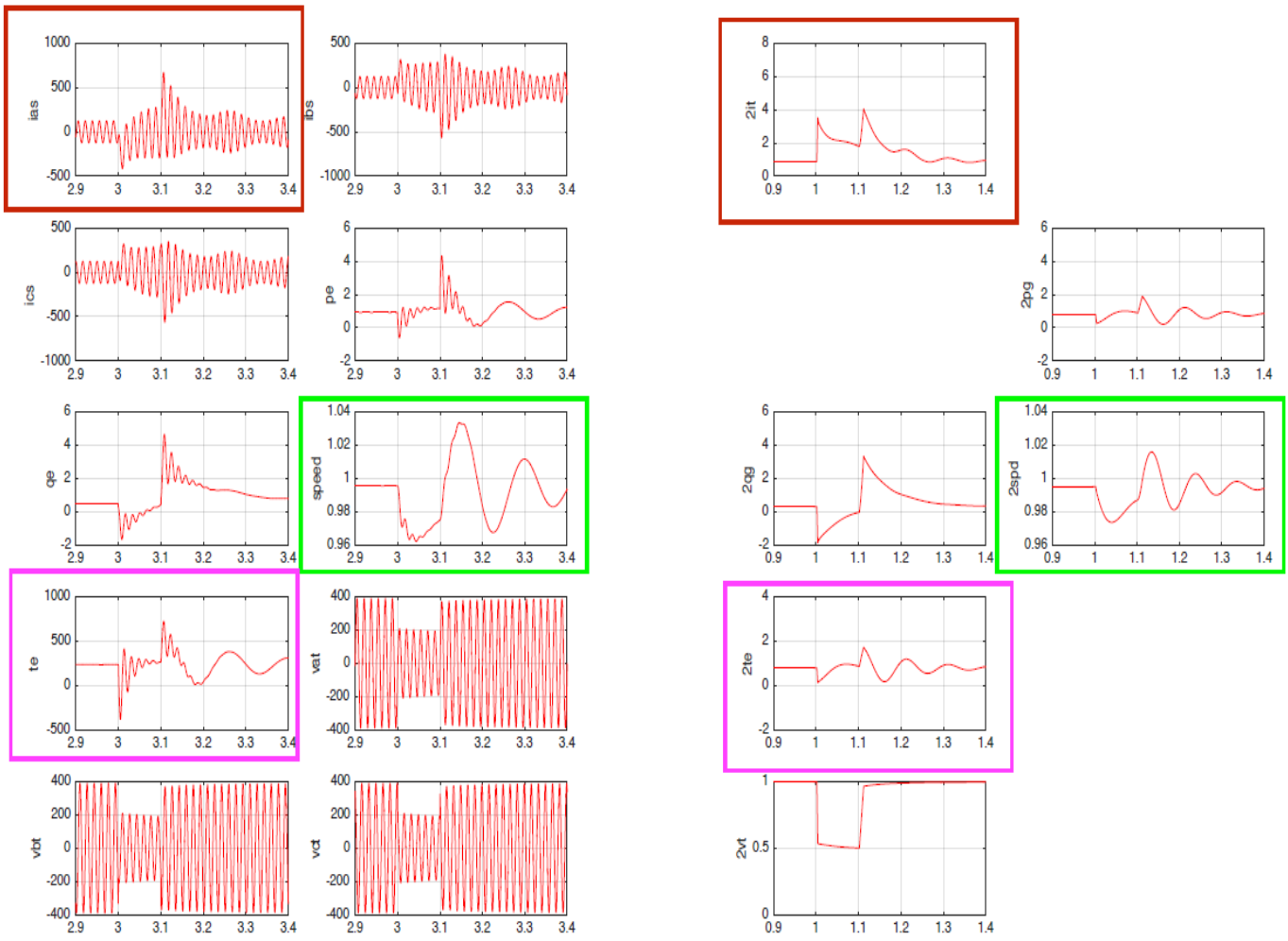


**Figure 75: Positive Sequence and Electromagnetic Transient Simulations**

The red color box on the left side highlights only the A phase current showing the presence of both the ac component and unidirectional component of current. The B phase and C phase currents are shown respectively to the right and below the A phase current. It can be inferred from the phase currents that there exists a high negative sequence current component at the time of disturbance. This negative sequence component of current is invisible to the positive sequence simulation. The presence of the negative sequence current is also visible from the graph of the electrical torque on the left side which shows the negative torque that is developed in the motor. This is not visible in the positive sequence simulation. Finally, the negative torque causes the speed to reduce to a much large value than that is shown in the positive sequence response.

The existing positive sequence motor models and simulations present a reasonably accurate picture of the operation of large size motors. However, with more emphasis being placed on studying the impact of aggregates of smaller motors in the distribution system along with the operation of the bulk power system, benchmarking with electromagnetic simulation programs is crucial.

# Appendix A – Composite Load Model Data

This section details the parameters of the composite load model and provides a reasoning behind the parameter value, if applicable. The parameters are broken up into sections for ease of reading – the composition of these parameters makes up the composite load model. The PSLF implementation of CMPLDW is used in the example provided.

Notes:

- Default parameter values that are not likely to change for during sensitivity analysis (fixed parameters) have a grey background.
- The values presented here are high-level "generic" values to help the industry get started, if necessary. To fully understand the impact of these parameter values, sensitivity analysis should be performed. Particularly for motor tripping values, the user should test various trip and reclose settings to ensure reasonable and robust simulation results.

## Substation & Feeder Parameters

```
"Bss"    0 "Rfdr" 0.04 "Xfdr" 0.04 "Fb" 0.75/
"Xxf" 0.08 "TfixHS" 1 "TfixLS" 1 "LTC" 0  "Tmin"    0.9 "Tmax" 1.1 "step" 0.00625 /
"Vmin"    1.025 "Vmax" 1.04 "Tdel" 30  "Ttap"    5 "Rcomp" 0 "Xcomp" 0 /
```

| Parameter | Default | Reason |
|---|---|---|
| Load MVA Base | -1.0 to -1.25 | If (-), MVA base = Load MW/Value Specified |
| Bss | 0.0 | Assumed no shunt compensation at bus |
| Rfdr | 0.04 | 4% impedance on load MVA base;<br>1:1 distribution feeder impedance X:R ratio |
| Xfdr | 0.04 | |
| Fb | 0.0 | No shunt compensation, so N/A |
| Xxf | 0.08 | 8% impedance on load MVA base |
| TfixHS | 1.0 | Assumed 1:1 T:D transformer turns ratio |
| TfixLS | 1.0 | |

# Transmission-Distribution Transformer Parameters

```
"Bss"    0 "Rfdr" 0.04 "Xfdr" 0.04 "Fb" 0.75/
"Xxf" 0.08 "TfixHS" 1 "TfixLS" 1 "LTC" 0  "Tmin"    0.9 "Tmax" 1.1 "step" 0.00625 /
"Vmin"    1.025 "Vmax" 1.04 "Tdel" 30  "Ttap"    5 "Rcomp" 0 "Xcomp" 0 /
```

| Parameter | Default | Reason |
|---|---|---|
| LTC | 1 or 0 | Based on whether LTC action enabled |
| Tmin | 0.9 | Based on common ULTC configuration:<br>• 32 steps<br>• +/- 0.1 tap<br>• +/- 1.25% voltage operation bounds |
| Tmax | 1.1 | |
| step | 0.00625 | |
| Vmin | 0.9875 | |
| Vmax | 1.0125 | |
| Tdel | 30-75 | Depends on utility practice for LTC action delay |
| Ttap | 5 | Time duration of LTC adjustment, commonly 5 seconds |
| Rcomp | 0 | Resistance and reactance compensation for LTC;<br>Generally not considered |
| Xcomp | 0 | |

# Load Composition Fraction Parameters

```
"Fma"    0.239538 "Fmb" 0.156309 "Fmc" 0.064766 "Fmd"    0.206375 "Fel"  0.116908  /
```

| Parameter | Default | Reason |
|---|---|---|
| Fma | Varies | These parameters are solely dependent on the load composition at the given bus. Many utilities use zonal or regional data when bus-level or feeder-level data is not available. Exact values depend on many factors – season, regional economies, industries, load type, etc. For example, heavy summer case parameters could = A: 25%, B: 15%, C: 5%, D: 15%, PE: 10%. But this is solely dependent on the load composition at the bus. |
| Fmb | Varies | |
| Fmc | Varies | |
| Fmd | Varies | |
| Fel | Varies | |

# Power Electronic Load Parameters

```
"PFel" 1 "Vd1" 0.7 "Vd2" 0.5 "Frcel" 0.8 /
```

| Parameter | Default | Reason |
|---|---|---|
| Pfel | 1.0 | Assumed power electronic load at unity power factor |
| Vd1 | 0.65 | Assume electronic load starts tripping at 70% voltage |
| Vd2 | 0.5 | Assume all electronic load is tripped by 50% voltage |
| Frcel | 0.8 | Assumed 80% of electronic load automatically reconnects upon acceptable voltage |

# Static Load Parameters

```
"Pfs"    -0.994504 "P1e" 2 "P1c" 0.295212 "P2e" 1 "P2c"    0.704788 "Pfreq" 0 /
         "Q1e" 2 "Q1c" -0.5 "Q2e" 1 "Q2c"    1.5 "Qfreq" -1 /
```

| Parameter | Default | Reason |
|---|---|---|
| Pfs | -0.99 to 1.0 | Generally near unity power factor (lighting); rather than specify shunt compensation, assume slight capacitive power factor for static load to account for shunt compensation at substation and down the feeder |
| P1e | 2.0 | $P=P_0*(P_{1c}*V/V_0^{P1e}+P_{2c}*V/V_0^{P2e}+P_3)*(1+P_{frq}*D_f)$<br>Polynomial fit for static load based on utility experience, measurement data, or laboratory testing; values provided are good assumption. |
| P1c | 0.3 | |
| P2e | 1.0 | |
| P2c | 0.7 | |
| Pfreq | 0.0 | Assume real power not frequency dependent |
| Q1e | 2.0 | Q=Q0*(Q1c*V/V0Q1e + Q2c*V/V0Q2e + Q3) * (1 + Qfrq * Df)<br>Polynomial fit for static load based on utility experience, measurement data, or laboratory testing; values provided are good assumption. |
| Q1c | -0.5 | |
| Q2e | 1.0 | |
| Q2c | 1.5 | |
| Qfreq | -1.0 | Assume Q inversely frequency dependent |

# Motor Type Parameters

```
"MtpA" 3  "MtpB" 3  "MtpC" 3  "MtpD" 1 /
```

| Parameter | Default | Reason |
|---|---|---|
| MtpA | 3 | Constant torque loads (e.g. commercial air conditioners and refrigerators) |
| MtpB | 3 | High inertia loads with torque proportional to speed squared (fans) |
| MtpC | 3 | Low inertia loads with torque proportional to speed squared (pumps) |
| MtpD | 1 | Single-phase induction motors (residential air conditioner compressors) |

# Motor A Parameters

```
"LfmA" 0.75 "RsA" 0.04 "LsA" 1.8 "LpA" 0.12 "LppA"   0.104 /
"TpoA" 0.095 "TppoA" 0.0021 "HA"   0.1 "etrqA" 0 /
"Vtr1A" 0.7 "Ttr1A" 0.02  "Ftr1A" 0.2 "Vrc1A" 1 "Trc1A" 99999 /
"Vtr2A" 0.5 "Ttr2A" 0.02  "Ftr2A" 0.7 "Vrc2A" 0.7 "Trc2A" 0.1 /
```

| Parameter | Default | Reason |
|---|---|---|
| LfmA | 0.75 | Load MVA = MW/MVA Rating |
| RsA | 0.04 | These are 'generic' motor parameters for this type of load, based on laboratory testing. |
| LsA | 1.8 | |
| LpA | 0.12 | |
| LppA | 0.104 | |
| TpoA | 0.095 | |
| TppoA | 0.0021 | |
| HA | 0.1 | Majority of these motors are small – low inertia |
| etrqA | 0* | $T_{mech} = T_{mech,0} * \omega^{E_{trq}}$ – Constant Torque |
| Vtr1A | 0.65 | Assumed performance of these motors:<br>• Represents higher performance motors – large commercial building chillers/air handlers<br>• First trip level at about 0.65 pu voltage, trip time around 100 ms<br>• 20% of these motors have this type of protection<br>• Manual reconnection |
| Ttr1A | 0.1 | |
| Ftr1A | 0.2 | |
| Vrc1A | 0.1 | |
| Trc1A | 9999 | |
| Vtr2A | 0.5 | Assumed performance of these motors:<br>• Represents majority of 'brute' motors – standard design, rugged, automated<br>• Contactor tripping levels - 0.50 pu voltage, trip time < 2 cycles<br>• 75% of these motors have this type of protection<br>• Contactors reclose around 0.65 pu within 100 ms.<br>NOTE: Vtr1A & Vtr2A should not equal 1; keep some fraction online at all times for numerical purposes with the model. |
| Ttr2A | 0.02 | |
| Ftr2A | 0.75 | |
| Vrc2A | 0.65 | |
| Trc2A | 0.1 | |

**3φ motors driving constant torque loads (commercial air conditioner compressors and refrigeration)*

# Motor B Parameters

```
"LfmB" 0.75 "RsB" 0.03 "LsB" 1.8 "LpB" 0.19 "LppB"   0.14 /
 "TpoB" 0.2 "TppoB" 0.0026 "HB"   0.5 "etrqB" 2 /
"Vtr1B" 0.6 "Ttr1B" 0.02  "Ftr1B" 0.2 "Vrc1B" 0.75 "Trc1B" 0.05 /
"Vtr2B" 0.5 "Ttr2B" 0.02  "Ftr2B" 0.3 "Vrc2B" 0.65 "Trc2B" 0.05 /
```

| Parameter | Default | Reason |
|---|---|---|
| LfmB | 0.75 | Load MVA = MW/MVA Rating |
| RsC | 0.03 | These are 'generic' motor parameters for this type of load, based on laboratory testing. |
| LsB | 1.8 | |
| LpB | 0.19 | |
| LppB | 0.14 | |
| TpoB | 0.2 | |
| TppoB | 0.0026 | |
| HB | 0.5 | Large inertia commercial/industrial fan motor loads |
| etrqB | 2* | $T_{mech} = T_{mech,0} * \omega^{E_{trq}}$ - Torque ∝ Speed-Squared |
| Vtr1B | 0.55 | Assumed performance of these motors:<br>• All fans assumed to only have contactor tripping – no controls-based protection; therefore<br>• Two sets of tripping levels representing diversity of motor load<br>• Level 1<br>  • Trip at 0.55 pu voltage, trip time < 2 cycles<br>  • 30% of these motors have this type of protection<br>  • Auto-reconnect – 0.65 pu voltage within 50 ms<br>• Level 2<br>  • Trip level at 0.50 pu voltage, trip time < 2 cycles<br>  • 30% of these motors have this type of protection<br>  • Auto-reconnect – 0.6 pu within 50 ms |
| Ttr1B | 0.02 | |
| Ftr1B | 0.3 | |
| Vrc1B | 0.65 | |
| Trc1B | 0.05 | |
| Vtr2B | 0.5 | |
| Ttr2B | 0.025 | |
| Ftr2B | 0.3 | |
| Vrc2B | 0.60 | |
| Trc2B | 0.05 | |

**3φ motors driving load proportional to speed-squared relationship with high inertia (large fans)*

# Motor C Parameters

```
"LfmC" 0.75 "RsC" 0.03 "LsC" 1.8 "LpC" 0.19 "LppC"   0.14 /
"TpoC" 0.2 "TppoC" 0.0026 "HC"   0.1 "etrqc" 2 /
 "Vtr1C" 0.65 "Ttr1C" 0.02 "Ftr1C" 0.2 "Vrc1C" 1 "Trc1C" 9999 /
 "Vtr2C" 0.5 "Ttr2C" 0.02 "Ftr2C" 0.3 "Vrc2C" 0.65 "Trc2C" 0.1 /
```

| Parameter | Default | Reason |
|---|---|---|
| LfmC | 0.75 | Load MVA = MW/MVA Rating |
| RsC | 0.03 | These are 'generic' motor parameters for this type of load, based on laboratory testing. |
| LsC | 1.8 | |
| LpC | 0.19 | |
| LppC | 0.14 | |
| TpoC | 0.2 | |
| TppoC | 0.0026 | |
| HC | 0.1 | Low inertia commercial/industrial fan motor loads |
| etrqC | 2* | $T_{mech} = T_{mech,0} * \omega^{E_{trq}}$ - Torque ∝ Speed-Squared |
| Vtr1C | 0.58 | Assumed motor protection is same as for Motor B (only contactors) – slightly offset to represent motor load diversity.<br>• Level 1<br>  • Trip at 0.58 pu voltage, trip time < 2 cycles<br>  • 20% fraction of motor trips<br>  • Contactors reclose at 0.68 pu in 50 ms<br>• Level 2<br>  • Trip at 0.53 pu voltage, trip time < 2 cycles<br>  • 30% fraction of motors trip<br>  • Contactors reclose at 0.62 pu in 50 ms |
| Ttr1C | 0.03 | |
| Ftr1C | 0.2 | |
| Vrc1C | 0.68 | |
| Trc1C | 0.05 | |
| Vtr2C | 0.53 | |
| Ttr2C | 0.03 | |
| Ftr2C | 0.3 | |
| Vrc2C | 0.62 | |
| Trc2C | 0.05 | |

**3φ motors driving load proportional to speed-squared relationship with low inertia (large fans)*

# Motor D Parameters

```
"LfmD"  1 "CompPF" 0.98 /
"Vstall" 0.6 "Rstall" 0.1  "Xstall" 0.1 "Tstall" 0.03  "Frst" 0.2 "Vrst" 0.95 "Trst" 0.3 /
"fuvr" 0.1 "vtr1" 0.6 "ttr1" 0.02 "vtr2" 1 "ttr2" 9999 /
"Vc1off" 0.5 "Vc2off" 0.4 "Vc1on" 0.6 "Vc2on" 0.5 /
"Tth" 15 "Th1t" 0.7 "Th2t" 1.9 "tv" 0.025
```

| Parameter | Default | Reason |
|---|---|---|
| LfmD | 1.0 | Load MVA = MW/MVA Rating |
| CompPF | 0.98 | Assumed slightly inductive motors load |
| Vstall | 0.45-0.60 | Stall voltage (range) based on laboratory testing |
| Rstall | 0.1 | Based on laboratory testing results of residential air-conditioners |
| Xstall | 0.1 | |
| Tstall | 0.033 | Stall time (range) based on laboratory testing |
| Frst | 0.2 | Captures diversity in load; also based on testing (fraction of motors capable of restart). |
| Vrst | 0.95 | Reconnect when acceptable voltage met |
| Trst | 0.3 | Induction motor restart time is relatively short |
| fuvr | 0.1 | Assumed fraction of A/C units with undervoltage relaying is relatively low. |
| vtr1 | 0.6 | Undervoltage relay settings (set higher than stall characteristic; therefore, small percentage of motors equipped with U/V protection will not stall). |
| ttr1 | 0.02 | |
| vtr2 | 0.1 | No second level undervoltage tripping specified. |
| ttr2 | 9999 | |
| Vc1off | 0.6 | Assume (based on lab testing) that contactors will start dropping out at this point. |
| Vc2off | 0.4 | Assume (based on lab testing) that all contactors dropped out at this point. |
| Vc1on | 0.65 | Assume all contactors have reclosed at this point. |
| Vc2on | 0.5 | Assume contactors will start reclosing at this point. |
| Tth | 15 | Varies based on manufacturer and external factors – sensitivity analysis required |
| Th1t | 0.7 | Assumed tripping starting at 70% temperature, with all tripped at 190% temperature |
| Th2t | 1.9 | |
| tv | 0.025 | Assumed generic transducer time lag |

# Motor D Parameters (for PSS®E)

PSS®E includes additional parameters in its DYRE file; these are described here for completeness.

| Parameter | Default | Reason |
|---|---|---|
| LFadj | 1 | Load factor adjustment to the stall voltage10 |
| Kp1 | 0 | Real power constant for running state 111 |
| Np1 | 1 | Real power exponent for running state 1 |
| Kq1 | 6 | Reactive power constant for running state 1 |
| Nq1 | 2 | Reactive power exponent for running state 1 |
| Kp2 | 12 | Real power constant for running state 2 |
| Np2 | 3.2 | Real power exponent for running state 2 |
| Kq2 | 11 | Reactive power constant for running state 2 |
| Nq2 | 2.5 | Reactive power exponent for running state 2 |
| Vbrk | 0.86 | Compressor motor "breakdown" voltage (pu) |
| CmpKpf | 1 | Real power constant for frequency dependency |
| CmpKqf | -3.3 | Reactive power constant for frequency dependency |

# Appendix B – Complex Load Model Data

This section provides a brief description of the Complex Load (CLOD) Model implemented in PTI PSS®E. This model is a simplified alternative to the composite load model. The dynamics record this model is represented as:

```
123456  'CLODBL'  *      15      45      0       20      6       1.25    0       0.1     /
```

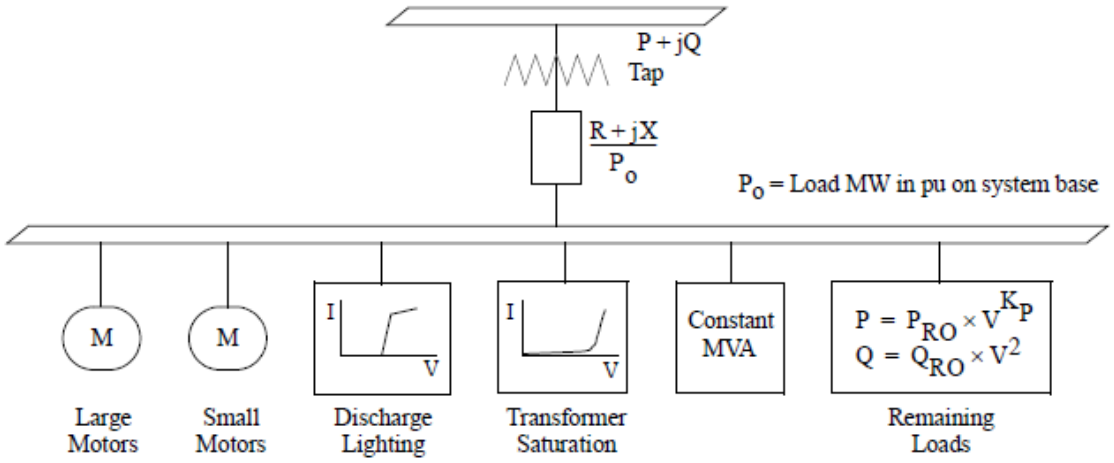


**Figure B1: Complex Load (CLOD) Model[34] (Source: PSS®E)**

The CLOD model replaces the constant MVA, current, and impedance load with a composition of loads as shown in Figure B1. These loads consist of large and small induction motors, discharge lighting, constant MVA load, and a static load response. Also included are transformer saturation effects and an equivalent distribution feeder and transformer impedance.

Some general comments and modeling considerations for the CLOD model:

- The model assumes that the load bus voltage is 0.98 pu, and adjusts the transformer tap ratio at initialization until that load bus voltage is attained.
- The motor curves for the large and small induction motor models are provided in the instruction manual. These motors models represent large and small motors with inertia constant H = 1.0 sec and H = 0.6 sec, respectively.
- The model does not consider single-phase induction motors such as residential air conditions.
- The distribution system equivalent modeled as $(R+jX)/P_0$ represents the transformer and/or feeder impedance; however, this does not represent shunt compensation at the substation or down the feeder.
- Under-load tap changing is not considered in the transformer model.
- Discharge lighting is modeled as constant current real part and imaginary part proportional to the voltage raised to 4.5 power. Voltage between 0.65-0.75 pu exhibits a linear reduction. For any voltage less than 0.65 pu, the load is assumed extinguished (no load).

[34] PTI PSS®E Application Guide Volume 2

# Appendix C – Estimating Polar Moment of Inertia

Consider a fan as shown in Figure C1 with the following known data:

- Number of blades is 6 and rotation speed of fan is 90 RPM.
- Root diameter of fan disc is 1m while tip diameter of fan disc is 4.5m.
- Fan blades taper linearly from root to tip and the mass per unit length of the blade varies from 8 Kg/m at the root to 3 Kg/m at the tip.

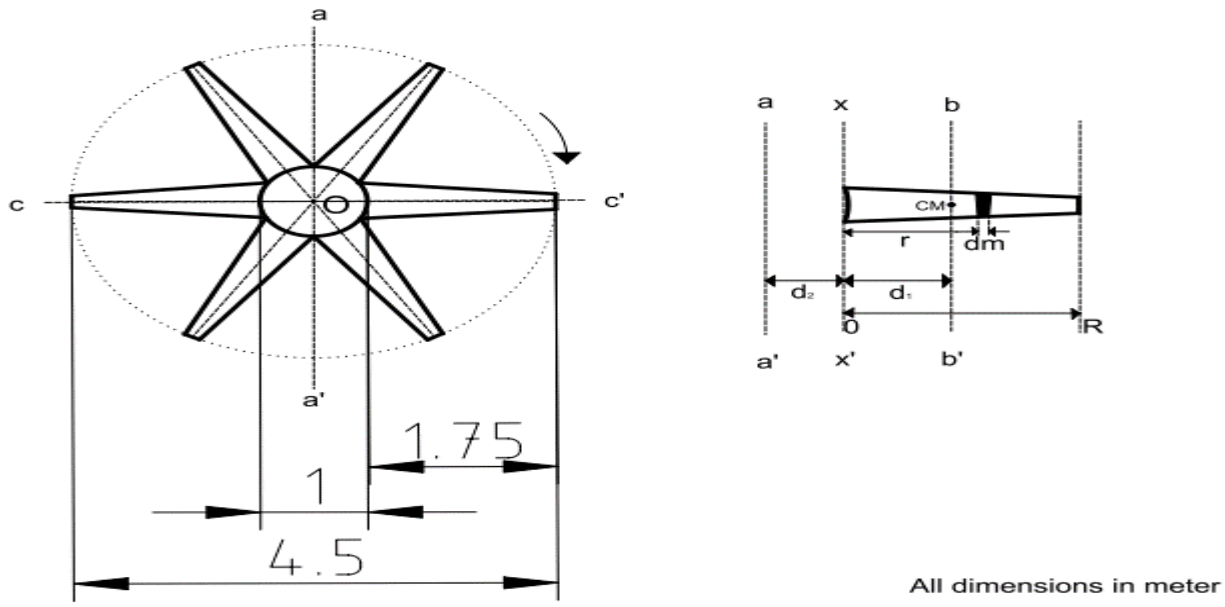


**Figure C1: 2D Schematic of Fan**

As the mass per unit length varies linearly from root to tip, the variation can be modelled as a straight line as:

$$m_r - 8 = \left(\frac{3-8}{1.75-0}\right)(r-0) \Rightarrow m_r = -2.857r + 8$$

where $m_r$ is the mass per unit length at length $r$ from the root to the blade. To obtain the polar moment of inertia, consider an infinitesimal element of mass $dm$ located at a distance $r$. The moment of inertia for this mass is given as,

$$dI = r^2 dm$$

The total moment of inertia is obtained by integrating this equation and using the quantity $m_r$ as,

$$\int_0^I dI = \int_0^M r^2 dm \Rightarrow \int_0^R r^2 m_r dr \Rightarrow \int_0^{1.75} r^2(-2.857r + 8)dr$$

The limits of integration are from *0* to *R* as the moment of inertia of the blade is being estimated about axis *xx'*. The integration yields the polar moment of inertia of the blade as $I_{xx'}$=7.6 kg-m$^2$. To obtain the polar moment of inertia about the central axis *aa'*, parallel axis theorem is invoked. However, since the mass per unit length of the blade is not uniform from root to tip, its center of mass will not be located at half the distance from either root or tip. The center of mass of the blade will be located at:

$$r_{cm} = \frac{\int_0^R r.m_r dr}{M} = \frac{\int_0^R r.m_r dr}{\int_0^R m_r dr} \Rightarrow M = 9.62kg; r_{cm} = 0.742m$$

In Figure C1, axis *bb'* passes through the center of mass. Thus, by parallel axis theorem,

$$I_{aa'} = I_{bb'} + M(d_1 + d_2)^2 = I_{xx'} + Md_2^2 + 2Md_1d_2 \Rightarrow I_{aa'} = 17.143kg - m^2$$

The above moment of inertia has been calculated assuming that the blade rotates about the axis *aa'*. However, actual rotation of the blade is about the axis through the center *O* and perpendicular to the axis *aa'*. Thus, by perpendicular axis theorem and since $I_{cc'}$=0, $I_{O1}$=17.143 kg-m2. By superposition,

$$I_O = 6 * I_{O1} = 102.858kg - m^2$$

Similarly, the polar moment of inertia of the rotor of the motor can be calculated.